

CONVECTIVE HEAT TRANSFER COEFFICIENTS  
FROM ELLIPSOIDAL MODELS AND  
IRREGULAR SHAPES TO AIR

By

BOBBY LELAND CLARY  
Bachelor of Science  
University of Georgia  
Athens, Georgia

1960

Submitted to the Faculty of the Graduate College  
of the Oklahoma State University  
in partial fulfillment of the requirements  
for the Degree of  
DOCTOR OF PHILOSOPHY  
May, 1969

SEP 29 1969

CONVECTIVE HEAT TRANSFER COEFFICIENTS  
FROM ELLIPSOIDAL MODELS AND  
IRREGULAR SHAPES TO AIR

*S. J. Mason*

Thesis Adviser

*Ernst Schneider*

*Gerald W. Parker*

*R. G. Newrickson*

*D. D. Durham*

Dean of the Graduate College

724790

## ACKNOWLEDGMENTS

This investigation was conducted as a part of the Oklahoma Agricultural Experiment Station Project 1268.

The author is especially grateful to his major adviser, Dr. Gordon L. Nelson, for his capable guidance during this study. He has been a source of real assistance, inspiration, and encouragement from the initiation of the study through the preparation of the manuscript.

Appreciation is extended to other members of the Advisory Committee. Professor E. W. Schroeder, Head of the Agricultural Engineering Department, Dr. J. D. Parker, Professor of Mechanical Engineering, and Dr. R. L. Henrickson, Professor of Animal Science served in this capacity. Their criticism and suggestions have been invaluable throughout this study.

A special thanks is extended to Professor Schroeder for his efforts as supervisor of the graduate program. Appreciation is extended to him and the Ford Foundation for providing the Forgivable Loan during the period of my graduate study.

My thanks is extended to Jack Fryrear and Don McCrackin for their assistance in the preparation of the figures.

To all of my fellow graduate students, who have so graciously endured my moments of despair, I am sincerely

grateful. A special word of thanks is extended to my office mate, Mr. Harvey B. Manbeck, for his encouragement during these periods of dejection.

I am grateful to Mrs. Linda Manning for her tireless efforts in typing the rough and final drafts of the manuscript.

For their many sacrifices throughout this study I dedicate this thesis to my wife Irene and my children, Debra, Teresa and Douglas.

## TABLE OF CONTENTS

Chapter	Page
I. INTRODUCTION . . . . .	1
The Problem . . . . .	1
Objectives . . . . .	3
Limitations of the Study . . . . .	3
Definition of Symbols . . . . .	5
II. REVIEW OF THE LITERATURE . . . . .	10
The Navier-Stokes Equation . . . . .	10
Boundary Layer Simplifications . . . . .	16
Solutions for the Temperature Distributions in Viscous Flow . . . . .	20
Couette Flow . . . . .	21
Poiseuille Flow Through a Channel with Flat Walls . . . . .	24
Parallel Flow Past Flat Plate- Blasius Solution . . . . .	25
Thermal Boundary Layers Over Other Shapes - Theoretical Results . . . . .	32
Turbulent Heat Transfer - External Boundary Layer . . . . .	33
Flow Over Bodies of Arbitrary Shape . . . . .	41
Ellipsoidal Shapes . . . . .	46
Wind Tunnel Turbulence . . . . .	49
The Critical Reynolds Number of Spheres . . . . .	53
Turbulence Effect on Heat Transfer . . . . .	57
III. EXPERIMENTAL DESIGN AND PROCEDURE . . . . .	60
Theory of Similitude . . . . .	60
Pi Terms . . . . .	63
Prediction Equations . . . . .	66
Range of Pi Terms . . . . .	67
Measurement of Nusselt Number . . . . .	69
IV. EQUIPMENT AND INSTRUMENTATION . . . . .	72
Model Construction . . . . .	72
Template Construction . . . . .	72
Model Instrumentation . . . . .	82

Chapter	Page
Data Collection . . . . .	85
Surface Areas of the Models . . . . .	86
Characteristics of the Wind Tunnel . . . . .	91
Summary of Turbulence Properties of the Tunnel . . . . .	98
V. DEVELOPMENT OF THE THEORY . . . . .	99
Component Equations for the Ellipsoidal Model . . . . .	100
Prediction Equation for the General Ellipsoid . . . . .	110
Irregular Shapes . . . . .	119
Transforming the Irregular Shape . . . . .	127
VI. SUMMARY AND CONCLUSIONS . . . . .	134
Summary . . . . .	134
Conclusion . . . . .	136
SELECTED BIBLIOGRAPHY . . . . .	139

## LIST OF TABLES

Table	Page
I. Values of $C_1$ for Various Prandtl Numbers for Heat Transfer to the Laminar Constant Property Boundary Layer . . . . .	30
II. Values for C and M for Calculating the Heat Transfer Coefficients from Cylinders with the Indicated Cross-Sectional Shape . . . . .	45
III. Pertinent Variables for the Convective Heat Transfer Coefficient from an Ellipsoidal Model . . . . .	61
IV. Experimental Design . . . . .	68
V. Surface Areas for General Ellipsoids . . . . .	92
VI. Nusselt Number as a Function of Reynolds Number with $\pi_4$ and $\pi_5$ Held Constant . . . . .	101
VII. Nusselt Number as a Function of the Length Ratio, $a/c$ , with $\pi_3$ and $\pi_5$ Held Constant . . . . .	104
VIII. Nusselt Number as a Function of the Length Ratio, $b/c$ , with $\pi_3$ and $\pi_5$ Held Constant . . . . .	108
IX. Nusselt Number vs. Reynolds Number For Shape I . . . . .	117
X. Nusselt Number vs. Reynolds Number For Shape II . . . . .	120
XI. Nusselt Number vs. Reynolds Number For Shape III . . . . .	123

## LIST OF FIGURES

Figure	Page
1. Velocity Distribution in Couette Flow . . . . .	22
2. Hydrodynamic Boundary Layer Formation . . . . .	25
3. Velocity and Thermal Boundary Layer Formation . . . . .	31
4. Variation of the Local Nusselt Number Around a Right Circular Cylinder . . . . .	34
5. Expected Temperature Distribution for a Fully Developed Turbulent Flow . . . . .	38
6. Local Heat Transfer Around a Cylinder for Different Reynolds Numbers . . . . .	43
7. Comparison of Methods for Calculation of Local Heat Transfer Coefficients Around an Elliptic Cylinder with Axis Ratio of 1:2 . . . . .	47
8. Comparison of Methods Used for Calculation of Local Heat Transfer Coefficients Around an Elliptic Cylinder with Axis Ratio of 1:4 . . . . .	48
9. Scale of Turbulence at Several Distances From the Screens . . . . .	52
10. Intensity of Turbulence at Several Distances From the Screens . . . . .	54
11. Critical Reynolds Number of Spheres as a Function of $\frac{(u^2)^{1/2}}{U_\infty} \left(\frac{D}{L}\right)^{1/5}$ . . . . .	55
12. Parametric Representation of the Ellipse . . . . .	73
13. Analog Computer Diagram for Plotting the Ellipsoid Cross-Sections . . . . .	74
14. Sheet Metal Templates in Position for Pouring the Paraffin Mold . . . . .	76



Figure	Page
15. Paraffin Mold Formed for Pouring the Plaster of Paris Pattern . . . . .	77
16. Unfinished Plaster of Paris Pattern Removed from Paraffin Mold . . . . .	78
17. Finished and Unfinished Plaster of Paris Pattern . . . . .	79
18. The Forming of the Pattern for the Outside Dimensions of the 13.5 x 10.0 x 5.75 inch Ellipsoid . . . . .	80
19. Patterns for the Inside and Outside Dimensions of the Ellipsoid Ready for Casting . . . . .	81
20. Location of Thermocouples on the Surface of the Ellipsoids . . . . .	83
21. Computer Program Error Function Related to the Increment Size . . . . .	88
22. Error Function for the Computer Program as a Function of the Length Ratio, A/B, of the Ellipsoid . . . . .	89
23. Agricultural Engineering Research Wind Tunnel . . . . .	93
24. Velocity Profiles Taken Along a Horizontal and Vertical Centerline of the Wind Tunnel . . . . .	94
25. Drag Coefficient on a Sphere as a Function of the Reynolds Number when Tested in the O.S.U. Wind Tunnel . . . . .	97
26. Nusselt Number vs. the Reynolds Number for the Ellipsoidal Model . . . . .	.102
27. Nusselt Number vs. the Length Ratio, a/c, for the Ellipsoidal Model . . . . .	.105
28. Hypothesized Shape of the Nusselt Number vs. a/c Function . . . . .	.107
29. Nusselt Number as a Function of the Length Ratio, b/c, for the Ellipsoidal Model . . . . .	.109

Figure	Page
30. The Nusselt Number vs. Reynolds Number Calculated From Equation 125 and Compared with the Results of Ko and Lewis . . . . .	114
31. Nusselt Number Calculated vs. Nusselt Number Observed for the General Ellipsoid . . . . .	115
32. Orientation of Shapes I, II, and III During the Experimental Tests . . . . .	116
33. Nusselt Number vs. Reynolds Number for Shape I . . . . .	118
34. Nusselt Number vs. Reynolds Number for Shape II . . . . .	121
35. Nusselt Number vs. Reynolds Number for Shape III . . . . .	124
36. Reynolds Number at Which Nusselt Number is Equal for the Irregular Shape and Ellipsoid with Equivalent Dimensions Using Equation 125 . . . . .	126
37. Effect of Geometry of the Object on the Nu vs. Re Relationship . . . . .	128
38. General Shape of Nu vs. Re for an Irregular Shape and Ellipsoidal Shape . . . . .	129
39. Values of $\gamma$ and $n$ as a Function of the Length Ratio $b/c$ . . . . .	130
40. Nusselt Number Calculated From Equation 136 vs. Nusselt Number Observed for the Irregular Shape . . . . .	133

## CHAPTER I

### INTRODUCTION

#### The Problem

Recent research on the processing of pork products concentrated attention on the problem of predicting heat transfer properties of irregular shaped objects. Past performances in the design of cooling equipment for biological materials have been based primarily on the designers experiences. Both over and under designed units are quite common. Most of these errors can be traced to a lack of available knowledge about the non-homogeneous, non-isotropic, irregular shaped objects encountered in biological materials.

Smith (40) at Oklahoma State University developed a procedure for predicting the temperature distribution within an irregular shape. He showed the temperature to be of the following form:

$$\theta = f_1 (Fo, Bi, L_d, G) \quad (1)$$

where:  $\theta$  = Dimensionless Temperature

$Fo$  = Fourier Number

$Bi$  = Biot Number

$L_d$  = Dimensionless distance

$G$  = Geometry of the shape.

In order to predict the temperature at any point within the shape requires a knowledge of the Biot Number  $\left(\frac{hc}{k_p}\right)$ . The characteristic dimension,  $c$ , and thermal conductivity of the shape can normally be determined by one of several methods. The heat transfer coefficient,  $h$ , is dependent upon the geometry of the shape as well as a number of other factors. Our knowledge of the heat transfer coefficient is limited to certain special surfaces such as spheres, flat plates, and cylinders. Should one wish to define the heat transfer coefficient for an irregular shape, such as a ham, he would have to define the shape in terms of a plate, cylinder, or sphere and then by one of several alternative approximations estimate the heat transfer coefficient. In many cases this approximation of the anomalous shape is a poor one. The final result is also a poor estimate--errors up to 100 percent have been observed of the heat transfer coefficient.

An ellipsoidal model would provide a more accurate means of defining the geometry of anomalous shapes since we have control of the size of the model in three principle directions. It is reasonable to expect that a model that more adequately defines the geometry of the shape will also give a better estimate of the heat transfer coefficient.

Therefore, there is a need for an equation that will predict the heat transfer coefficient of a wide variety of ellipsoidal models. With these two tools, a redefinition of anomalous shapes in terms of ellipsoids and a general

prediction equation for the heat transfer coefficient of these ellipsoids, it is thought that less "guess work" and more accuracy could be derived in estimating the heat transfer coefficient of anomalous shapes.

### Objectives

The objectives of this study are:

1. To design ellipsoidal models which will be representative of a typical agricultural product.
2. To develop a general prediction equation for the heat transfer coefficient from the ellipsoidal models in a gas stream with a specified orientation relative to the fluid flow.
3. To correlate the results of the general prediction equation with those obtained by direct measurement of the heat transfer coefficient from an anomalous shape.
4. To determine an adequate criterion for replacing an anomalous shape with an ellipsoidal model for convective heat transfer.

### Limitations of the Study

Several factors that are known to have an effect on the convective heat transfer rates from blunt bodies have not been considered in this work. This was generally done either to hold the scope of the work to a manageable level

or because it was considered unnecessary to accomplish the objectives of this work.

The surfaces of all models were buffed using a jewelers rouge to give a smooth shiny surface. As long as the boundary layer flow is laminar the surface roughness will have little, if any, effect on the convective heat transfer rate. However in the transition, turbulent and separated regions of the boundary layer large variations in heat transfer rates can occur with small fluctuations in surface roughness. One of the noticeable effects of increased roughness would be an earlier transition from laminar to turbulent boundary layer flow. Results for surfaces with large irregularities would be expected to yield results different than those presented here.

In all cases the model was orientated so that the dimensions a and c were perpendicular to fluid flow and dimension b was parallel to fluid flow. Variation in the orientation of the model with respect to fluid flow was not considered important in fulfilling the objectives of this study.

Air was used as the only fluid medium throughout the study so that Prandtl Number dependence could not be determined. However since the Prandtl Number for other gases closely approximates that for air these results should introduce small errors when using gases other than air. Kays (19) and others have shown the Nusselt Number to vary approximately as the Prandtl Number to the one-third

power. Using this approximation these results can be extended to cover fluids whose Prandtl Number varies significantly from the value for air.

The maximum and minimum levels of the independent  $\pi$  terms are tabulated in Chapter III. Extrapolation of these results beyond the range of these values is not recommended. Extrapolation to values of the length ratios below the minimum is particularly discouraged for reasons detailed in Chapter V.

### Definition of Symbols

The symbols used in this report are generally the same as those finding common usage in the literature of heat transfer. Those symbols finding general usage throughout the report are tabulated below. Subscripts on the variable symbol generally refer to a particular location in space and is not necessarily included in the list given below. The subscript,  $\infty$ , always refers to the free stream condition while a subscript of  $o$  or  $w$  usually refers to the condition at a stationary surface. Where special symbols that are not tabulated below are used a special effort is made to define those quantities.

Symbol	Quantity	Units
$a$	Length of the major axis of the ellipsoid perpendicular to fluid flow	ft.
$A$	$a/2$	ft.
$A_i$	Surface area represented by node $i$	ft <sup>2</sup>

<u>Symbol</u>	<u>Quantity</u>	<u>Units</u>
$A_p$	Area projected on a plane perpendicular to fluid flow	ft <sup>2</sup>
$A_s$	Total surface area	ft <sup>2</sup>
b	Length of the horizontal axis of ellipsoid perpendicular to major axis and parallel to fluid flow	ft.
B	b/2	ft.
Bi	Biot Number	-
c	Length of vertical axis of ellipsoid perpendicular to major axis and fluid flow	ft.
C	c/2	ft.
$C_1, C_2$	Constants	-
$C_D$	Drag Coefficient	-
$C_p$	Specific heat at constant pressure	Btu/(lb <sub>m</sub> °F)
d, e, g, j	Dimensionless exponents	-
D	Diameter of sphere	ft.
E	emf	volts
Ek	Eckert Number	-
f	A function of	-
$f_x$	Friction factor	-
F	Drag force	lb <sub>f</sub>
Fo	Fourier Number	-
g	Acceleration due to gravity strength	ft/sec <sup>2</sup>
G	Geometry index	-
$G_1$	Mass fluid velocity	lb <sub>m</sub> /(secft <sup>2</sup> )
Gr	Grashof Number	-
h	Average convective heat transfer coefficient	Btu/(hrft <sup>2</sup> °F)



<u>Symbol</u>	<u>Quantity</u>	<u>Units</u>
$h_1$	Distance from centerline to wall in couette flow problem	ft.
I	Current flow	Amperes
k	Fluid thermal conductivity	Btu/(hrft <sup>°F</sup> )
$k_p$	Product thermal conductivity	Btu/(hrft <sup>°F</sup> )
K	Constant	-
L	Scale of turbulence	-
$L_d$	Dimensionless length ratio	-
m	Dimensionless exponent	-
M	Screen mesh size	ft.
n	Exponent on Reynolds Number of general prediction equation	-
Ne	Newton's Second Law Coefficient	(lb <sub>f</sub> sec <sup>2</sup> )/(lb <sub>m</sub> ft)
Nu	Nusselt Number	-
P	Pressure	lb <sub>f</sub> /ft <sup>2</sup>
P	Power	watts
Pr	Prandtl Number	-
Q	Correlation Coefficient	-
q	Heat Energy Flow	Btu/hr
$\dot{q}''$	Heat Energy Flow per unit area	Btu/(hrft <sup>2</sup> )
r	Regression Correlation Coefficient	-
$r_1, r_2$	Dimensionless exponent	-
R	Universal Gas Constant	(ftlb <sub>f</sub> )/(lb <sub>m</sub> <sup>°R</sup> )
Re	Reynolds Number	-
Re <sub>crit</sub>	Reynolds Number when $C_D = 0.3$	-
S	Total length of ellipsoidal surface measured from the stagnation point along the meridian profile	ft.

<u>Symbol</u>	<u>Quantity</u>	<u>Units</u>
St	Stanton Number	-
T	Temperature	°F
Tu	Intensity of Turbulence	-
u	Local velocity in x-direction	ft/sec
u'	Instantaneous velocity fluctuation in x-direction	ft/sec
U <sub>1</sub>	Velocity of plate in couette flow	ft/sec
U <sub>∞</sub>	Free Stream Velocity	ft/sec
v	Local velocity in y-direction	ft/sec
v'	Instantaneous velocity fluctuation in y-direction	ft/sec
w	Local velocity in z-direction	ft/sec
w'	Instantaneous velocity fluctuation in z-direction	ft/sec
x <sub>1</sub>	Unheated starting length	ft.
x,y,z	Coordinate directions	ft.
X	Body Forces in x-direction	lb <sub>f</sub> /ft <sup>3</sup>
Y	Body Forces in y-direction	lb <sub>f</sub> /ft <sup>3</sup>
Z	Body Forces in z-direction	lb <sub>f</sub> /ft <sup>3</sup>
ℓ	Characteristic Length	ft.
ln	Naperian logarithm	-
log	Logarithm to Base 10	-
α	Thermal diffusivity	ft <sup>2</sup> /hr
β	Coefficient of volumetric expansion	1/°F
γ	Coefficient for general prediction equation	-
δ <sub>S</sub>	Hydrodynamic boundary layer thickness	ft.
δ <sub>T</sub>	Thermal boundary layer thickness	ft.

<u>Symbol</u>	<u>Quantity</u>	<u>Units</u>
$\epsilon$	Roughness index	-
$\epsilon_H$	Eddy diffusivity for heat	ft <sup>2</sup> /hr
$\eta$	Similarity Variable	-
$\theta$	Dimensionless temperature	-
$\Theta$	Angle	degrees
$\mu$	Dynamic viscosity	lb <sub>f</sub> sec/ft <sup>2</sup>
$\nu$	Kinematic viscosity, $\mu/(\rho Ne)$	ft <sup>2</sup> /sec
$\xi$	$(\nu x U_\infty)$	ft <sup>2</sup> /sec
$\rho$	Density of fluid	lb <sub>m</sub> /ft <sup>3</sup>
$\tau_0$	Shear stress at the wall	lb <sub>f</sub> /ft <sup>2</sup>
$\phi$	Viscous dissipation function	1/sec
$\phi_1$ $\phi_2$	A function of	-
$\Psi$	Stream function	ft <sup>2</sup> /sec
$\omega$	Number of nodes	-
$P^*$	Dimensionless pressure - $P/(\rho U_\infty^2)$	-
$T^*$	Dimensionless temperature - $T/(T_w - T_\infty)$	-
$U^*$	Dimensionless velocity - $u/U_\infty$	-
$U^+$	Dimensionless velocity - $u/(\tau_0/\rho Ne)^{1/2}$	-
$V^*$	Dimensionless velocity - $v/U_\infty$	-
$W^*$	Dimensionless velocity - $w/U_\infty$	-
$y^+$	Dimensionless Distance - $y \rho Ne (\tau_0/\rho Ne)^{1/2} / \mu$	-
$\psi^*$	Dimensionless stream function - $\Psi/\xi$	-
$\nabla^2$	Differential operator, $\frac{\partial^2}{\partial x^2} + \frac{\partial^2}{\partial y^2} + \frac{\partial^2}{\partial z^2}$	-

## CHAPTER II

### REVIEW OF THE LITERATURE

A complete report of the literature in the heat transfer area relating both directly and indirectly to this problem is impossible because of the large number of volumes coming off the press each year. Because of this the author has selected those areas considered to be most applicable to this particular problem for review.

The derivation of those basic governing laws generally covered in most advanced heat transfer courses are not reproduced here. Instead the reader is referred to at least one reference for derivation and proof of these equations. These derivations are generally reproduced in numerous heat transfer texts that are not referenced in this report.

#### The Navier-Stokes Equations

Schlichting (36) shows the Navier-Stokes equations for steady compressible flow with constant viscosity to be:

continuity:

$$\frac{\partial(\rho u)}{\partial x} + \frac{\partial(\rho v)}{\partial y} + \frac{\partial(\rho w)}{\partial z} = 0$$

momentum:

$$\rho(u \frac{\partial u}{\partial x} + v \frac{\partial u}{\partial y} + w \frac{\partial u}{\partial z}) = -\frac{\partial P}{\partial x} + \rho \beta \theta g_x + \mu[\nabla^2 u + \frac{1}{3} \frac{\partial}{\partial x} \text{div} \vec{w}] + X \quad (3)$$

$$\rho(u \frac{\partial v}{\partial x} + v \frac{\partial v}{\partial y} + w \frac{\partial v}{\partial z}) = -\frac{\partial P}{\partial y} + \rho \beta \theta g_y + \mu[\nabla^2 v + \frac{\partial}{\partial y} \text{div} \vec{w}] + Y \quad (4)$$

$$\rho(u \frac{\partial w}{\partial x} + v \frac{\partial w}{\partial y} + w \frac{\partial w}{\partial z}) = -\frac{\partial P}{\partial z} + \rho \beta \theta g_z + \mu[\nabla^2 w + \frac{1}{3} \frac{\partial}{\partial z} \text{div} \vec{w}] + Z \quad (5)$$

where:

$$\nabla^2 = \frac{\partial^2}{\partial x^2} + \frac{\partial^2}{\partial y^2} + \frac{\partial^2}{\partial z^2}$$

$$\text{div} \vec{w} = \frac{\partial w}{\partial x} + \frac{\partial w}{\partial y} + \frac{\partial w}{\partial z}$$

These equations with the energy equation are used to solve for the temperature distribution in a viscous fluid. The energy equation with constant fluid properties becomes

$$\rho C_p (u \frac{\partial T}{\partial x} + v \frac{\partial T}{\partial y} + w \frac{\partial T}{\partial z}) = k(\frac{\partial^2 T}{\partial x^2} + \frac{\partial^2 T}{\partial y^2} + \frac{\partial^2 T}{\partial z^2}) + u \frac{\partial P}{\partial x} + v \frac{\partial P}{\partial y} + w \frac{\partial P}{\partial z} + \mu \phi \quad (6)$$

where:

$\phi$  = viscous dissipation function

$$\begin{aligned} \phi = & 2[(\frac{\partial u}{\partial x})^2 + (\frac{\partial v}{\partial y})^2 + (\frac{\partial w}{\partial z})^2] + (\frac{\partial v}{\partial x} + \frac{\partial u}{\partial y})^2 + (\frac{\partial w}{\partial y} + \frac{\partial v}{\partial z})^2 \\ & + (\frac{\partial u}{\partial z} + \frac{\partial w}{\partial x})^2 - \frac{2}{3}(\frac{\partial u}{\partial x} + \frac{\partial v}{\partial y} + \frac{\partial w}{\partial z})^2 \end{aligned}$$

The equation of state for a perfect gas may be written as:

$$P = \rho RT \quad (7)$$

These six equations, eqns. 2 to 7, form a system of six simultaneous equations for the six variables:  $u$ ,  $v$ ,  $w$ ,  $P$ ,  $\rho$ , and  $T$  for the general case of a compressible medium.

By introducing non-dimensional variables into this set of governing differential equations, we will determine the dimensionless groups on which the solutions must depend. Denoting these non-dimensional variables with  $*$ , they are

$$\begin{aligned} u^* &= \frac{u}{U_\infty} \\ v^* &= \frac{v}{U_\infty} \\ w^* &= \frac{w}{U_\infty} \\ P^* &= \frac{P}{\rho U_\infty^2} \\ T^* &= \frac{T}{\Delta T_0} = \frac{T}{T_w - T_\infty} \end{aligned} \quad (8)$$

Introducing these variables into eqns. 3 and 4 we obtain for the two-dimensional equation of motion in the  $x$ -direction and the two-dimensional energy equation as follows:

$$u^* \frac{\partial u^*}{\partial x^*} + v^* \frac{\partial u^*}{\partial y^*} = -\frac{\partial P^*}{\partial x^*} + \frac{g\beta\theta l}{U_\infty^2} + \frac{\mu}{U_\infty^2 \ell \rho Ne} \left( \frac{\partial^2 u^*}{\partial x^{*2}} + \frac{\partial^2 u^*}{\partial y^{*2}} \right) \quad (9)$$

$$\begin{aligned} u^* \frac{\partial T^*}{\partial x^*} + v^* \frac{\partial T^*}{\partial y^*} &= \frac{kNe}{\rho C_p U_\infty \ell} \left( \frac{\partial^2 T^*}{\partial x^{*2}} + \frac{\partial^2 T^*}{\partial y^{*2}} \right) + \frac{U_\infty^2}{C_p (\Delta T_0)} \left( u^* \frac{\partial P^*}{\partial x^*} + v^* \frac{\partial P^*}{\partial y^*} \right) \\ &+ \frac{\mu U_\infty Ne}{\rho C_p \ell (\Delta T_0)} \Phi^* \end{aligned} \quad (10)$$

The dimensionless dissipation function is given by:

$$\phi^* = 2 \left[ \left( \frac{\partial u^*}{\partial x^*} \right)^2 + \left( \frac{\partial v^*}{\partial y^*} \right)^2 \right] + \left( \frac{\partial v^*}{\partial x^*} + \frac{\partial u^*}{\partial y^*} \right)^2 - \frac{2}{3} \left( \frac{\partial u^*}{\partial x^*} + \frac{\partial v^*}{\partial y^*} \right)^2$$

It is seen from these equations that the solution depends only on the following five dimensionless groups:

$$\frac{\mu}{U_\infty \rho \ell \text{Ne}}; \frac{g \beta \theta \ell}{U_\infty^2}; \frac{k \text{Ne}}{C_p U_\infty \ell}; \frac{U_\infty^2 \text{Ne}}{C_p (\Delta T_o)}; \frac{\mu U_\infty \text{Ne}}{\rho C_p \ell (\Delta T_o)}$$

The first group will be recognized as the reciprocal of the Reynolds Number.

$$\text{Re} = \frac{U_\infty \ell \rho \text{Ne}}{\mu}$$

The second dimensionless group will be recognized as the ratio of the Grashof Number to the Reynolds Number squared, or:

$$\frac{g \beta \theta \ell}{U_\infty^2} = \frac{\text{Gr}}{\text{Re}^2}$$

where:

$$\text{Gr} = \frac{\beta \theta \ell^3 \rho^2 \text{Ne}^2}{\mu}$$

The third group can be written as:

$$\frac{k \text{Ne}}{C_p U_\infty \ell} = \frac{k \rho \text{Ne}}{C_p \rho \mu} \cdot \frac{\mu}{U_\infty \ell \text{Ne}} = \frac{1}{\text{PrRe}}$$

where:

$$\text{Pr} = \text{Prandtl Number} = \frac{\mu C_p}{k \text{Ne}}$$

The fourth and fifth dimensionless groups are not independent because multiplying the fifth group by the Reynolds Number will yield the fourth dimensionless group. The fourth dimensionless group then gives the Eckert Number.

$$Ek = \frac{U_{\infty}^2 Ne}{C_p (\Delta T_o)}$$

The Eckert Number is a measure of the temperature increase caused by adiabatic compression. Schlichting (36) uses the equation of state for a perfect gas to show that the work of compression, i.e., the Eckert Number, becomes important only when the free-stream velocity approaches the speed of sound.

This dimensional analysis leads to the conclusion that the dimensionless velocity and dimensionless temperature fields for the governing system of equations depend upon the following four dimensionless groups:

$$\text{Reynolds Number: } Re = \frac{U_{\infty} \rho Ne}{\mu}$$

$$\text{Prandtl Number: } Pr = \frac{\mu C_p}{k Ne}$$

$$\text{Grashof Number: } Gr = \frac{g \beta \theta l^3 \rho^2 Ne^2}{\mu^2}$$

$$\text{Eckert Number: } Ek = \frac{U_{\infty}^2 Ne}{C_p (\Delta T_o)}$$

In practical engineering heat transfer problems, however, we are generally interested in determining the heat energy transfer from a body to the fluid field. The velocity and temperature fields generally are of interest only in so much



as they aid in finding the heat transferred. This problem is generally solved by introducing the heat transfer coefficient,  $h$ , which may be defined either as a local or as an average heat transfer value. This heat transfer coefficient is defined by Newton's Law of Cooling as:

$$q = h A_s (T_w - T_\infty) \quad (11)$$

where:

$q$  = rate of heat energy transferred in Btu/hr.

$A_s$  = surface area in ft.<sup>2</sup>

$T_w$  = wall temperature, °F.

$T_\infty$  = fluid temperature, °F.

This defines  $h$  as the heat transferred per unit time per unit area per unit temperature change or Btu/(hrft<sup>2</sup>°F).

Energy is transferred entirely by conduction at the boundary between the body and fluid. Therefore, by Fourier's heat conduction law:

$$q = -k A_s \left( \frac{\partial T}{\partial n} \right)_{n=0} \quad (12)$$

Equating these two expressions we obtain a dimensionless heat transfer coefficient known as the Nusselt Number. This becomes

$$\text{Nusselt Number} = Nu = \frac{h \ell}{k} = - \left( \frac{\partial T^*}{\partial n^*} \right)_{n^*=0} = - \frac{\ell}{(\Delta T_o)} \left( \frac{\partial T}{\partial n} \right)_{n=0} \quad (13)$$

The heat transfer problem then becomes one of determining the heat transfer coefficient since:

$$q = \frac{k}{l} \text{Nu} (T_w - T_\infty) \quad (14)$$

The preceding discussion leads to the conclusion that

$$\text{Nu} = f_2(\text{Re}, \text{Pr}, \text{Gr}, \text{Ek}) \quad (15)$$

for geometrically similar surfaces.

For flows where the temperature differences are not large the buoyancy forces are generally very small compared to the viscous forces and may be neglected. Parker (30) states that as a rule if

$$\frac{\text{Gr}}{(\text{Re})^2} \ll 1$$

the buoyancy forces may be neglected. This gives what is normally called forced convection.

For flow conditions where the fluid velocities are much less than the speed of sound, the Eckert Number becomes very small and can be neglected.

Under these limiting conditions then

$$\text{Nu} = f_3(\text{Re}, \text{Pr}) \quad (16)$$

#### Boundary Layer Simplifications

For all except the most simple geometries, a complete viscous fluid solution for flow about a body poses considerable mathematical difficulty. Prandtl (34) made an

important contribution when, in 1904, he discovered that the influence of viscosity is confined to an extremely thin region very close to the body. The remainder of the flow field can be closely approximated by considering it an inviscid fluid. The region over which the viscosity has considerable influence is called the velocity boundary layer,  $\delta_s$ .

Since the boundary layer is very thin in comparison to the dimensions of the body, the Navier-Stokes equations become simplified so that the analysis for a number of shapes are relatively simple. One fundamental assumption (19) of the boundary layer approximation is that the fluid immediately adjacent to the body surface is at rest relative to the body. This assumption appears valid except for very low pressures where the mean free path of molecules become large relative to the body dimensions. Therefore, the velocity boundary layer may be defined as the region where the velocity changes from zero at the surface to its free-stream value,  $U_\infty$ . Since the velocity in the boundary layer approaches the free-stream velocity asymptotically, the outer edge of the velocity boundary layer is usually considered to be where  $u = 0.99 U_\infty$  (30).

Considering a two-dimensional boundary layer for simplicity, Kays (19) shows that the assumption of the boundary layer approximation requires the following conditions to exist in the boundary layer.

$$u \gg v$$

$$\frac{\partial u}{\partial y} \gg \frac{\partial u}{\partial x}, \frac{\partial v}{\partial x}, \frac{\partial v}{\partial y} \quad (17)$$

$$\frac{\partial P}{\partial y} \approx 0$$

$$\frac{\partial P}{\partial x} \approx \frac{dP}{dx}$$

Introducing these approximations into the continuity equation, eqn. 2, and the Navier-Stokes equations 3 and 4, for two-dimensional, steady, compressible fluid flow with constant fluid properties, we obtain the following simplified equations of motion.

$$\frac{\partial(\rho u)}{\partial x} + \frac{\partial(\rho v)}{\partial y} = 0 \quad (18)$$

$$\left(u \frac{\partial u}{\partial x} + v \frac{\partial u}{\partial y}\right) = \frac{\partial^2 u}{\partial y^2} - \frac{dP}{dx} + \rho \beta (T - T_\infty) \quad (19)$$

Schlichting (36) estimates that the thickness of the laminar velocity boundary layer is:

$$\begin{aligned} \frac{\delta_s}{L} &\approx \frac{1}{(\text{Re})^{1/2}} \\ &= \frac{C}{(\text{Re})^{1/2}} \end{aligned}$$

where the constant, C, depends on the geometry of the body.

When a body is placed in a fluid field so that the temperature of the body is different from that for the fluid field, the temperature field around the body will generally be of the boundary layer type (36)(19). This

essentially means that the fluid temperature will change from the free-stream temperature some distance from the body to the body temperature at the body boundary. The distance over which this occurs being called the thermal boundary layer,  $\delta_T$ . Eckert (7) shows that the relationship between the velocity boundary layer and thermal boundary layer is

$$\frac{\delta_T}{\delta_S} = \frac{1}{(Pr)^{1/3}} \quad (21)$$

This indicates for gases where the Prandtl Number is approximately unity that the thermal boundary layer is of the same magnitude as the velocity boundary layer.

The thermal boundary layer approximation infers that

$$\frac{\partial T}{\partial y} \gg \frac{\partial T}{\partial x} \quad (22)$$

Applying this approximation into equation 6 and limiting to the two-dimension case yields the energy equation for the boundary layer.

$$\rho C_p \left( u \frac{\partial T}{\partial x} + v \frac{\partial T}{\partial y} \right) = k \frac{\partial^2 T}{\partial y^2} + \mu \left( \frac{\partial u}{\partial y} \right)^2 + u \frac{dP}{dx} \quad (23)$$

The equation of state for the boundary layer is unchanged.

$$P = \rho RT \quad (7)$$

In boundary layer theory the pressure is considered to be known from an inviscid flow solution. We then have a system of four simultaneous equations to solve for the

four unknowns  $\rho$ ,  $u$ ,  $v$ , and  $T$ . For the incompressible case where  $\rho=C$  the equation of state is no longer needed to effect a solution.

These boundary layer approximations have reduced the set of governing differential equations to a form that can be simply solved to give the flow patterns and temperature distributions around a number of bodies. As shown by equation 14 this will allow a means for predicting the heat transfer from the surface of these bodies. Although no attempt will be made to develop these solutions here, several of the results will be presented in the following section.

#### Solutions for the Temperature Distributions in Viscous Flow

Equations 2 to 7 may be solved for several geometries to yield the temperature distribution in the fluid field in the neighborhood of a body of different temperature. A few restricted examples exist whereby an exact solution is available. Still other problems can be solved by invoking the boundary layer approximations discussed in the previous section. A review, without detailed solutions, of several of these problems are presented here.

The Fourier law, equation 12, and Newton's law of cooling, equation 11, enables us to use the temperature distribution in the fluid to predict the heat transferred from the body to the fluid.

The following two examples of Couette and Poiseuille flow are examples of exact solutions to equations 2 to 7. These systems are restricted to the case of incompressible two-dimensional steady flow along a horizontal x, y-plane with constant fluid properties. Boundary layer approximations are not needed in these solutions.

With these restrictions equations 2 to 7 reduce to

$$\frac{\partial u}{\partial x} + \frac{\partial v}{\partial y} = 0 \quad (24)$$

$$\rho \left( u \frac{\partial u}{\partial x} + v \frac{\partial v}{\partial y} \right) = -\frac{\partial P}{\partial y} + \left( \frac{\partial^2 u}{\partial x^2} + \frac{\partial^2 u}{\partial y^2} \right) \quad (25)$$

$$\rho \left( u \frac{\partial v}{\partial x} + v \frac{\partial v}{\partial y} \right) = -\frac{\partial P}{\partial x} + \left( \frac{\partial^2 v}{\partial x^2} + \frac{\partial^2 v}{\partial y^2} \right) \quad (26)$$

$$\rho C_P \left( u \frac{\partial T}{\partial x} + v \frac{\partial T}{\partial y} \right) = k \left( \frac{\partial^2 T}{\partial x^2} + \frac{\partial^2 T}{\partial y^2} \right) + \mu \phi \quad (27)$$

where:

$$\phi = 2 \left[ \left( \frac{\partial u}{\partial x} \right)^2 + \left( \frac{\partial v}{\partial y} \right)^2 \right] + \left( \frac{\partial v}{\partial x} + \frac{\partial u}{\partial y} \right)^2$$

### Couette Flow (36)

Flow between two parallel flat plates of which one is at rest, the other moving with a constant velocity  $U_1$  in its own plane is called couette flow and is shown in Figure 1. The solution of the continuity and momentum equations in the absence of a pressure gradient in the x-direction is

$$u(y) = U_1 \left( \frac{y}{L} \right) ; \quad v = 0 ; \quad P = \text{const} \quad (28)$$

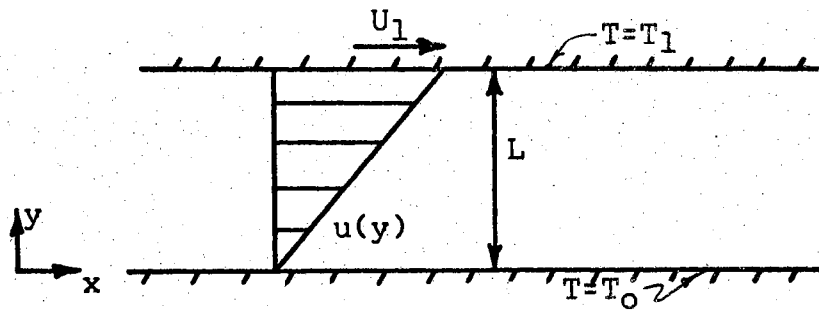


Figure 1. Velocity Distribution in Couette Flow

If the temperature of the wall is held constant, a simple solution is available for the temperature distribution. The boundary conditions become

$$y = 0 : T = T_0$$

$$y = L : T = T_1$$

with these restrictions the viscous dissipation function reduces to

$$\phi = \left( \frac{\partial u}{\partial y} \right)^2$$

and the energy equation then becomes

$$\rho C_p \left( u \frac{\partial T}{\partial x} + v \frac{\partial T}{\partial y} \right) = k \left( \frac{\partial^2 T}{\partial y^2} \right) + \mu \left( \frac{\partial u}{\partial y} \right)^2 \quad (29)$$

The solution to this equation which satisfied the boundary conditions is

$$\frac{T - T_0}{T_1 - T_0} = \frac{y}{L} + \frac{\mu U_1^2}{2k(T_1 - T_0)} \frac{y}{L} \left( 1 - \frac{y}{L} \right) \quad (30)$$



but

$$(\text{Pr})\text{Ek} = \frac{\mu U_1^2}{k(T_1 - T_0)}$$

therefore

$$\frac{T_1 - T_0}{T_1 - T_0} = \frac{y}{L} + \frac{1}{2} \text{Pr} \cdot \text{Ek} \frac{y}{L} \left(1 - \frac{y}{L}\right) \quad (31)$$

In the case when the two walls in couette flow have equal temperatures ( $T_1 = T_0$ ) equation 30 leads to a simple parabolic temperature distribution which is symmetrical with respect to the centerline between the walls. The solution gives the temperature rise due to frictional energy and is

$$T(y) - T_0 = \frac{\mu U_1^2}{2k} \frac{y}{L} \left(1 - \frac{y}{L}\right) \quad (32)$$

If one of the walls is made adiabatic so that all of the heat energy due to friction is transferred to the other wall, the boundary conditions become

$$y = h_1 \quad : \quad T = T_0$$

$$y = 0 \quad : \quad \frac{dT}{dy} = 0$$

The solution of equation 29 to satisfy these boundary conditions is

$$T(y) - T_0 = \frac{\mu U_1^2}{2k} \left(1 - \frac{y}{L}\right) \quad (33)$$

DeGroff (5) modified the solution for the Couette flow problem so that the viscosity of the fluid is a function of temperature.

### Poiseuille Flow Through a Channel With Flat Walls

Another exact solution to the above equations for temperature distributions is the two-dimensional flow through a channel with parallel flat walls. Kays (19), Schlichting (36) and others show the velocity distribution for Poiseuille flow to be parabolic:

$$u(y) = u_{\max} \left(1 - \frac{y^2}{L^2}\right) \quad (34)$$

Assuming constant and equal wall temperatures, the boundary conditions are

$$y = \pm h_1 : T = T_0$$

where  $y = 0$  is the centerline between the plates.

For these conditions equation 29 reduces to

$$k \frac{d^2 T}{dy^2} = -\frac{4\mu u_{\max}^2}{L^4} y^2 \quad (35)$$

whose solution is

$$T(y) - T_0 = \frac{1}{3} \frac{\mu u_{\max}^2}{k} \left[1 - \left(\frac{y}{L}\right)^4\right] \quad (36)$$

Hausenblas (17) modified the solution for the Poiseuille flow problem to include the case of temperature

dependent viscosity. A similar solution to the problem for a circular pipe has been given by Grigull (16).

Parallel Flow Past Flat Plate-Blasius Solution (28)(36)

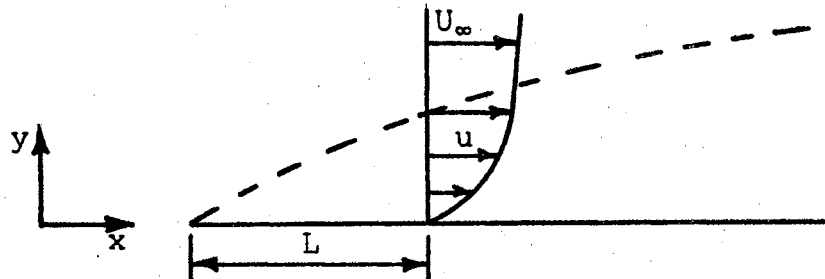


Figure 2. Hydrodynamic Boundary Layer Formation

The boundary layer equations for this case assuming incompressible flow with constant fluid properties and assuming that buoyancy forces and  $dP/dx$  are equal to zero are

$$\frac{\partial u}{\partial x} + \frac{\partial v}{\partial y} = 0$$

$$\rho \left( u \frac{\partial u}{\partial x} + v \frac{\partial u}{\partial y} \right) = \mu \frac{\partial^2 u}{\partial y^2} \quad (37)$$

$$\rho C_p \left( u \frac{\partial T}{\partial x} + v \frac{\partial T}{\partial y} \right) = k \frac{\partial^2 T}{\partial y^2} + \mu \left( \frac{\partial u}{\partial y} \right)^2 \quad (38)$$

The boundary conditions are

$$u = v = 0 \text{ at } y = 0$$

$$u = U_\infty \text{ at } y = \infty$$

$$T = T_w \text{ at } y = 0$$

$$\frac{\partial T}{\partial y} = 0 \text{ at } y = 0$$

$$T = T_\infty \text{ at } y = \infty$$

Since the velocity field is independent of the temperature field, the two flow equations above can be solved first and the results used to determine the temperature field.

Blasius (3) introduced similarity variables for the solution of the flow equations as follows:

$$\eta = y (U_{\infty}/\nu x)^{1/2} \quad (39)$$

$$\psi = (\nu x U_{\infty})^{1/2} f(\eta) \quad (40)$$

where  $\psi$  is the stream function defined by

$$u = \frac{\partial \psi}{\partial y} \text{ and } v = -\frac{\partial \psi}{\partial x} \quad (41)$$

Let

$$u^* = \frac{u}{U_{\infty}} + \frac{1}{U_{\infty}} \frac{\partial \psi}{\partial y} + \frac{\xi}{U_{\infty}} \frac{\partial \eta}{\partial y} \frac{d\psi^*}{d\eta} \quad (42)$$

where

$$\psi^* = \frac{\psi}{\xi} \quad (43)$$

therefore

$$u^* = \frac{\xi}{U_{\infty}} \left( \frac{U_{\infty}}{\nu x} \right)^{1/2} \frac{d\psi^*}{d\eta} \quad (44)$$

Let

$$\xi = (\nu x U_{\infty})^{1/2} \quad (45)$$

then

$$\psi^* = (\nu x U_\infty)^{1/2} \psi = f(\eta) \quad (46)$$

and

$$u = U_\infty f'(\eta) \quad (47)$$

Transforming the momentum equation, equation 37, yields

$$f''' + \frac{1}{2}ff'' = 0 \quad (48)$$

The boundary conditions transform to yield

$$f = f' = 0 \text{ at } \eta = 0$$

$$f' = 1 \text{ at } \eta = \infty$$

The general solution of this third order non-linear differential equation is not available in closed form. The solution is available in tabular form on page 121, Table 7.1 in Schlichting (36).

If the heat of friction ( $\mu \frac{\partial^2 u}{\partial y^2}$ ) is neglected the energy equation becomes

$$\rho C_p (u \frac{\partial T}{\partial x} + v \frac{\partial T}{\partial y}) = Nek \frac{\partial^2 T}{\partial y^2} \quad (49)$$

The energy and momentum equations are identical if we replace  $u$  by  $T$  and restrict

$$\frac{\mu}{\rho} = \frac{kNe}{C_p \rho} \text{ or } \nu = \alpha$$

therefore

$$Pr = \frac{\nu}{\alpha} = 1$$

It follows that for the flat plate described above for the Prandtl Number equal to unity that

$$\frac{T - T_w}{T_\infty - T_w} = \frac{u}{U_\infty}$$

is the solution to the energy equation by analogy.

The preceding solution suggests a similarity solution for the general case as outlined for the flow field. If we assume  $T = T(\eta)$  as defined previously, the partial differential energy equation reduces to the following total differential equation.

$$\frac{d^2 T}{d\eta^2} + \frac{\text{Pr}}{2} f \frac{dT}{d\eta} = -P \frac{U_\infty^2 \text{Ne}}{C_p} f''^2 \quad (50)$$

The solution to this equation can be represented by the superposition of two solutions of the form (36):

$$T(\eta) - T_\infty = (T_w - T_\infty) \theta_1(\eta) + \frac{U_\infty^2 \text{Ne}}{2 C_p} \theta_2(\eta) \quad (51)$$

where

$$\theta = \frac{T(\eta) - T_\infty}{T_w - T_\infty}$$

$\theta_1(\eta)$  denotes the general solution of the homogeneous equation while  $\theta_2(\eta)$  denotes a particular solution of the non-homogeneous equation. It is convenient to choose the boundary conditions for  $\theta_1(\eta)$  and  $\theta_2(\eta)$  such that  $\theta_1$  is the solution of a cooling problem with a given temperature

difference between the wall and the external stream and  $\theta_2$  is the solution for the adiabatic wall. The following equations must then be satisfied.

$$\theta'' + \frac{1}{2}Prf\theta' = 0 \quad (52)$$

$$\theta_1 = 1 \text{ at } \eta = 0$$

$$\theta_1 = 0 \text{ at } \eta = \infty$$

and

$$\theta_2'' + \frac{1}{2}Prf\theta_2' = -2Prf''^2 \quad (53)$$

$$\theta_2' = 0 \text{ at } \eta = 0$$

$$\theta_2 = 0 \text{ at } \eta = \infty$$

Polhausen (31) first solved the cooling problem. The following analysis is given in Kays (19).

$$\theta_1'' + \frac{1}{2}Prf\theta_1' = 0 \quad (54)$$

Integrating this equation twice and evaluating at the boundary conditions yields

$$\theta_1 = \frac{\int_0^\eta [\exp(-\frac{Pr}{2} \int_0^\eta f d\eta)] d\eta}{\int_0^\infty [\exp(-\frac{Pr}{2} \int_0^\eta f d\eta)] d\eta} \quad (55)$$

The Nusselt Number is defined as

$$Nu = \frac{hx}{k} = \frac{x}{(\nu x/U_\infty)^{1/2}} (\theta_1')_0 = (Re)^{1/2} (\theta_1')_0 \quad (56)$$

From the first integration it can be shown that

$$(\theta_1')_{\eta=0} = C_1 \quad (57)$$

therefore

$$\text{Nu} = C_1 (\text{Re})^{1/2} \quad (58)$$

Values for  $C_1$  can be calculated for moderate Prandtl Number ranges. Several values are tabulated in Table I.

TABLE I

VALUES OF  $C_1$  FOR VARIOUS PRANDTL NUMBERS FOR  
HEAT TRANSFER TO THE LAMINAR CONSTANT  
PROPERTY BOUNDARY LAYER

Pr	0.5	0.7	1.0	7.0	10.0	15.0
$C_1$	0.259	0.292	0.332	0.645	0.730	0.835

These results are closely approximated by (19):

$$\text{Nu} = 0.332 (\text{Pr})^{1/3} (\text{Re})^{1/2} \quad (59)$$

Temperature distributions are tabulated in graphical form for the cooling problem in Schlichting (36).

Eckert and Drake (7) provides the solution for the flat plate with an unheated starting length,  $x_1$ . A laminar incompressible boundary layer is assumed to develop with



no pressure gradient. Using the energy integral equation Kays assumed the velocity profile to be

$$\frac{u}{U_\infty} = \frac{3}{2}\left(\frac{y}{\delta_s}\right) - \frac{1}{2}\left(\frac{y}{\delta_s}\right)^3 \quad (60)$$

The terms are defined in Figure 3. The choice of the cubic parabola to approximate the velocity profile makes the second derivative zero at the wall. This condition is demanded by the differential equation of the boundary layer.

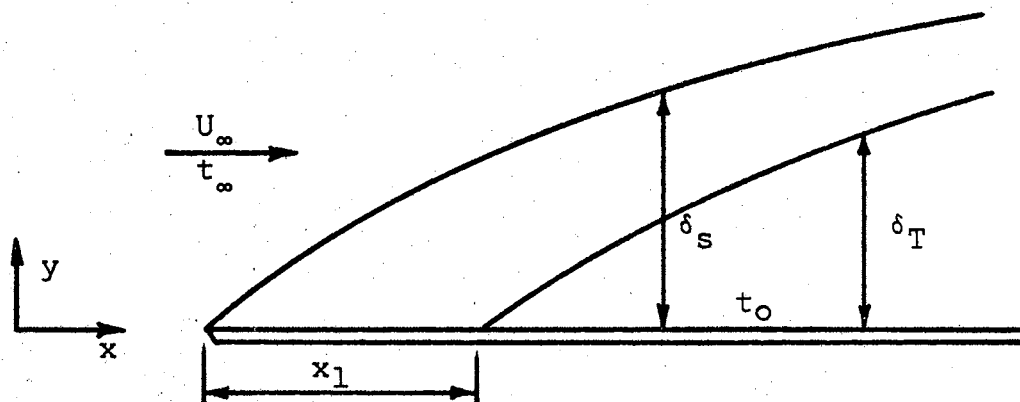


Figure 3. Velocity and Thermal Boundary Layer Formation

The differential energy equation also suggests that a cubic parabola will provide a satisfactory approximation for the temperature profile. Eckert approximated the temperature profile as

$$\frac{\theta}{\theta_0} = \frac{3}{2}\left(\frac{y}{\delta_T}\right) - \frac{1}{2}\left(\frac{y}{\delta_T}\right)^3 \quad (61)$$

where

$$\theta = T_{\infty} - T$$

$$\theta_0 = T_{\infty} - T_0$$

Eckert showed the ratio of the thermal boundary layer thickness to the hydrodynamic boundary layer thickness to be

$$\frac{\delta_T}{\delta_s} = (\text{Pr})^{-1/3} \left[ 1 - \left( \frac{x_1}{x} \right)^{3/4} \right]^{1/3} \quad (62)$$

The local Nusselt Number is derived to be

$$\text{Nu}_x = \frac{0.332 (\text{Pr})^{1/3} (\text{Re})^{1/2}}{\left[ 1 - \left( \frac{x_1}{x} \right)^{3/4} \right]^{1/3}} \quad (63)$$

### Thermal Boundary Layers Over Other Shapes-Theoretical Results

Froessling (12) carried out calculations on the temperature distribution in the laminar boundary layer about a body of arbitrary shape for two-dimensional axial symmetrical cases. He neglected frictional and compression work in his analysis.

Froessling assumed a power series for the potential velocity distribution around the body expanded in terms of the arc length,  $x$ , of the form.

$$U_{\infty} = u_1 x + u_3 x^3 + u_5 x^5 + \dots \quad (64)$$

The velocity distribution in the boundary layer is assumed to have the form

$$u(x,y) = u_1 x \phi_1(y) + u_3 x^3 \phi_2(y) + \dots \quad (65)$$

The corresponding assumption for the temperature distribution is of the form

$$T(x,y) = T_0 + x^2 T_2(y) + x^4 T_4(y) \quad (66)$$

Froessling's results for the local rate of heat transfer around a circular cylinder is shown in Figure 4 for the region covered with a laminar boundary layer.

Squire (41) used the energy integral equation

$$\frac{d}{dx} \int_0^{\infty} [u(T-T_{\infty})] dy = -\delta_s \left( \frac{\partial T}{\partial y} \right)_y = 0 \quad (67)$$

To outline a solution based on numerical techniques for the heat flux from a body of arbitrary shape with a laminar boundary layer.

Kays (19) used the Mangler transformation with the wedge flow solution to show that the Nusselt Number based on the radius for the two-dimensional stagnation point is:

$$Nu_R = 0.81 (Re_R)^{1/2} (Pr)^{0.4} \quad (68)$$

and for the axisymmetric stagnation point is

$$Nu_R = 0.93 (Re_R)^{1/2} (Pr)^{0.4} \quad (69)$$

#### Turbulent Heat Transfer-External Boundary Layer

Turbulent flow theory is still in an unsatisfactory state because of the complexity of the fluid motion. The

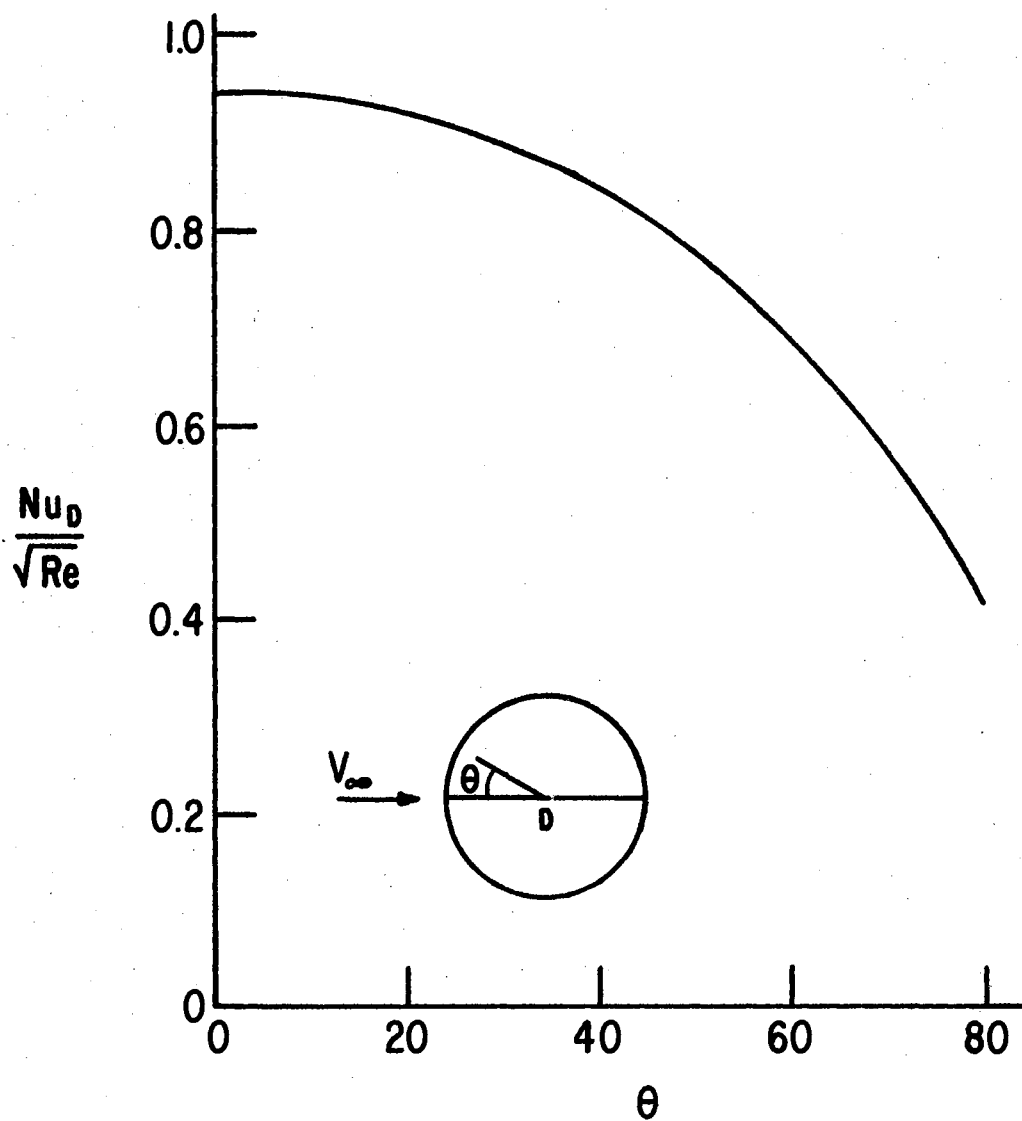


Figure 4. Variation of the local Nusselt Number around a right circular cylinder. From Froessling (12)

fluid motion is normally viewed statistically with no attempt to follow the motion of the individual fluid particles. This normally requires a dependence upon experimental observations and correlations for predicting heat and mass transfer under these conditions.

Kays (19) described the turbulent flow phenomena qualitatively as follows. In a turbulent flow process there appears to be a region very close to the wall where the fluid motion is predominately laminar. The velocity gradient in this region is very large. This region is generally referred to as the laminar sub-layer. Farther away from the wall the flow becomes unsteady until a region is reached where the entire flow is involved in turbulent motion. This region is called the turbulent region. The transition region between the laminar sub-layer and the turbulent region is known as the buffer zone and exhibits momentum transport characteristics of both the laminar sub-layer and the turbulent region. Experimental studies have shown that even the laminar region is not stable. Periodically and unpredictably large elements of relatively low velocity fluid lifts off the surface and enters the turbulent region of flow. Obviously a fluid with a velocity higher than that existing in the laminar sub-layer must move into the laminar region to replace this fluid element. The

mechanism for this phenomenon is not fully understood but it is thought to be the result of an instability in the laminar region (19).

A dimensional analysis of the velocity profile near the wall leads to

$$u = f_4(y, \tau_0, \rho, \mu, Ne) \quad (70)$$

This relationship can be reduced to two independent and dimensionless groups through Buckingham's Pi theorem.

$$\pi_1 = u^+ = \frac{u}{(\tau_0/\rho Ne)^{1/2}}$$

$$\pi_2 = y^+ = \frac{Ne y \rho (\tau_0/\rho Ne)^{1/2}}{\mu}$$

Therefore

$$u^+ = f_5(y^+) \quad (71)$$

Martinelli (24) described the turbulent velocity behavior near the wall in three separate algebraic equations. These equations commonly referred to as the "law of the wall" are

$$\begin{aligned} u^+ &= y^+ & y^+ &< 5 \\ u^+ &= -3.05 + 5.0 \ln y^+ & 5 &< y^+ < 30 \\ u^+ &= 5.5 + 2.5 \ln y^+ & 30 &< y^+ \end{aligned} \quad (72)$$

A number of investigators have solved the problem for heat transfer from a flat plate with a turbulent boundary layer. Consider the case of the infinite flat plate with constant property fluids, low velocity flow and negligible flow. The energy equation of the boundary layer reduces to

$$\frac{\partial}{\partial y} \left[ \left( \frac{k}{C_p \rho} \right) \frac{\partial T}{\partial y} \right] = u \frac{\partial T}{\partial x} + v \frac{\partial T}{\partial y} \quad (73)$$

In turbulent energy exchange the energy transport is due to turbulent diffusivity as well as molecular diffusivity. Replacing the thermal diffusivity  $k/C_p \rho$  with a total turbulent diffusivity  $(\alpha + \epsilon_H)$  we have

$$\frac{\partial}{\partial y} \left[ (\alpha + \epsilon_H) \frac{\partial T}{\partial y} \right] = u \frac{\partial T}{\partial x} + v \frac{\partial T}{\partial y} \quad (74)$$

The appropriate boundary conditions are

$$T = T_0 \text{ at } y = 0$$

$$T = T_\infty \text{ at } y = \infty$$

$$T = T_\infty \text{ at } x = 0$$

Employing the Reynolds analogy for the region  $y^+ < 30$  and recognizing that this region corresponds to only a small part of the boundary layer thickness we can solve this problem. The shear stress will be essentially constant throughout these layers and approximately equal to the shear stress at the wall,  $\tau_0$ . The energy equation reduces to

$$\frac{\partial}{\partial y}[(\alpha + \epsilon_H) \frac{\partial T}{\partial y}] = 0 \quad (75)$$

Since  $v = 0$  and  $\frac{\partial T}{\partial y} = 0$

Kays (19) solves this problem to give

$$T_\ell - T_o = 5 \left( \frac{\dot{q}_o''}{C_p \rho} \right) \frac{Pr}{(\tau_o / \rho Ne)^{1/2}} \quad (76)$$

$$T_b - T_\ell = 5 \left( \frac{\dot{q}_o''}{C_p} \right) \frac{(5 Pr + 1)}{(\tau_o / \rho Ne)^{1/2}} \quad (77)$$

where

$T_o$ ,  $T_\ell$  and  $T_b$  are defined in Figure 5.

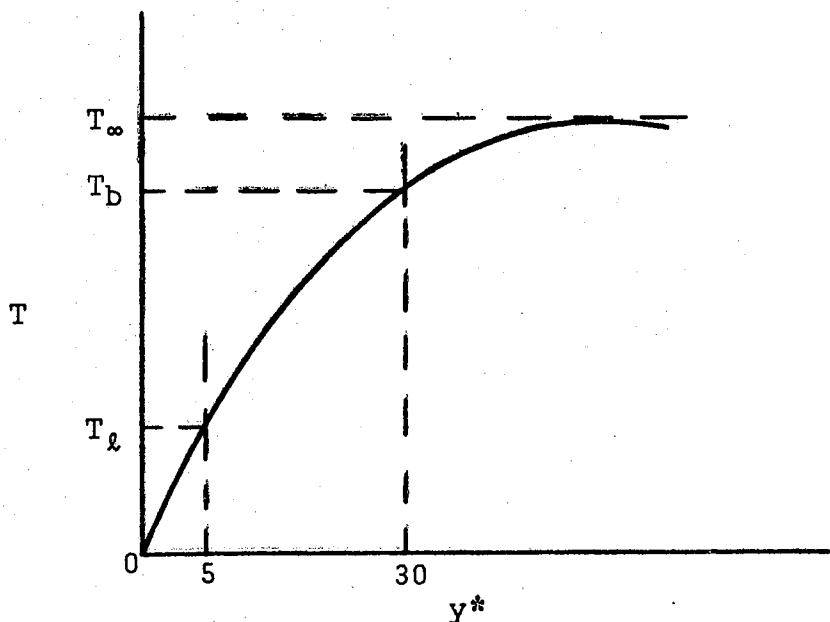


Figure 5. Expected Temperature Distribution for a Fully Developed Turbulent Flow

For moderate Prandtl Numbers the eddy diffusivities are much larger than the molecular diffusivities and the molecular diffusivities can be neglected in the momentum



and energy differential equations. If the Reynold's analogy is again invoked the equations can be solved to give

$$T_{\infty} - T_b = \left( \frac{\dot{q}_o''}{C_p \rho} \right) \frac{1}{(\tau_o / \rho Ne)^{1/2}} - \frac{U_{\infty}}{(\tau_o / \rho Ne)^{1/2}} - 14 \quad (78)$$

summing equations 76, 77, and 78 gives

$$T_{\infty} - T_o = \left( \frac{\dot{q}_o''}{C_p \rho} \right) \left( \frac{Ne \rho}{\tau_o} \right)^{1/2} [5Pr + 5 \ln(5Pr + 1) + \frac{U_{\infty}}{(\tau_o / \rho Ne)^{1/2}} - 14] \quad (79)$$

Defining the local friction factor, the local convective heat transfer coefficient and the Stanton Number as

$$\frac{\tau_o}{\rho} = f_x \frac{U_{\infty} Ne}{2} \quad (80)$$

$$\dot{q}_o'' = h_x (T_o - T_{\infty}) \quad (81)$$

$$St_x = \frac{h_x}{C_p \rho U_{\infty}} \quad (82)$$

and combining with equation 86 gives

$$St_x = \frac{(f_x/2)^{1/2}}{[5Pr + 5 \ln(5Pr + 1) + \frac{1}{(f_x/2)^{1/2}} - 14]} \quad (83)$$

The local friction factor has been derived as (19):

$$f_x = 0.059 (Re_x)^{-0.2}$$

Substituting into equation 83 gives

$$St_x = \frac{h_x}{C_p \rho V_\infty} = \frac{0.0295 (Re_x)^{-0.2}}{1 + 0.172 (Re_x)^{-0.1} [5Pr + 5 \ln(5Pr + 1) - 14]} \quad (84)$$

As Kays points out this result is not valid for extremely low or extremely high Prandtl Numbers. Based on experimental observations he suggested limiting the results to the Prandtl Number range 0.5 to 10.

For the same problem Reynolds (35) noted the similarity between heat and momentum transfer and derived an expression for the heat transfer from a flat plate with  $Pr = 1$  as

$$Nu_x = 0.0296 (Re_x) \quad (85)$$

Prandtl (33), Taylor (42), Von Karman (46) and others have also extended the Reynolds analogy to cases where the Prandtl Number is not equal to unity. Their results yield for the flat plate with a turbulent boundary layer

$$Nu_x = 0.0296 (Pr)^{1/3} (Re)^{0.8} \quad (86)$$

A number of other approximate solutions are available for varying boundary conditions. Some examples are provided in detail in Schlichting (36), Kays (19), Pappas (29), Seiff (39), and Van Driest (44). Generally these solutions require experimental observations for validation.

## Flow Over Bodies of Arbitrary Shape

The hydrodynamic and thermal boundary layers on blunt bodies of arbitrary shape are not as easily described analytically as those discussed previously for well defined geometries. Under a number of conditions the velocity gradient at the body surface can decrease to zero so that the entire boundary layer separates from the surface leaving a region of reversed flow near the wall. Separation generally occurs anywhere there is an abrupt step in the surface and often occurs on smooth continuous surfaces. There is no general theory for calculating heat transfer to the fluid in the region of separation, primarily because this flow regime has not been extensively studied (19).

Because of the lack of a general theory researchers have resorted to experimental correlations when design data was needed for some specific shape.

Giedt (13) (14), Zapp (47) and others (37), (43), (45), have measured the local heat transfer coefficient on the surface of blunt bodies. Figure 6 is typical results from the work of Giedt on the flow around a cylinder placed normal to an air-stream.

The curve for the Reynolds Number equal to 99,300 is typical of the body where a laminar boundary layer develops without a transition to turbulence. The local Nusselt Number decreases from the value at the stagnation point

until it reaches the minimum value at the point of laminar boundary layer separation (about 80 degrees F). As the turbulent wake begins, the Nusselt Number begins to increase and may reach a value higher than those existing at the stagnation point on the front part of the cylinder.

The curves for Reynolds Numbers equal to 167,500 and 213,000 are rather typical of the case where the laminar boundary layer changes to a turbulent boundary layer before separation occurs. The local Nusselt Number decreases from the value at the stagnation point until transition to the turbulent boundary layer occurs at approximately 90 degrees. Due to the turbulence the local Nusselt Number rapidly increases to another maximum and then decreases again as the turbulent boundary layer thickness increases. Separation of the turbulent boundary layer occurs about 140 degrees from the stagnation point and the local Nusselt Number again increases in the wake.

The average Nusselt Number may be obtained by integrating the local Nusselt Number over the surface. A more typical approach is to develop an experimental correlation based on dimensional analysis. This analysis will yield

$$Nu = f_3(Re, Pr)$$

for each specified geometric shape. Experimental evidence indicates that the component equations combine as straight lines in log-log space. Therefore the general prediction equation will take the form

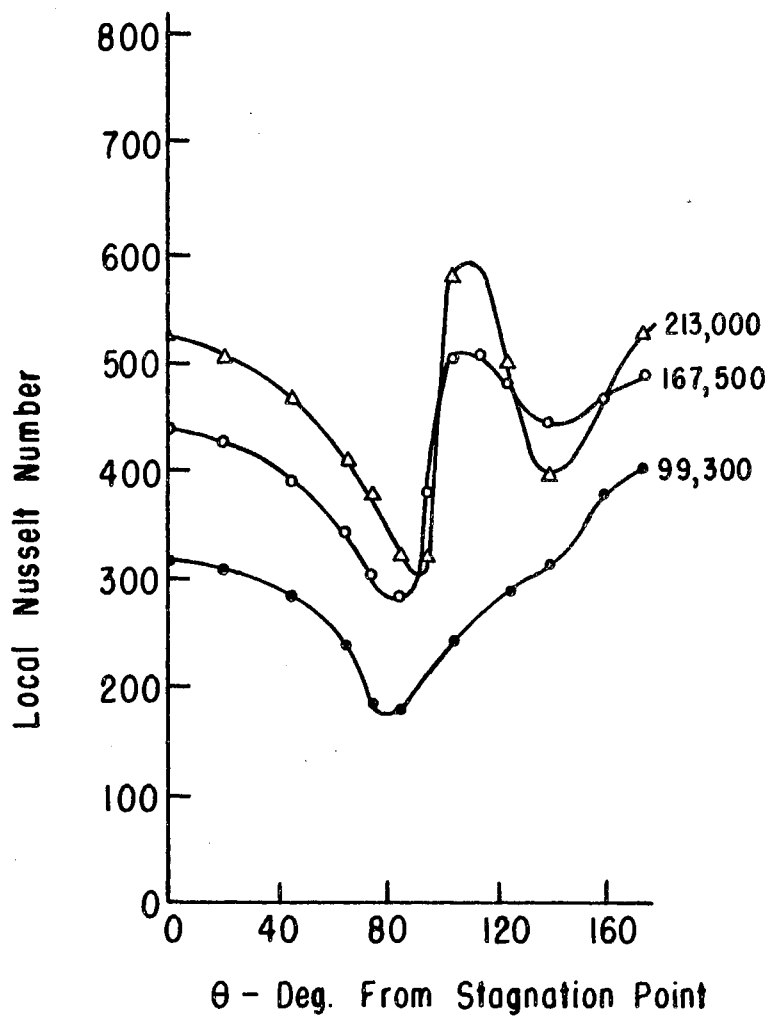


Figure 6. Local heat transfer around a cylinder for different Reynolds Numbers. From Giedt (13).

$$\text{Nu} = C_1 (\text{Re})^d (\text{Pr})^e \quad (87)$$

where  $C_1$ ,  $d$ , and  $e$  are all constants for a specified shape. Correlations are normally developed for gases and the Prandtl Number is considered to be constant for all gases. This is not a bad assumption since the Prandtl Number for most gases fall within 10% of the value for air. The above correlation then reduces to

$$\text{Nu} = C_2 (\text{Re})^d \quad (88)$$

where

$$C_2 = C_1 (\text{Pr})^e$$

A number of investigators (13), (14), (43), (45), used this procedure to estimate the average Nusselt Numbers from infinite right circular cylinders. One of the most commonly used is due to Hilpert (18)

$$\text{Nu} = 0.174(\text{Re})^{0.618} \quad 4000 \leq \text{Re} \leq 40,000 \quad (89)$$

$$\text{Nu} = 0.0239(\text{Re})^{0.805} \quad 40,000 \leq \text{Re} \leq 250,000 \quad (90)$$

For the sphere McAdams (25) recommended that the average convective heat transfer coefficient may be predicted over the Reynolds Number range from about 25 to 100,000 by

$$\text{Nu} = 0.37(\text{Re})^{0.6} \quad (91)$$

Hilpert (18) measured the heat transfer coefficient from several cylinders with different cross-sections to an

air flow normal to their axes. He correlated the results with the equation


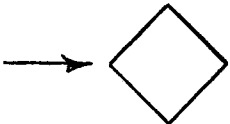
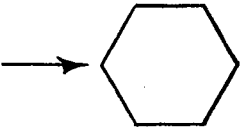
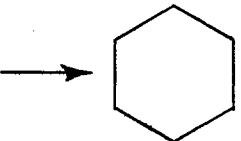
$$\text{Nu} = C(\text{Re})^m \quad (92)$$

where the values of  $C$  and  $m$  are given in Table II.

It is difficult to predict the exact nature of the flow around bodies of this type. However, it is expected that boundary layer separation will occur at the points where sharp corners exist. Beyond this point, a wake area is generally considered to exist although it is not impossible for reattachment to occur in some instances.

TABLE II

VALUES FOR  $C$  AND  $m$  FOR CALCULATING THE HEAT TRANSFER COEFFICIENTS FROM CYLINDERS WITH THE INDICATED CROSS-SECTIONAL SHAPE

Cross Section	Re	$C$	$m$
	5,000-100,000	0.0921	0.675
	5,000-100,000	0.222	0.588
	5,000-100,000	0.138	0.638
	5,000-19,500	0.144	0.638
	19,500-100,000	0.0347	0.782

## Ellipsoidal Shapes

Several investigators have studied the heat transfer properties in the boundary layer of ellipsoids of revolution. Most of this work has been concerned only with the local heat transfer coefficients over that portion of the surface ahead of boundary layer separation. One such result is reported in graphical form by Lewis and Ruggeri (22).

Needs of the aircraft industry have also caused the flow around elliptical cylinders to be investigated. Again the investigators have limited themselves to the flow region preceding boundary layer separation. The works of Seban (38), Drake (6), Eckert and Livingood (10), Frick (11), and Allen (1) are all typical examples of these results.

Figure 7 is the results from Eckert (10), Allen (1), and Frick (11) for the local Nusselt Number as a function of the dimensionless distance from the stagnation point.  $X^+$  is the distance along the surface from the stagnation point divided by the major axis of the elliptical cylinder. This elliptic cylinder has a 2:1 axis ratio and is valid for fluids whose Prandtl Number is approximately 0.7. Figure 8 is similar results from Eckert along with the wedge flow and flat plate solutions for an elliptic cylinder with an axis ratio of 4:1.

Ko and Sogin (20) experimentally determined the average heat transfer coefficient from an ellipsoid of revolution in axisymmetrical flow in air with an axis ratio of 4:1 as



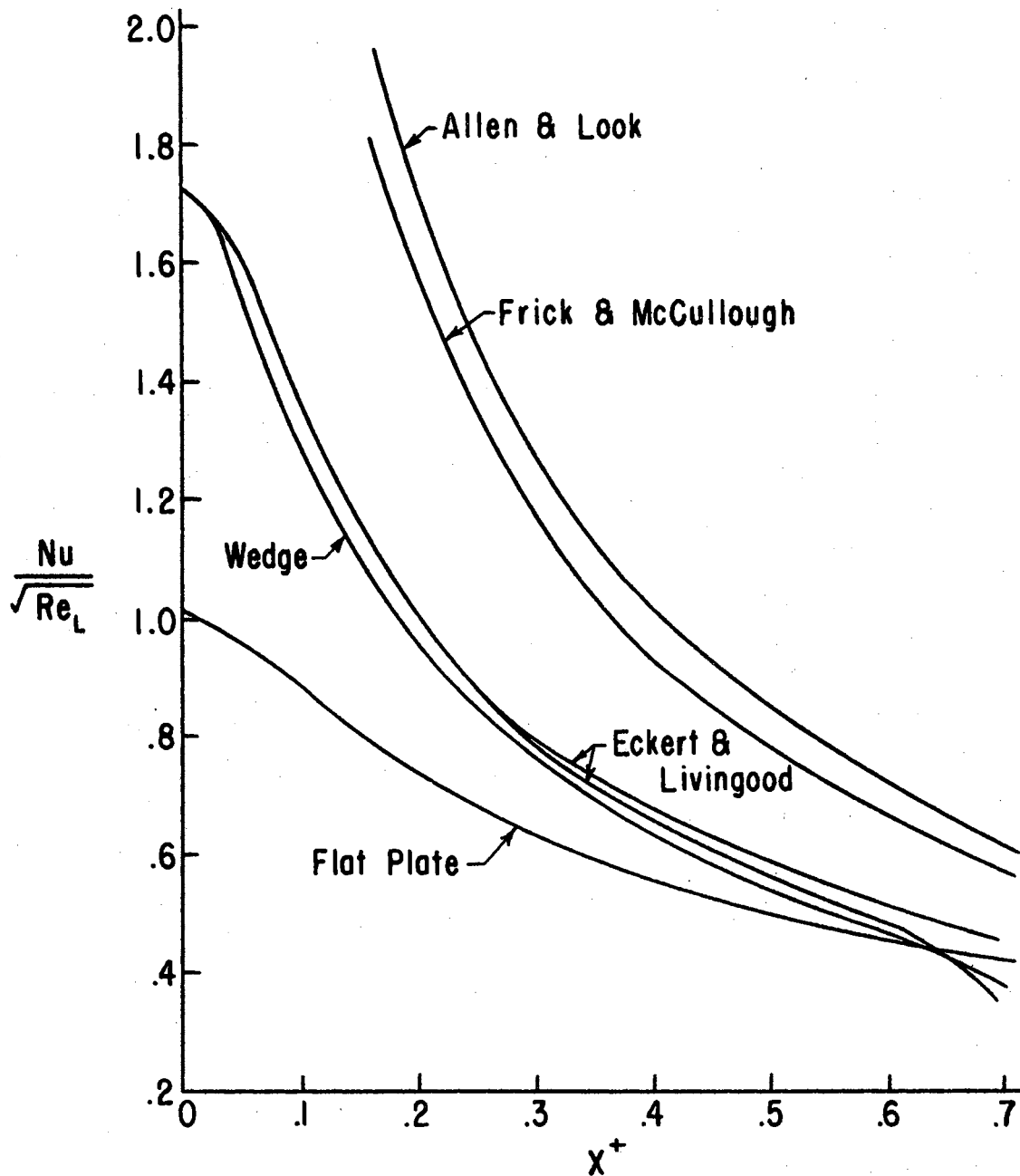


Figure 7. Comparison of methods for calculation of local heat transfer coefficients around an elliptic cylinder with axis ratio of 1:2  
From Eckert (10)

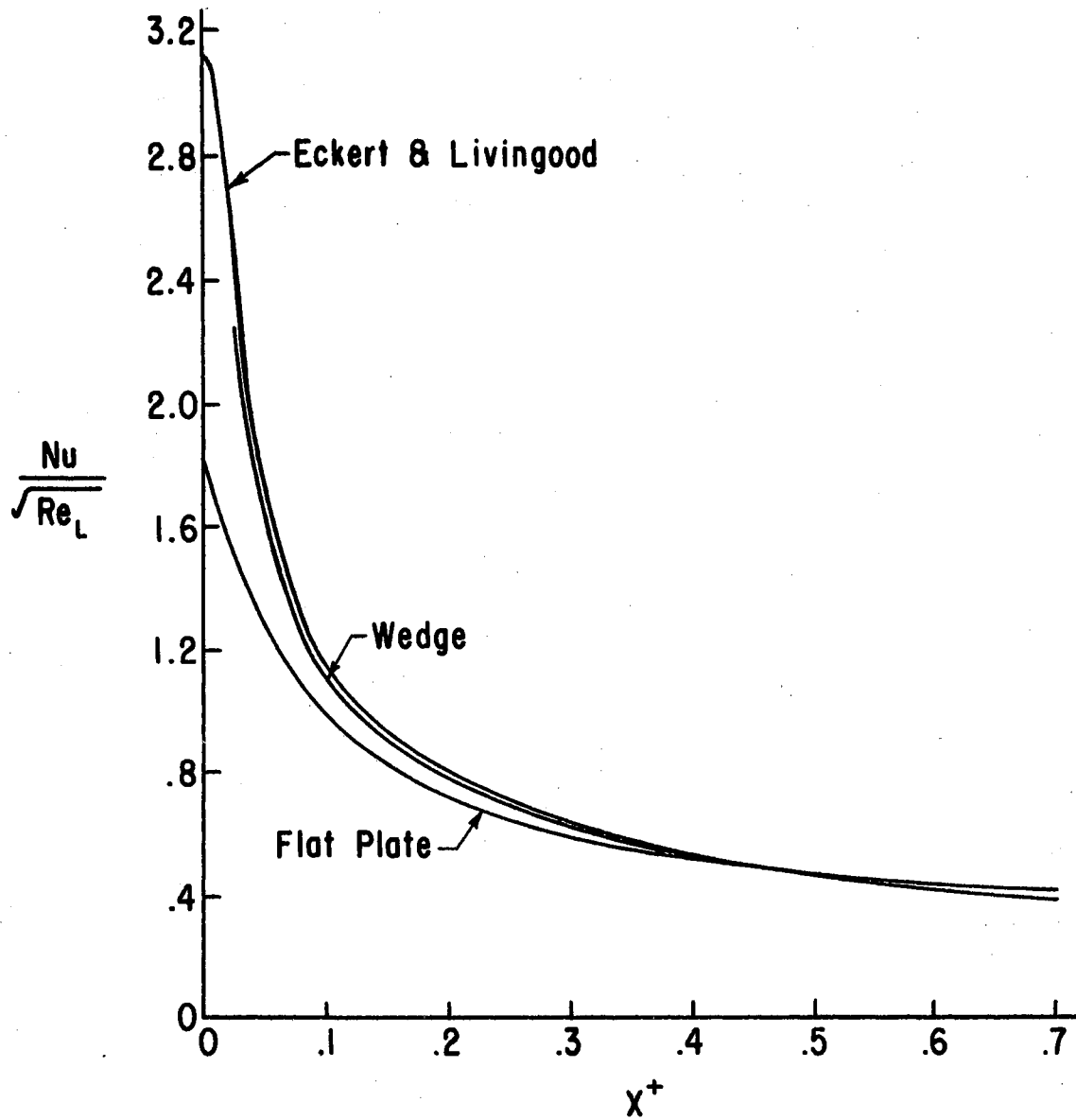


Figure 8. Comparison of methods used for calculation of local heat transfer coefficients around an elliptic cylinder with axis ratio of 1:4  
From Eckert (10)

$$\left[ \frac{h}{G_1 C_p} (\text{Pr})^{2/3} \right] (\text{Re}_D)^{1/2} = 0.52 \quad (93)$$

These results were verified for the Reynolds Number range, based on diameter, from 15,000 to 130,000. Ko also transformed the work of Lewis and Ruggeri (22) for flow about an ellipsoidal model with an axis ratio of 3:1 to give

$$\left[ \left( \frac{h}{G_1 C_p} \right) (\text{Pr})^{2/3} \right] (\text{Re}_D)^{1/2} = 0.60 \quad (94)$$

The work of Ko was entirely in the laminar boundary layer flow regime while transition occurred in most of Lewis and Ruggeri tests.

More complete results for the convective heat transfer coefficient for ellipsoidal and other shapes would be desirable but they are not generally available in the literature.

#### Wind Tunnel Turbulence

The intensity of turbulence of an air stream is defined (36) as

$$\text{Tu} = \text{Intensity} = \left[ \left( \frac{1}{3} \right) (\overline{u'^2} + \overline{v'^2} + \overline{w'^2}) \right]^{1/2} / U_\infty \quad (95)$$

where  $u$ ,  $v$ , and  $w$  are the instantaneous velocity fluctuations in the  $x$ ,  $y$ , and  $z$  directions. The bar indicates that the values are time averaged. At a short distance downstream from the screen, grid, or honeycomb of the tunnel the turbulence becomes isotropic which means that the

instantaneous velocity fluctuations become equal in all three co-ordinate directions. That is

$$\overline{u'^2} = \overline{v'^2} = \overline{w'^2}$$

In this case the intensity of turbulence becomes

$$Tu = \text{Intensity} = (\overline{u'^2})^{1/2}/U_{\infty} \quad (96)$$

The determination of turbulent intensity is accomplished by determining the value of Reynolds Number of a sphere in the wind tunnel for which the drag coefficient is 0.3. The value of this Reynolds Number is called the critical Reynolds Number. The work described in reference 7 shows a good correlation between the intensity of turbulence and the critical Reynolds Number. The work of Millikan and Klein in reference 26 indicated that the critical Reynolds Number also depends upon the diameter of the sphere in a wind tunnel where the entrance conditions were modified with various honeycomb type entrance sections. Generally the critical Reynolds Number decreased as the diameter of the sphere increased.

Dryden, et.al. (8) showed by measuring the turbulent intensity with a hot-wire anemometer that this variation in the critical Reynolds Number with sphere diameter could not be due to a variation in the intensity of turbulence with a variation of air velocity in the wind tunnel. They further showed that the critical Reynolds Number was dependent upon another turbulence property as well as turbulent

intensity. They called this value the scale of turbulence and defined it as

$$L = \int_0^{\infty} Q(y) dy \quad (97)$$

where

$L$  = Scale of Turbulence

$Q$  = Correlation Coefficient

$Q$  defines the correlation between the velocity fluctuations at two points in the stream separated by known distances.

It is defined

$$Q = \frac{\overline{u'_1 u'_2}}{(\overline{u_1'^2})^{1/2} (\overline{u_2'^2})^{1/2}}$$

where

$u'_1$  = instantaneous velocity at point 1

$u'_2$  = instantaneous velocity at point 2

Using a series of geometrically similar screens Dryden correlated the scale of turbulence as a function of distance from the screen for several screen sizes. The results showed the scale of turbulence to increase linearly as distance from the screen increased. Some of his results are shown in Figure 9.

In measuring the intensity of turbulence with the hot-wire anemometer over a large number of wind speeds, Dryden, et.al. found it to be independent of air velocity.

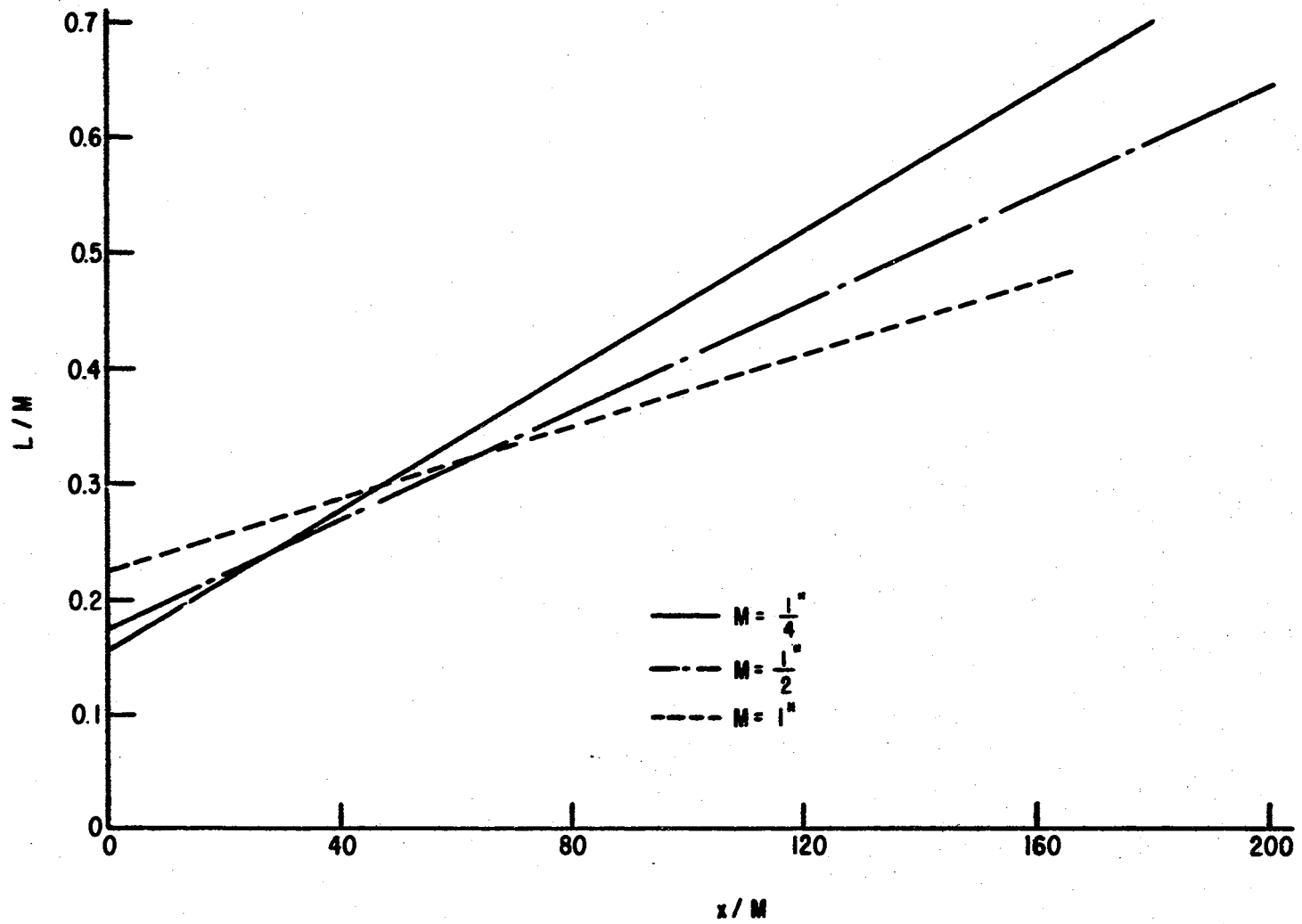


Figure 9. Scale of Turbulence at several distances from the screens.  
From Dryden (8)

After about 80 mesh diameters downstream from the screen inducing the turbulence, the intensity was found to be independent of distance also. These results are shown in Figure 10.

#### The Critical Reynolds Number of Spheres

Prandtl (32) originally proposed the use of the sphere as a means of indicating the turbulence in an air stream. By measuring the drag force on a sphere in an air stream, the drag coefficient can be calculated. The drag coefficient being defined as

$$C_D = \frac{F}{1/2\rho U_\infty^2 A_p Ne} \quad (99)$$

where

$C_D$  = Drag coefficient

$F$  = Drag force

$\rho$  = Fluid Density

$U_\infty$  = Free stream velocity

$A_p$  = Projected area of sphere

$Ne$  = Newton's Second Law Coefficient

A plot of the drag coefficient against the Reynolds Number will show that for low Reynolds Numbers  $C_D$  is approximately constant and equal to 0.4. At some range of Reynolds Numbers, the drag coefficient decreases rather rapidly to a value of about 0.1. This drop in the drag coefficient is caused by the transition of the laminar boundary layer

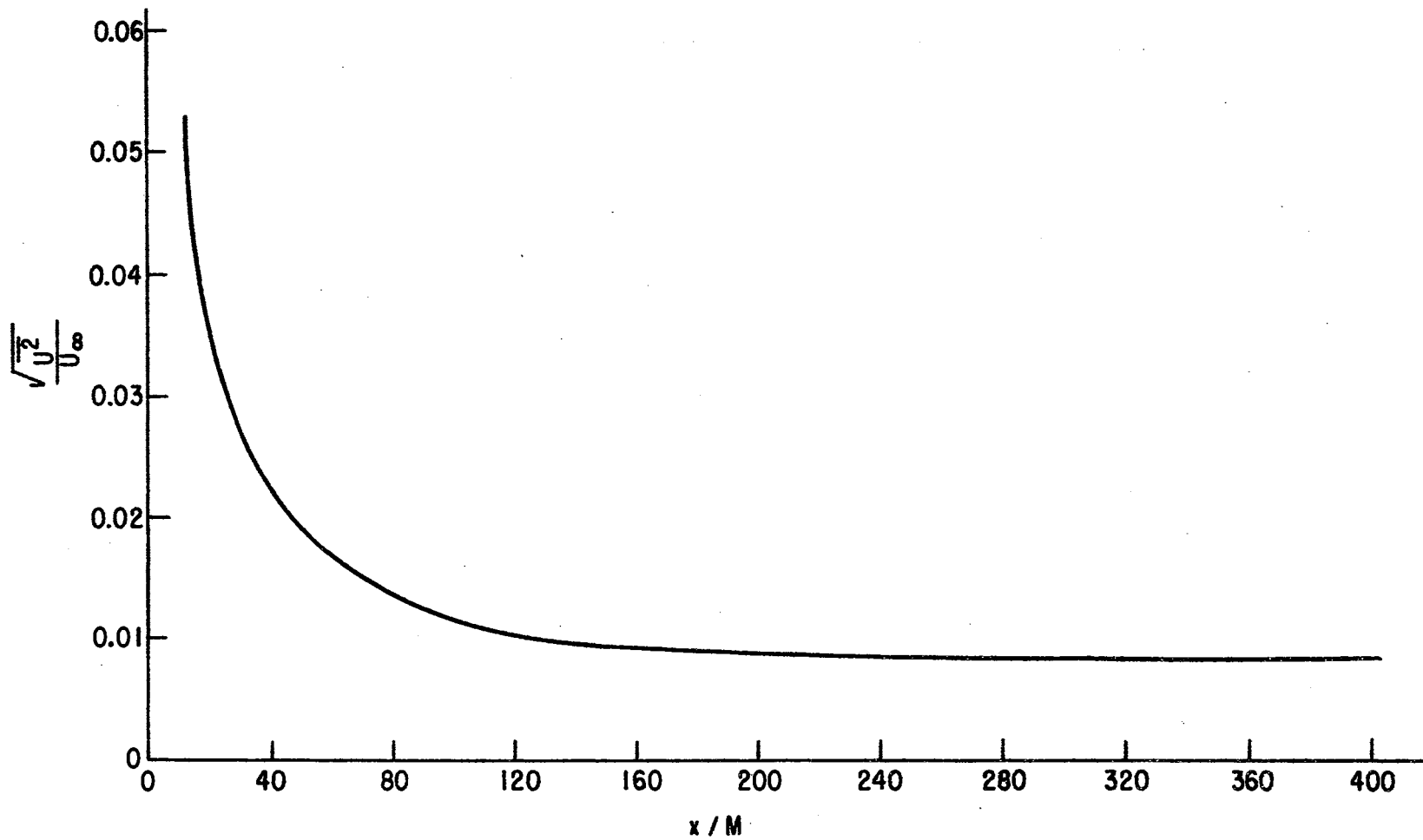


Figure 10. Intensity of Turbulence at several distances from the screens.  
From Dryden (8)



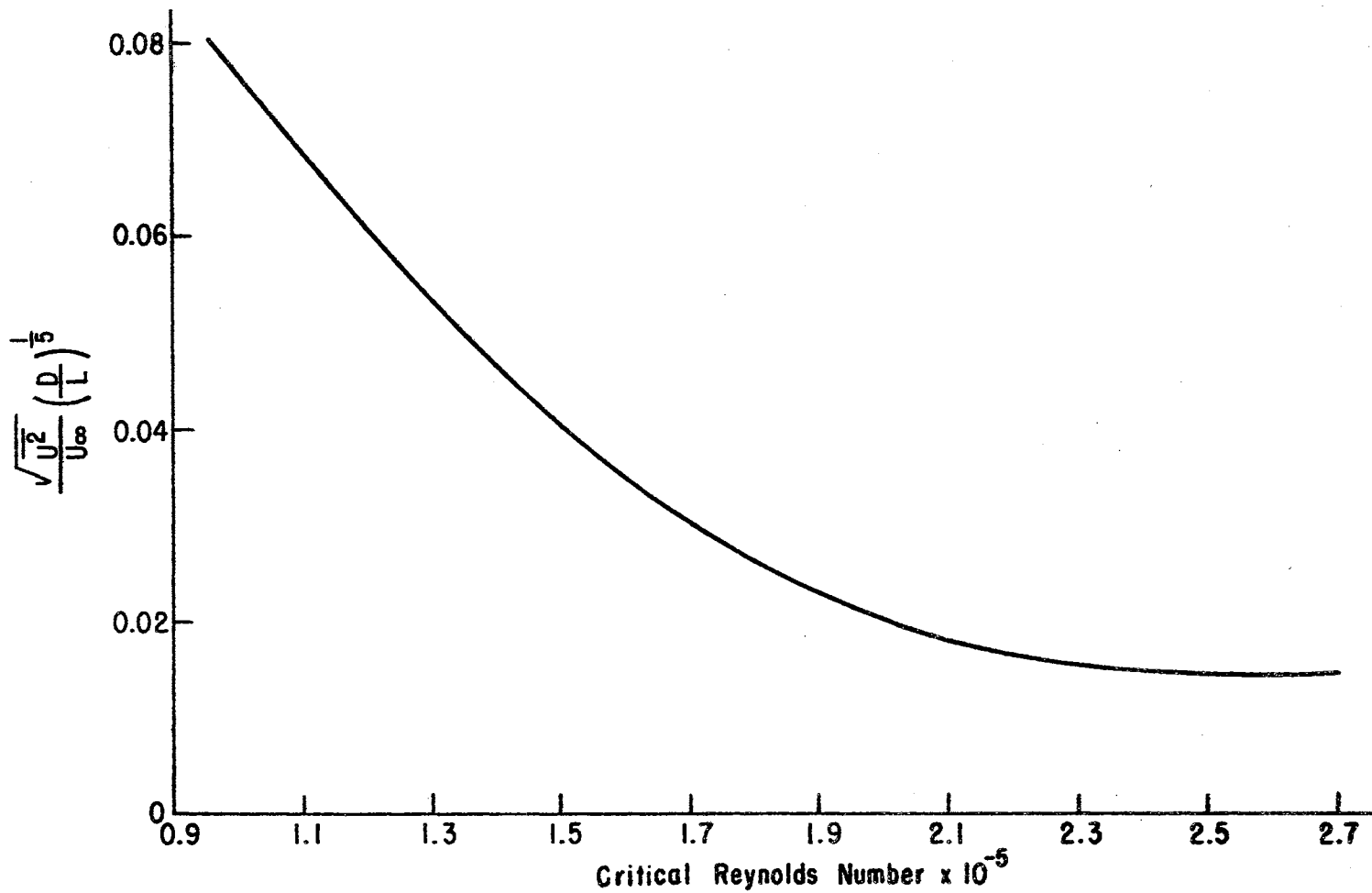


Figure 11. Critical Reynolds Number of spheres as a function of  $\frac{(u^2)^{1/2}}{U_\infty} \left(\frac{D}{L}\right)^{1/5}$  From Dryden (8).

to a turbulent boundary layer over a part of the sphere surface. The range of Reynolds Numbers over which this drop in the drag coefficient occurs is dependent upon the turbulence of the air stream. The decrease in  $C_D$  occurs at higher Reynolds Numbers in air streams of lower turbulence levels.

Several experimenters have attempted with some success to calibrate the sphere as a means of measuring the turbulence levels of an air stream. Dryden and Kuethe (7) proposed that the critical Reynolds Number of a sphere be defined as the value of the Reynolds Number at which the drag coefficient is 0.3. This criteria for determining the critical Reynolds Number for a wind tunnel has been generally accepted.

Dryden (8) in his work was able to prove that the critical Reynolds Number of a wind tunnel is dependent upon the intensity of turbulence, scale of turbulence and the diameter of the sphere. He showed that a good correlation exists between the critical Reynolds Number and the dimensionless quantity  $\frac{(\overline{u^2})^{0.5}}{U_\infty} \left(\frac{D}{L}\right)^{1/5}$  where D is the diameter of the sphere and the other quantities are as previously defined. These results are shown in Figure 11. As noted by Dryden these results indicate that a small change in intensity of turbulence will produce about the same effect as a change of 5 times as much in the scale of turbulence or diameter of the sphere.

An elaborate hot-wire anemometer system is necessary to measure either the intensity of turbulence or scale of turbulence. Because of this the turbulence properties of a wind tunnel is generally reported by specifying the critical Reynolds Number and wind tunnel entrance conditions. Generally, no attempt is made to separate the effects of intensity and scale of turbulence. From Figures 9 and 10 it can be observed that as the distance from the screen or entrance section of the tunnel increases, the intensity rapidly approaches a constant value whereas the scale of turbulence continues to increase linearly. This net effect is to increase the critical Reynolds Number as distance from the entrance section increases.

#### Turbulence Effect on Heat Transfer

The turbulence level of an air stream has a large effect upon the local and mean Nusselt Number from a body. This is easily accepted if we realize that specification of the Reynolds Number and Prandtl Number do not necessarily guarantee similarity between air streams. The Reynolds Number is generally defined using the average free stream **velocity**. This does not in any way specify the turbulence level of the stream in steady flow since the velocity fluctuations time-average to zero over sufficiently long time intervals.

Schlichting (36) observed that Hilpert (18) and Griffith (15) et.al. obtained large differences in measuring the

Nusselt Number from infinite circular cylinders in cross-flow. The experimental procedure for the two works was the same leaving the turbulence level of the tunnel as the only variable. The thirty percent difference between these two investigators was attributed to differences in the turbulence properties of the air streams by Schlichting (36). This leads to the conclusion that the Nusselt Number is a function of the Reynolds Number, Prandtl Number, object geometry and turbulence of the air stream.

$$Nu = f_6(Re, Pr, Gr, Tu) \quad (100)$$

To look at the effect of an increase in turbulence on the heat transfer from a body, let's look at the case of a blunt body such as a cylinder. The major effect will be in the effect the turbulence has on the boundary layer. At low Reynolds Numbers the flow pattern consists of a laminar boundary layer in front and a wake behind the body caused by laminar separation. This will be recognized as a subcritical flow pattern. An increase in turbulence will cause earlier separation and thereby cause a larger segment of the surface to be covered by the separated region. This will cause a change in the average Nusselt Number because the local Nusselt Number is different for these two flow regions. At higher Reynolds Numbers the flow pattern consists of a laminar layer, followed by a turbulent layer behind the point of transition. Finally a wake exists behind the point of turbulent separation.

This flow pattern will be recognized as the supercritical flow pattern. The increase in turbulence has little effect on the point of separation but does effect the point of transition. This causes a larger portion of the surface to be covered with a turbulent layer and thereby increases the average Nusselt Number. An increase in turbulence may also cause a sudden change from subcritical to supercritical flow causing a sudden change in the Nusselt Number. An increase in turbulence must also cause an increase in the local Nusselt Numbers of the laminar boundary layer, the turbulent boundary layer and the wake.

## CHAPTER III

### EXPERIMENTAL DESIGN AND PROCEDURE

A general ellipsoidal model is visualized as an adequate model for predicting the convective heat transfer coefficient from irregular shapes. The control of the three orthogonal axes of the ellipsoid will provide for a close approximation of the irregular shape.

Because of a lack of available information on the convective heat transfer from general ellipsoidal shapes, it is necessary to experimentally determine the convective heat transfer properties.

#### Theory of Similitude

Much of the theory of model systems is based on a theorem due to Buckingham (4). The pi theorem states that a relationship existing among physical quantities that is completely described by an equation can be reduced to an expression of the form

$$f_7(\pi_1, \pi_2, \dots) = 0 \quad (101)$$

where the  $\pi$ 's are all independent and dimensionless products that are formed by a suitable combination of the pertinent variables.

TABLE III  
 PERTINENT VARIABLES FOR THE CONVECTIVE HEAT TRANSFER  
 COEFFICIENT FROM AN ELLIPSOIDAL MODEL

No.	Symbol	Quantity	Unit
1	$h$	Heat transfer coefficient	Btu/(hrft <sup>2</sup> °F)
2	$\mu$	Viscosity of the gas	(lb <sub>f</sub> -sec)/ft <sup>2</sup>
3	$\rho$	Mass density of gas	lb <sub>m</sub> /ft <sup>3</sup>
4	$k$	Thermal conductivity of gas	Btu/(hrft°F)
5	$C_p$	Specific heat of gas	Btu/(lb <sub>m</sub> °F)
6	$\epsilon$	Roughness index of the surface	-
7	$a$	Length of major axis of the ellipsoid perpendicular to fluid flow	ft
8	$b$	Length of horizontal axis of ellipsoid to major axis and parallel to fluid flow	ft
9	$c$	Length of vertical axis of ellipsoid perpendicular to major axis and fluid flow	ft
10	$U_\infty$	Mean velocity of gas flowing by ellipsoid	ft/sec
11	$Ne$	Newton's Second Law Coefficient	(lb <sub>f</sub> -sec <sup>2</sup> )/(lb <sub>m</sub> ft)
12	$\lambda$	Angle of attack	Radians

The physical system for predicting the convective heat transfer coefficient from an ellipsoidal model to a fluid stream may be adequately described by the pertinent variables listed in Table III. The units utilized in this study are also shown in Table III for each variable.

The heat transfer coefficient,  $h$ , is the dependent quantity and is the quantity to be determined. Since  $h$  cannot be measured directly, techniques must be employed which provide a means of computing  $h$ . One such technique will be discussed later.

Since the ability to transfer heat from the body surface to the fluid is partially dependent upon the ease with which heat is conducted through the fluid and upon the heat capacity of the fluid, both the thermal conductivity and the specific heat of the fluid are pertinent.

Researchers have shown that the nature of the flow about the body is an important consideration when predicting the heat transfer coefficient; i.e., laminar flow, turbulent flow, and boundary layer separation. Previous research has also shown that the nature of the flow about a body is dependent upon  $\rho$ ,  $\mu$ ,  $U_\infty$ ,  $Ne$ , and  $\epsilon$ . Also, the dimensions and geometry of the body affect the nature of flow around the ellipsoid. In the special case of an ellipsoid, three length dimensions are required to adequately describe the shape.

The angle of attack,  $\lambda$ , is the angle between the direction of fluid flow and the major axis,  $a$ , measured in



the horizontal plane. The orientation of the body is important since the boundary layer characteristics are altered as the angle of attack changes. For example, as  $\lambda$  changes, the location at which boundary layer separation occurs also changes.

The other possible rotations of the body will be equally as important as the angle  $\lambda$ . However, the effect of the orientation is not to be considered in this work, as will be described later, and therefore the other angles are not listed in the set of pertinent quantities.

#### Pi Terms

There appear to be six independent dimensions in the list of pertinent quantities. However, where  $H$  and  $\theta$  appear, they appear in the combination  $H\theta^{-1}$ . Thus, they are not independent and the combination must be treated as one independent dimension.

A dimensional matrix for the variables will show that the rank of the matrix is five indicating that five independent dimensions exist. Langhaar (21) showed that the number of pi terms necessary to adequately describe the system is always equal to the number of independent physical variables minus the rank of the dimensional matrix. Therefore we have  $12-5=7$  independent and dimensionless groups or pi terms to adequately describe this system. One set of pi terms is:

$\pi_1 = hc/k$	(Nusselt Number)
$\pi_2 = \mu C_p / (Ne k)$	(Prandtl Number)
$\pi_3 = \frac{Ne U_\infty c \rho}{\mu}$	(Reynolds Number)
$\pi_4 = a/c$	(length ratio)
$\pi_5 = b/c$	(length ratio)
$\pi_6 = \epsilon$	(roughness index)
$\pi_7 = \lambda$	(orientation)

The effect of the roughness index,  $\pi_6$ , will not be included in this study since we are primarily interested in the variation of the heat transfer coefficient as a function of the geometry of the body. This parameter will be held constant throughout the study by working with "smooth" surfaces only.

The angle of orientation,  $\lambda$ , is held constant at zero degrees throughout the experiment. Although the heat transfer coefficient will vary as  $\pi_7$  changes; a constant value of  $\lambda$  is selected so that the experimental plan may be reduced to meet the time limitations of the study. The investigation of the effect of  $\lambda$  is not necessary for the completion of the objectives of this study.

The Reynolds Number,  $\pi_3$ , is an index of the ratio of inertial to viscous forces of the fluid as it comes in contact with the body. The value of this index will affect

the nature of the boundary layer at any point on the ellipsoid.

The Prandtl Number,  $\pi_2$ , is an index of the similarity in the temperature and momentum transport boundary layers when the temperature transport occurs by convective and diffusive effects and momentum transport by inertial (convective) and viscous (diffusive) effects. For a gas in the temperature range of 0°F to 400°F the Prandtl Number remains nearly constant. Even between gases the variation in the Prandtl Number is not large being within 10% of the value for air for most gases. This study, due to physical limitations, uses air as the only fluid media so that the Prandtl Number is held constant at 0.72. Kays (19) and other investigators have shown that the Nusselt Number varies as the Prandtl Number raised to the one-third power. This will allow the results from this work to be extended to fluids whose Prandtl Number differs significantly from the value for air.

The Nusselt Number,  $\pi_1$ , is the dependent  $\pi$  term since it contains the heat transfer coefficient. Physically, it is an index of the ratio of the heat transfer rate through the boundary layer when the fluid is moving to the heat transfer rate through a thickness of fluid equal to the boundary layer thickness when the fluid is stationary.

## Prediction Equations

The general prediction equation for determining the heat transfer coefficient can be written as:

$$\pi_1 = f_8(\pi_2, \pi_3, \pi_4, \pi_5), \quad (102)$$

or

$$hc/k = \phi_1 \left( \frac{C_p}{Nek} \right)^d \left( \frac{NeU_\infty \rho c}{\mu} \right)^e \left( \frac{a}{c} \right)^g \left( \frac{b}{c} \right)^j,$$

or

$$Nu = \phi_1 (Pr)^d (Re)^e \left( \frac{a}{c} \right)^g \left( \frac{b}{c} \right)^j \quad (103)$$

where

Nu = Nusselt Number,

Pr = Prandtl Number,

Re = Reynolds Number,

and

$\phi$  = Dimensionless coefficient.

Previous research has shown that Nusselt Number, and therefore the heat transfer coefficient, is a function of the Reynolds Number and the Prandtl Number for flat, spherical and cylindrical shaped bodies. It is reasonable to assume that the heat transfer coefficient of an ellipsoidal body would be similarly related; that is, it also would be a function of the Prandtl and Reynolds Numbers.

The prediction equation will not be continuous for all conditions. For example, if abrupt changes in boundary layer characteristics occur due to variations of the angle of attack, high Reynolds Number, or geometry, we can expect a discontinuous function. The general prediction equation presented here will be for the case of turbulent flow and no abrupt changes in the shape. The experimental design conditions which satisfy this criterion will be discussed in the following section.

#### Range of Pi Terms

The values through which the pi terms are varied is tabulated in Table IV. The Prandtl Number,  $\pi_2$ , is held constant at 0.72 by using air as the only fluid medium. The Reynolds Number based on the characteristic dimension  $c$  is varied from 30,000 to 150,000 in 9 steps. This range of Reynolds Number was controlled by the limitations of the wind tunnel used for these tests. However this range is satisfactory since most convective cooling of agricultural products is done within this range.

Before the levels of the two geometric pi terms were determined the following criteria were established for the ellipsoidal model. One of the objectives of this work was to design models that would adequately represent a typical agricultural product. The basic dimension of the ellipsoidal models were therefore selected to span the range of dimensions

TABLE IV  
EXPERIMENTAL DESIGN

$\pi_1$	$\pi_2$	$\pi_3$	$\pi_4$	$\pi_5$
$\frac{hc}{k}$	$\frac{\mu C_D}{kNe}$	$\frac{U_\infty c_D Ne}{\mu}$	a/c	b/c
Measure	0.72	30,000	2.50	1.75
		41,000		
		52,000		
		70,000		
		88,000		
		106,000		
		123,000		
		141,000		
146,000				
Measure	0.72	123,000	1.33	1.75
			1.67	
			2.00	
			2.33	
			2.50	
			2.80	
			3.00	
Measure	0.72	123,000	2.50	1.00
				1.25
				1.50
				1.75
				2.00
				2.25
				2.50

normally expected in commercial cuts of pork. The limits on a, b, and c are then

a: 8 to 14 inches

b: 4 to 11 inches

c: 4 to 6 inches

The maximum and minimum levels of  $\pi_4$  and  $\pi_5$  were determined using these values of a, b, c and the remaining levels were uniformly distributed between these limiting conditions. These limits are

$$1.33 \leq \pi_4 \leq 3.00$$

$$1.00 \leq \pi_5 \leq 2.50$$

A large number of other agricultural products will fall within this range of values for  $\pi_4$  and  $\pi_5$ .

This experimental design will require a total of thirteen ellipsoidal models within the ranges indicated above.

#### Measurement of Nusselt Number

In order to determine Nusselt Number, it is necessary to measure the heat transfer coefficient. Since it is not possible to directly measure the heat transfer coefficient, the following procedure will be used. The surface temperature of the fluid moving past the body will be measured. Using numerical integration the average surface temperature

can be determined; and by placing a known heat source inside the model and allowing the system to reach the steady state condition, the amount of heat flow out of the ellipsoidal model is established. The heat transfer coefficient can then be computed directly by the equation:

$$h = q / (A_s (T_s - T_f)) \quad (104)$$

where

$q$  = total heat flow out of the body, Btu/hr

$A_s$  = surface area of the body,  $\text{ft}^2$

$T_s$  = average body surface temperature,  $^{\circ}\text{F}$

$T_f$  = temperature of gas moving by the body,  $^{\circ}\text{F}$

An electric resistance heater element made of nichrome wire is used as the heat source. The power input to the system is measured by monitoring the voltage and current input to the system. The electrical energy is converted into heat energy according to the relationship

$$q = KEI \quad (105)$$

where

$K = 3.413 \text{ Btu/hr-watt}$

$I = \text{current flow in heating element, amperes}$

$E = \text{emf across heating element, volts.}$



The fluid temperature,  $t_f$ , is measured directly with a thermocouple. A weighted average of the local surface temperatures measured on the model is obtained by

$$T_{\text{avg}} = \frac{\sum T_i A_i}{\sum A_i} \quad i = 1, \omega \quad (106)$$

where

$T_{\text{avg}}$  = weighted average of measured surface temperatures, °F.

$T_i$  = temperature of the surface at node  $i$ , °F.

$A_i$  = surface area represented by node  $i$ , ft<sup>2</sup>.

$\omega$  = number of nodes at which surface temperature is measured.

Location of the temperature sensors will be described in detail later in this report.

## CHAPTER IV

### EQUIPMENT AND INSTRUMENTATION

The experimental design discussed in the previous chapter required the construction of thirteen different general ellipsoids. A hollow ellipsoid was required for the placing of a heat source in the center. Since the necessary milling machinery was not available, the models were cast from aluminum. The patterns were constructed in the Agricultural Engineering Research Shop at Oklahoma State University.

#### Model Construction

For each ellipsoid a pattern was required for the inside (or core) and for the outside dimensions of the model. The patterns were constructed of rapid curing plaster of Paris. In order to accurately construct the plaster of Paris patterns, paraffin molds were constructed for pouring the plaster of Paris.

#### Template Construction

In the construction of the mold for each ellipsoid, a template was constructed at one inch intervals along the major axis of the ellipsoid. In regions of high curvature

this interval was reduced to one-half inch. The major and minor axis of the ellipse obtained at each point along the major axis of the ellipsoid was calculated from the equation for the surface of a general ellipsoid

$$\frac{x^2}{A^2} + \frac{y^2}{B^2} + \frac{z^2}{C^2} = 1 \quad (107)$$

Since  $z$  is specified then the major axis of the ellipse at the given  $z$  is determined by letting  $y = 0$  and solving for  $x$ . The minor axis is likewise obtained by letting  $x = 0$  and solving for  $y$ . The equation for the ellipse is then

$$\frac{x^2}{A^2} + \frac{y^2}{B^2} = 1$$

This can be expressed parametrically by:

$$\begin{aligned} x &= A \cos \theta \\ y &= B \sin \theta \end{aligned} \quad (108)$$

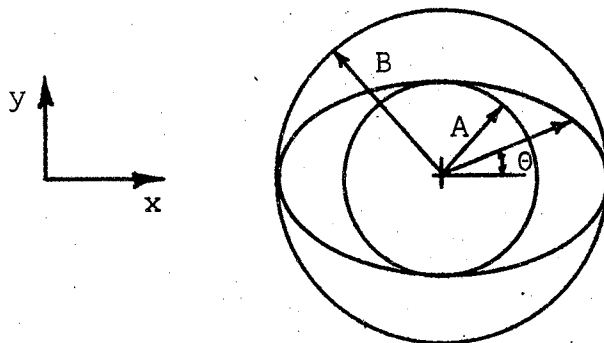


Figure 12. Parametric Representation of the Ellipse

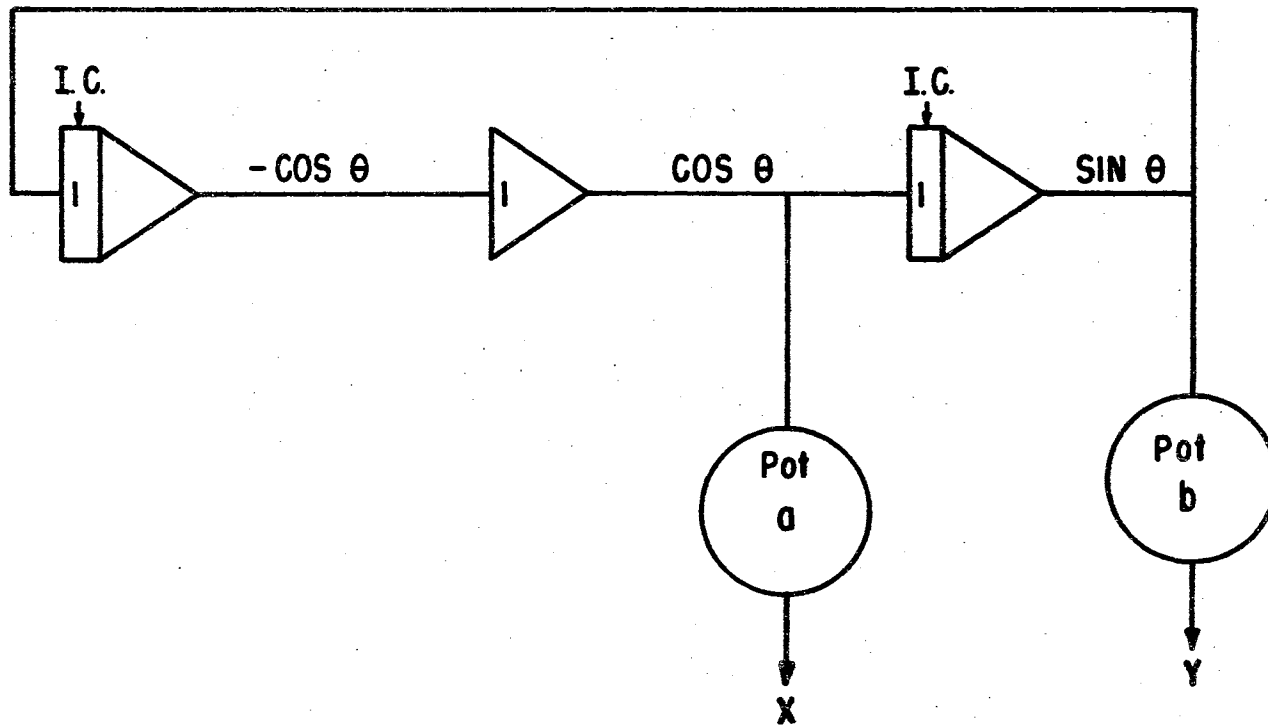


Figure 13. Analog computer diagram for plotting the ellipsoid cross sections

An analog computer circuit to solve for  $x$  and  $y$  is shown in Figure 13.

The  $x$ - $y$  plotter printed the cross-section on a thin sheet of cardboard that was used to construct sheet metal templates for the ellipsoidal model.

After fastening the templates in position hot paraffin was poured over the templates and allowed to solidify. Using the templates as a guide a mold of the approximate ellipsoid dimensions was formed so that the plaster of Paris pattern could be constructed. The finishing work on the rough patterns was completed using hand tools to give an accurate ellipsoidal surface. Step-by-step pictures of the construction process are shown in Figures 14 through 19.

Using the plaster of Paris patterns, a commercial foundry formed sand molds and cast the ellipsoidal models from aluminum alloy 355-T51. It was desired to construct the models with as thin walls as possible to minimize the temperature gradient that exist in the wall. The foundry could control the wall thickness to a minimum of 1/8 inch, therefore this was the thickness selected. The thermal conductivity of this aluminum is listed in reference 48 as 97 Btu/(hrft<sup>0</sup>F). The resistance to heat flow through the wall is very small compared to the resistance to heat flow at the inside and outside boundaries of the wall. The temperature of the wall is, therefore, essentially constant throughout the thickness of the wall. This allows

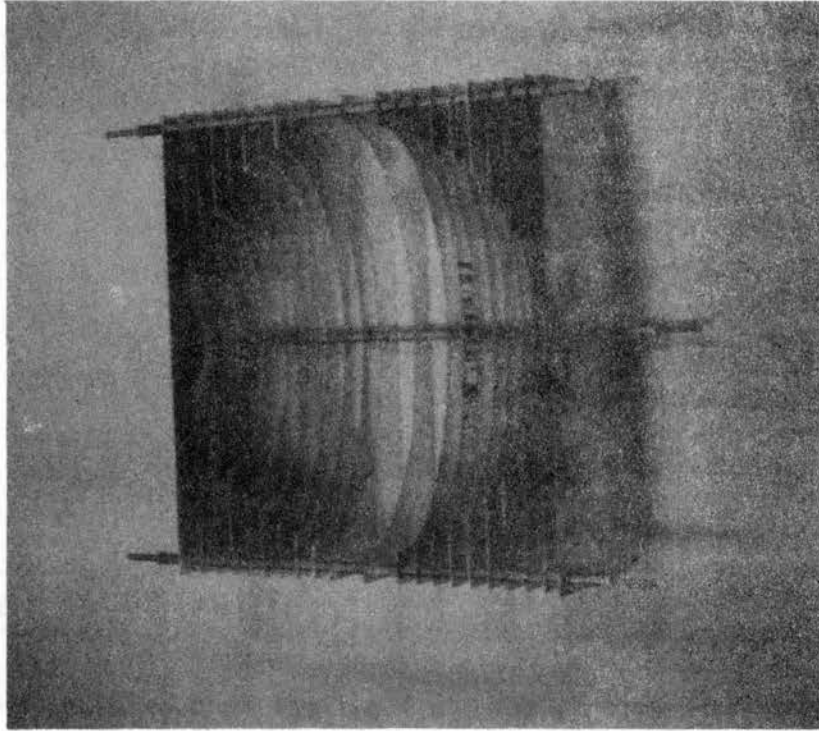


Figure 14. Sheet Metal Templates in Position for Pouring the Paraffin Mold.

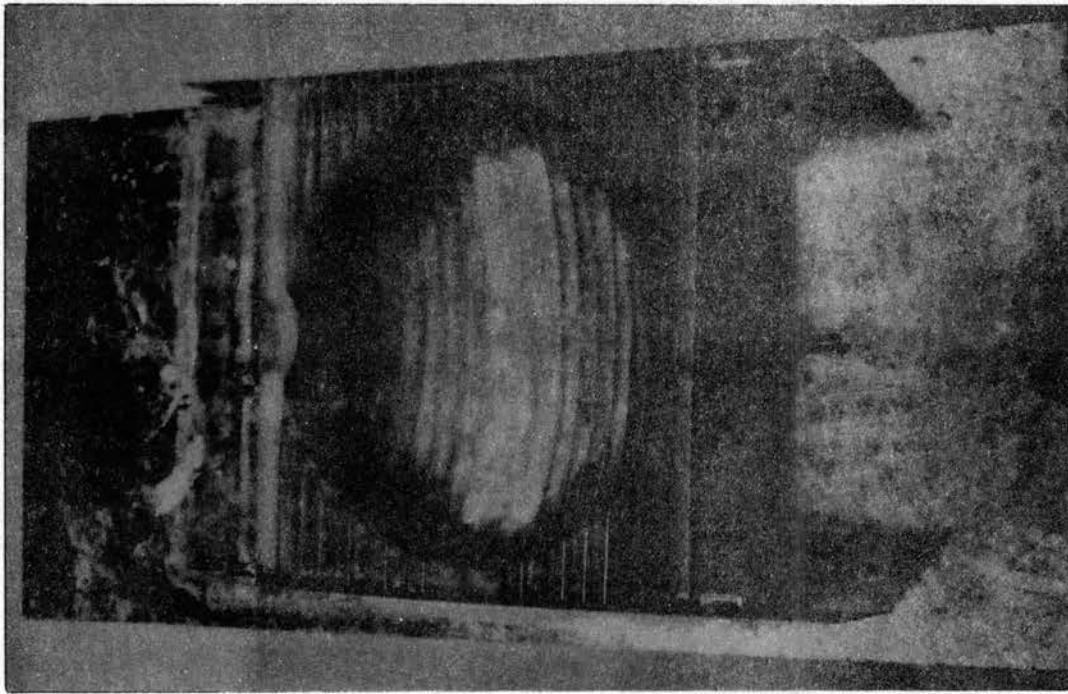


Figure 15. Paraffin Mold Formed for  
Pouring the Plaster of  
Paris Pattern

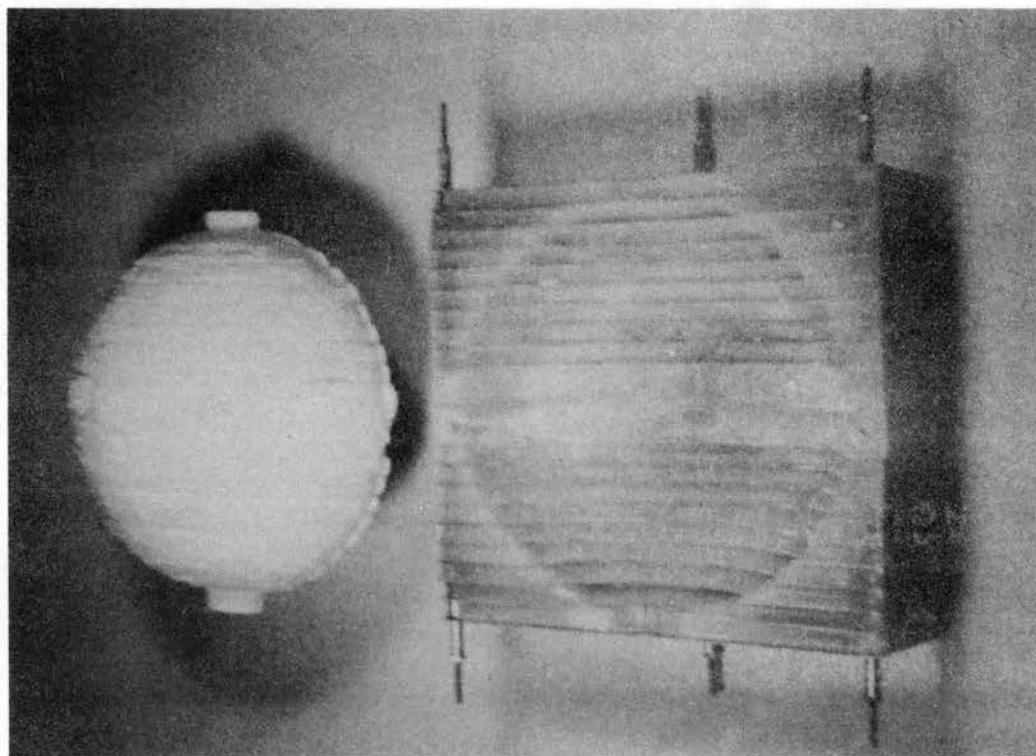


Figure 16. Unfinished Plaster of Paris Pattern  
Removed from Paraffin Mold



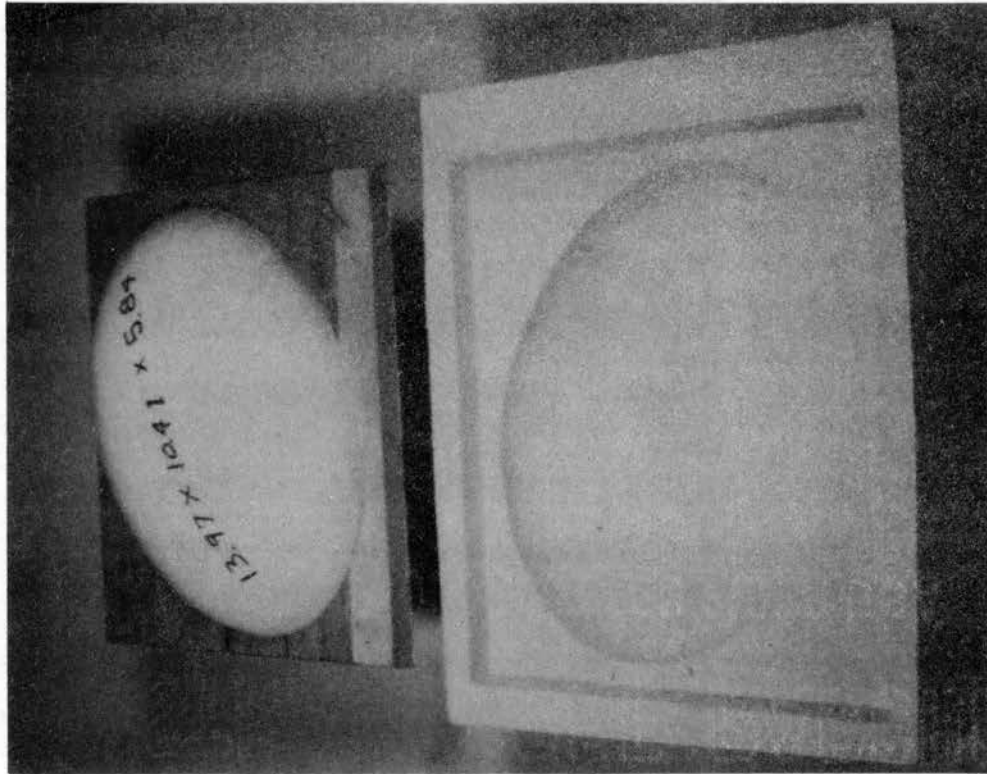


Figure 17. Finished and Unfinished Plaster of Paris Pattern

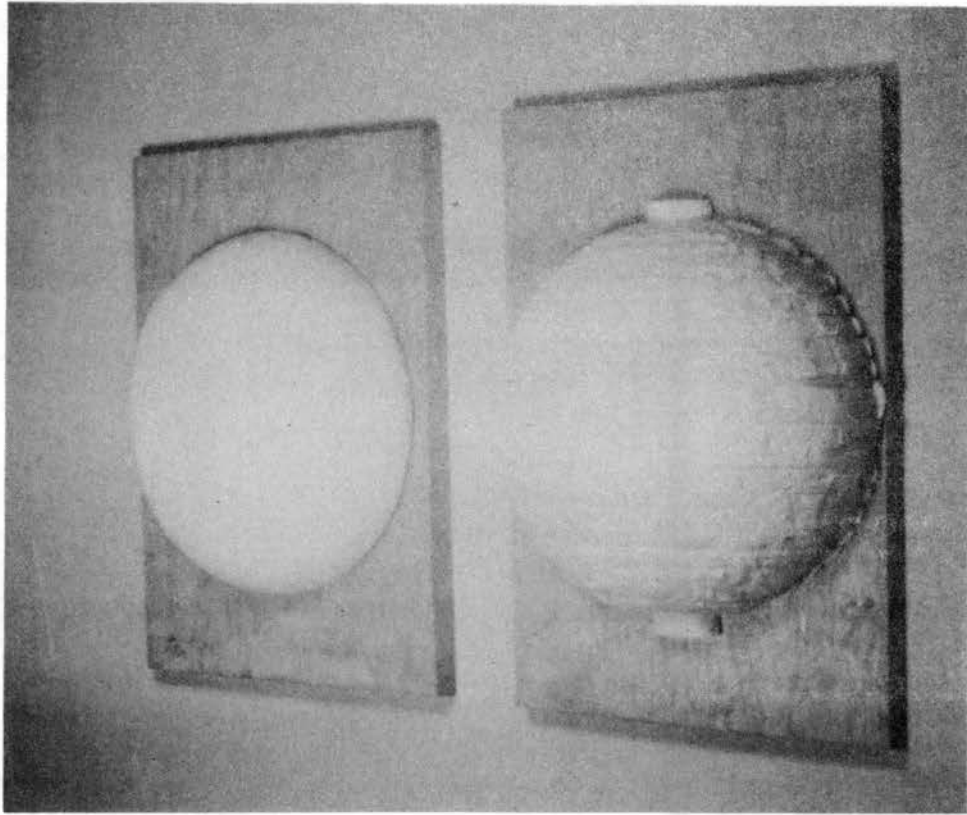


Figure 18. The Forming of the Pattern for the Outside Dimensions of the 13.5 x 10.0 x 5.75 Ellipsoid

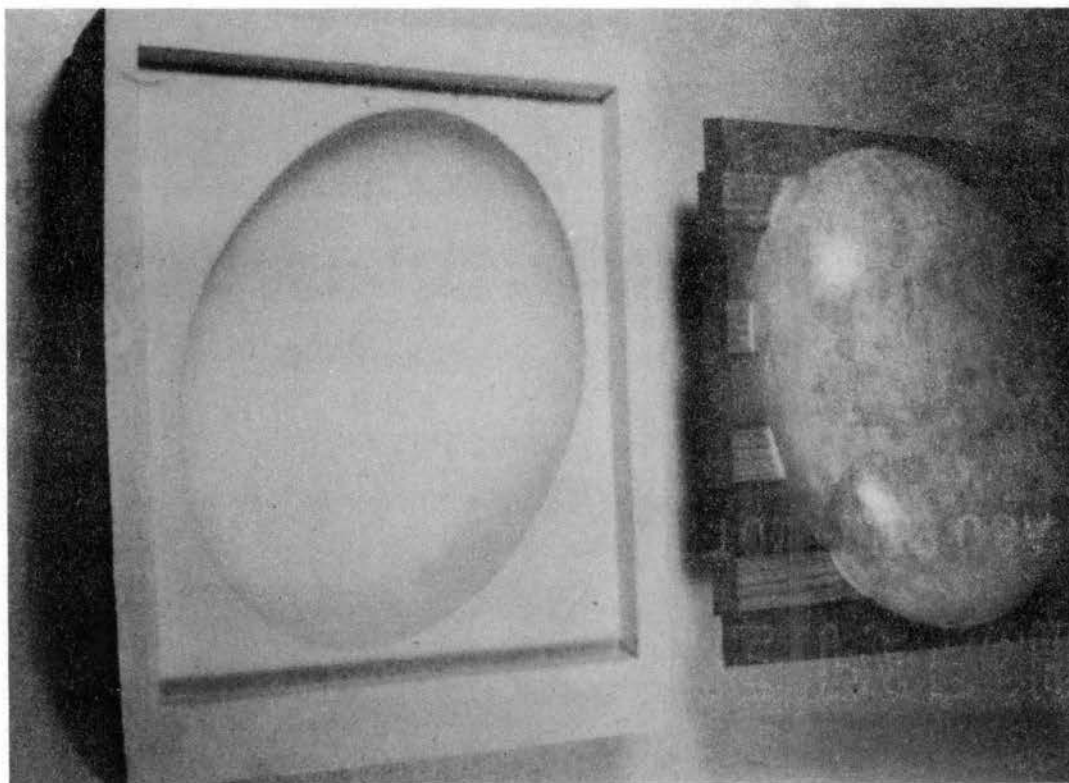


Figure 19. Patterns for the Inside and Outside Dimensions of the Ellipsoid Ready for Casting

the placement of the thermocouples for measuring surface temperature to be in error without inducing appreciable error in the temperature measurement.

The outer surface of all the models were buffed using jeweler's rouge to provide a smooth shiny surface. This insured that the surface roughness was the same for all models and therefore did not confound the results of the experiments.

#### Model Instrumentation

Each ellipsoid was instrumented with forty nine 36-gage copper-constantan thermocouples. These thermocouples were distributed over one half of the model surface as indicated in Figure 20. At each cross-section the thermocouples were spaced so that the arc-length between thermocouples was constant.

At each thermocouple location a hole was drilled in the model just large enough to allow the thermocouple to be inserted from the inside of the model. The thermocouple was mounted so that it was located at the external surface of the model but not extending into the boundary layer. To insure good thermal contact with the walls of the model, the thermocouple was embedded in a mixture of epoxy cement and a Honeywell thermometer-well compound. The thermocouple leads were fastened to the inside surface of the model with contact cement to a point on the leeward side of the model where the leads entered the air stream and

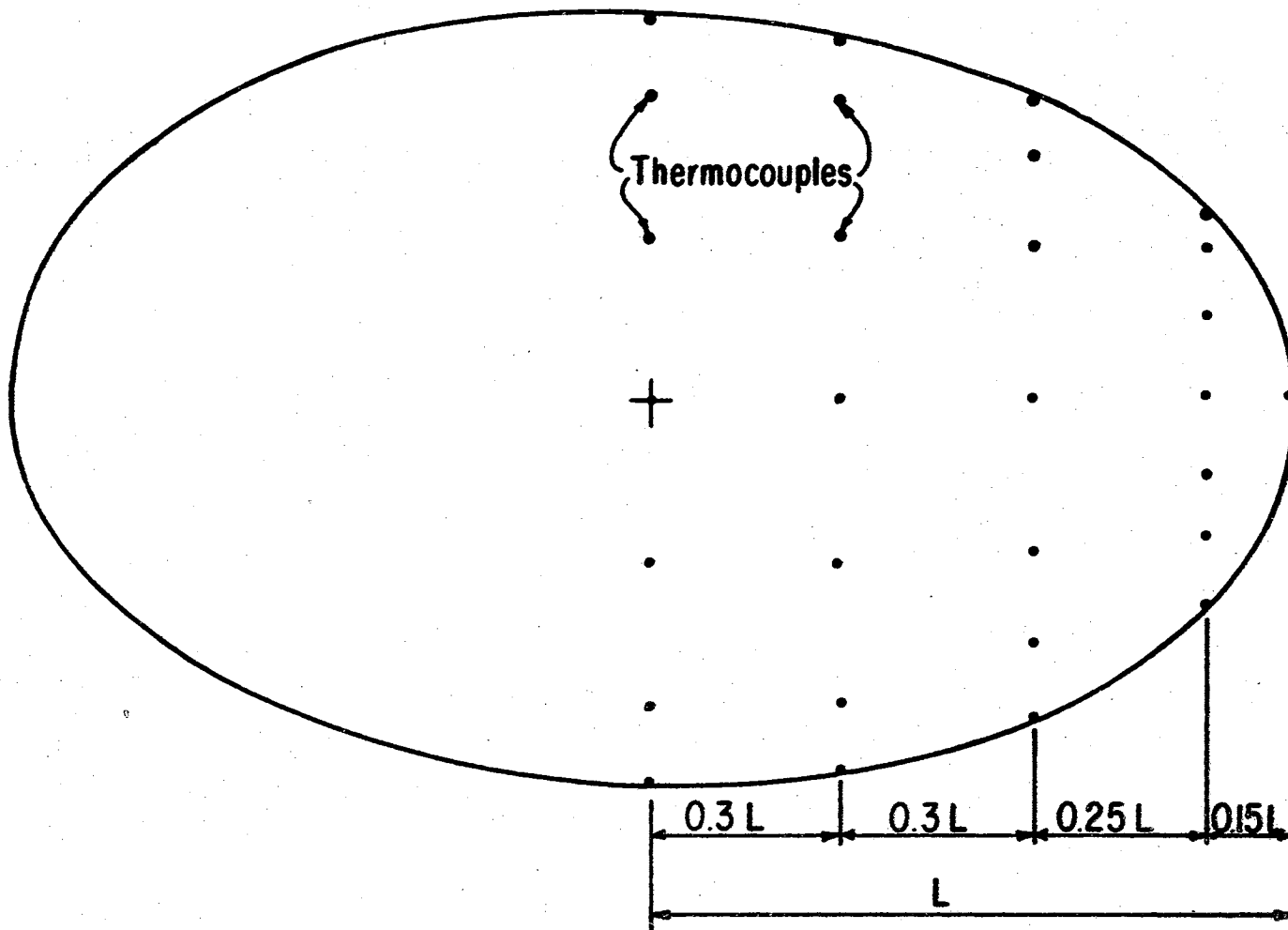


Figure 20. Location of thermocouples on the surface of the ellipsoids

traveled parallel to air flow for several inches before leaving the tunnel and connecting to the recording potentiometer.

A resistance type electric heater was suspended in the center of the model by four 30-gage steel wires. The unit was shielded so that the mode of heat transfer from the heater to the model walls was primarily due to free convection. The radiant energy transfer was small because of the relatively small temperature difference between the heater surface and wall of the model.

The energy input was monitored by a voltmeter and ammeter. The power input was then:

$$P = EI$$

$$P = \text{Power, watts}$$

$$E = \text{Voltage, volts}$$

$$I = \text{Current, amperes}$$

therefore:

$$q = (3.413) \frac{\text{Btu}}{\text{hr-watt}} (P)$$

$$= (3.413) EI \quad (109)$$

$$q = \text{energy, Btu/hr.}$$

After mounting the thermocouples and heater, the two halves of the model were sealed together with a mixture of epoxy cement and the Honeywell thermometer well compound.

This mixture provided good thermal contact as well as adequate strength to support the models while in the wind tunnel.

These models were mounted in the wind tunnel by eight 30-gage steel wires extending from the surface of the model to stationary supports in the tunnel. Tension on these wires was controlled to eliminate vibration of the model during the test and to hold the model in the correct position throughout the test.

#### Data Collection

The models were mounted in the tunnel and the air velocity adjusted by varying the speed of the fan and monitoring the velocity head with a pitot-static tube. Variations in the velocity head were measured with an accuracy of  $\pm 0.001$  of an inch of water.

Energy input to the system was controlled by a variable voltage transformer. The energy level was controlled at a value so that the maximum temperature difference existing between the model surface and ambient air temperature did not exceed  $30^{\circ}\text{F}$ . Higher temperature differences would require higher temperatures inside the model and could possibly cause damage to the nylon insulation on the copper-constantan thermocouple wires.

Depending upon the air velocity, the transient period was from 30 to 45 minutes. The model was considered to have reached the steady state condition when the surface

temperature was observed to vary no more than one-half degree in a 10 minute period. At this time all surface temperatures, air temperature, energy input and air velocity were measured. Surface temperatures were recorded by a 10 point recording potentiometer. Recording of all points required a twenty-five minute time period. To insure that the surface temperatures had not changed during this period, a check was run at the end of the test to insure that the first points recorded had not changed in value.

The test on each model was repeated three times. Sometimes the tests were run on the same day while at other times a day or more intervened between tests. Generally once a model was in the tunnel, tests were performed as quickly as schedules permitted. In all cases the model was brought into equilibrium with ambient conditions before a new test was begun.

#### Surface Areas of the Models

The surface of a general ellipsoid is described by:

$$\frac{x^2}{A^2} + \frac{y^2}{B^2} + \frac{z^2}{C^2} = 1 \quad (110)$$

where

A = one-half the semi-major axis-parallel to the  
x-axis.



B = one-half the major axis-parallel to the y-axis.

C = one-half the semi-major axis-parallel to the z-axis.

Then

$$z = \pm C \left(1 - \frac{x^2}{A^2} - \frac{y^2}{B^2}\right)^{1/2}$$

In most advanced calculus textbooks it is shown that:

$$A_s = 8 \int_0^B \int_0^A \left(1 + \left(\frac{\partial z}{\partial x}\right)^2 + \left(\frac{\partial z}{\partial y}\right)^2\right)^{1/2} dx dy \quad (111)$$

The surface area of a general ellipsoid after differentiating and simplifying is then:

$$A_s = 8 \int_0^B \int_0^A \left( \frac{A B + \left(\frac{B^2 C^2}{A^2} - B^2\right)x^2 + \left(\frac{A^2 C^2}{B^2} - A^2\right)y^2}{A^2 B^2 - B^2 x^2 - A^2 y^2} \right) dx dy \quad (112)$$

Since this function is not readily integrable, a solution for the surface area is obtained by a numerical approximation. The surface of each model is broken into a series of small finite size surface elements. The sides of these elements are approximated as straight lines and the areas of each element calculated and summed to give the total area of the model. As the size of the surface elements approach zero in the limit, the approximated surface area will equal the true value. However, the use of very small element sizes causes large roundoff errors in the computer as well as increasing the computer time to an excessively high value. To solve this problem the

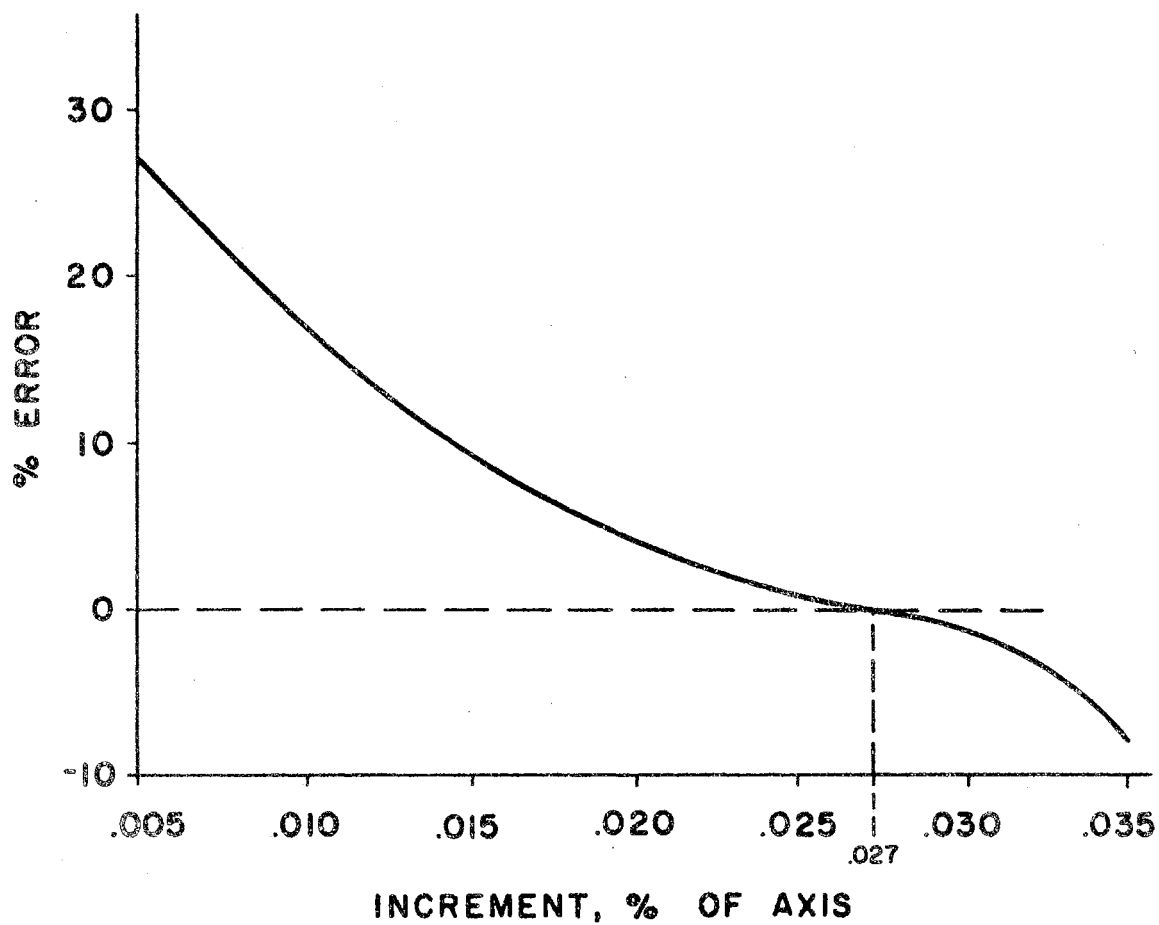


Figure 21. Computer program error function related to the increment size

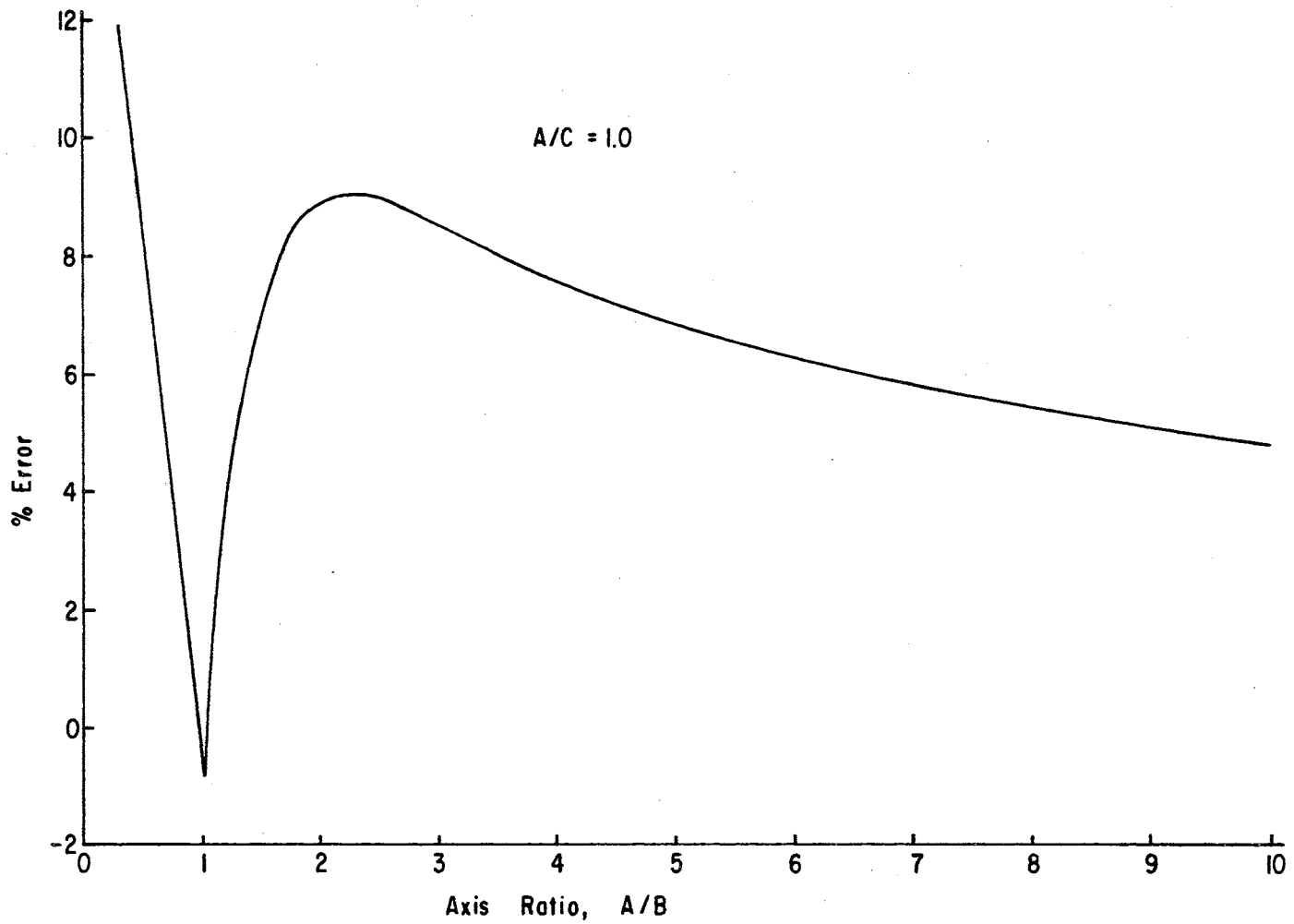


Figure 22. Error function for the computer program as a function of the length ratio, A/B, of the ellipsoid

surface area of a sphere was calculated using several surface element sizes. The percent error as a function of element size is shown in Figure 21. The element size selected was such that the projection of any side on its corresponding axis would be 0.025 times that maximum axis dimension. The surface areas of spheres of varying sizes were calculated using this surface element size. The error in all cases was independent of sphere size. This surface element size was used to calculate the surface area of the general ellipsoid.

With this surface element size, the surface area of several ellipsoids of revolution was calculated. A new error function was calculated and is plotted in Figure 22. It is hypothesized that the error in calculating the surface area by this method is:

$$\% \text{ error} = f(A/B, A/C) \quad (113)$$

For the range of ellipsoids used the component equations of the error function was approximated by several straight line segments in arithmetic coordinates. Since these component equations are straight lines in cartesian coordinates they can be added to predict the error for any given ellipsoid. This error function is of the form:

$$\% \text{ error} = K_1 + K_2(A/B)^{r1} + K_3(A/C)^{r2} \quad (114)$$

where:

$K_1$ ,  $K_2$  and  $K_3$  are dimensionless coefficients

$r_1$  and  $r_2$  are exponents.

Using these results surface areas for the general ellipsoids were calculated as shown in Table V.

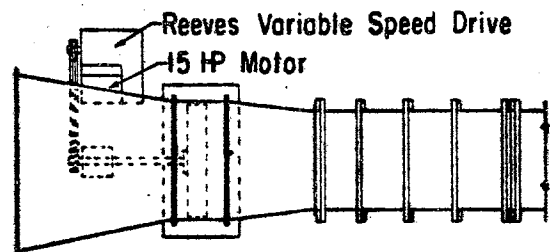
#### Characteristics of the Wind Tunnel

The experiments were conducted in the wind tunnel in the Agricultural Engineering Laboratory at Oklahoma State University. The tunnel has a test section that is 4 ft. by 4 ft. in cross-section. The maximum velocity is limited to approximately 70 ft/sec. A schematic diagram of the tunnel is shown in Figure 23.

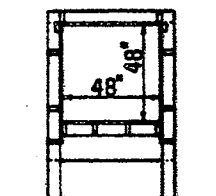
Maher (23) measured both horizontal and vertical velocity profiles along the centerline of the tunnel and perpendicular to the air flow. His results indicated the velocity to be constant across the tunnel except for the six inches immediately adjacent to the wall. A typical velocity profile is shown in Figure 24. Maher measured the average velocity to be 0.9 times the velocity at the center of the tunnel. In this study, the models were all located in the center of the tunnel in the region where the velocity does not vary with location. The center velocity does not vary with location. The center velocity as measured with the pitot-static tube was considered to be the approach velocity throughout this study.

TABLE V  
SURFACE AREAS FOR GENERAL ELLIPSOIDS

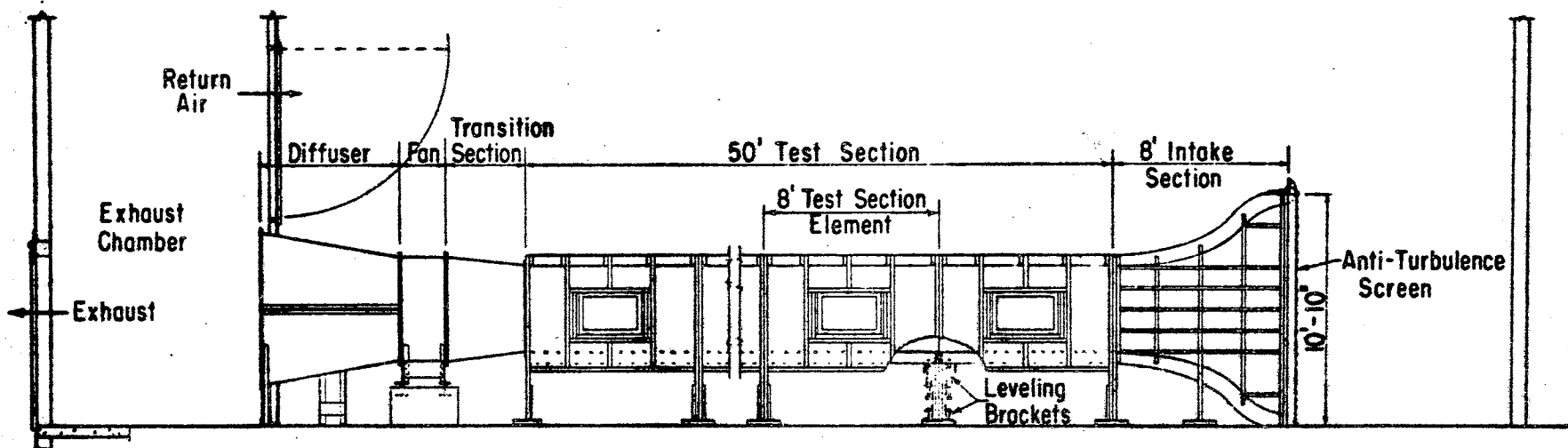
Ellipsoid Axis a in.	Ellipsoid Axis b in.	Ellipsoid Axis c in.	Surface Area in <sup>2</sup>
10.0	7	4	158.71
8.0	10.5	6	212.94
10.0	10.5	6	249.01
10.0	8.75	5	202.34
14.0	10.5	6	336.00
14.0	8.75	5	275.09
12.0	7.0	4	187.51
14.0	7.0	4	215.23
10.0	4.0	4	110.41
10.0	5.0	4	127.09
10.0	6.0	4	143.49
12.5	10.0	5	272.70
10.0	9.0	4	188.45
10.0	10.0	4	202.85



PLAN VIEW - EXHAUST END



CROSS SECTION



ELEVATION - WIND TUNNEL

Figure 23. Agricultural Engineering Research Wind Tunnel

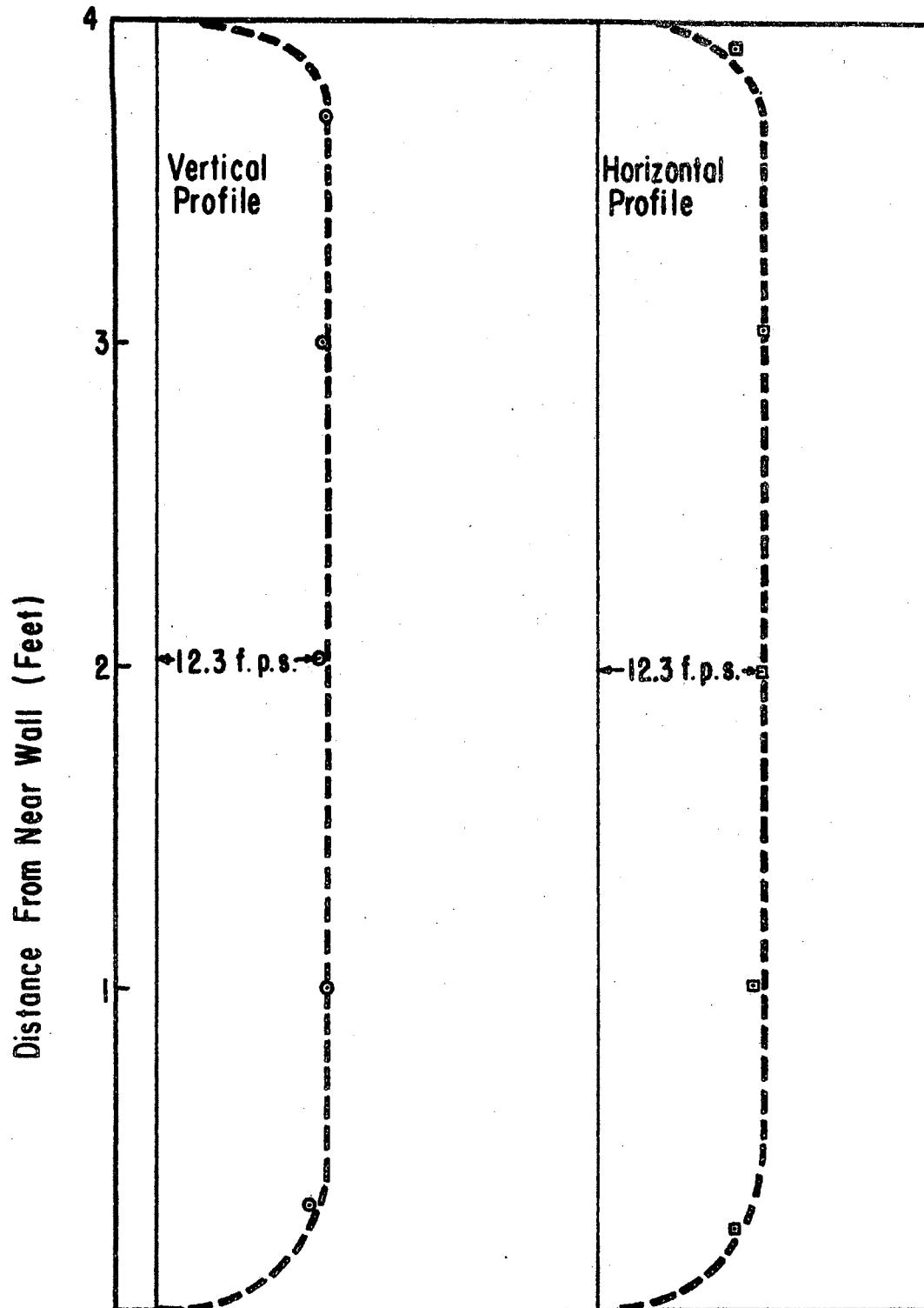


Figure 24. Velocity profiles taken along a horizontal and vertical center line of the wind tunnel. From Maher (23)



A 22-mesh stainless steel screen was installed over the entrance to the intake section of the wind tunnel. This screen was made of number 304 stainless steel wire 0.0132 inches in diameter and had an opening area of 50.5 percent of the gross area. The screen's primary purpose was to smooth out any large fluctuations in velocity that occur during a test.

The turbulence conditions of the air stream can be adequately described by the intensity and scale of turbulence as outlined in Chapter II. It will be recalled that the intensity of turbulence is a measure of the magnitude of the velocity fluctuations while the scale of turbulence may be considered a measure of the size of the turbulent eddies in the flow. As pointed out in Chapter II, one method for defining the turbulent conditions in the tunnel is to measure and report the critical Reynolds Number of a sphere in the specified tunnel. The critical Reynolds Number is defined as the value when the drag coefficient is equal to 0.3. This method was used in this study to define the turbulent conditions existing in the wind tunnel at Oklahoma State University.

A hard rubber bowling ball whose diameter is 8.55 inches was used as the sphere in the turbulence tests. The smooth surfaced ball was mounted on a vertical steel shaft so that the drag force placed the shaft in bending similar to that encountered in a fixed end cantilever beam. The beam was instrumented with a strain gage and calibrated

in test position in the tunnel using a set of dead weights. Thus the drag force exerted on the bowling ball and beam could be measured at any value of Reynolds Number. Because of the weight of the ball, the correction for the drag force on the shaft had to be measured with the ball in test position. To accomplish this the ball was placed in the test position and completely enclosed in a solid and separately supported sheet metal box. The deflection was measured and subtracted from the value for the unshielded ball to give the true deflection due to the drag force on the ball only. Using these values for the drag force, the drag coefficient was computed from

$$C_D = \frac{F}{1/2\rho U_\infty^2 A_p N_e} \quad (99)$$

The results for a number of tests are shown in Figure 25 where the drag coefficient is plotted as a function of the Reynolds Number. The critical Reynolds Number is read from this chart at the point where the drag coefficient is 0.3. The value is

$$Re_{crit.} = 270,000$$

This procedure is in agreement with the method suggested by Dryden and Kuethe (7) for standardizing the reporting of level of wind tunnel turbulence. According to Schlichting (36) page 471 this value for the critical Reynolds Number corresponds to an intensity of turbulence of 0.006.

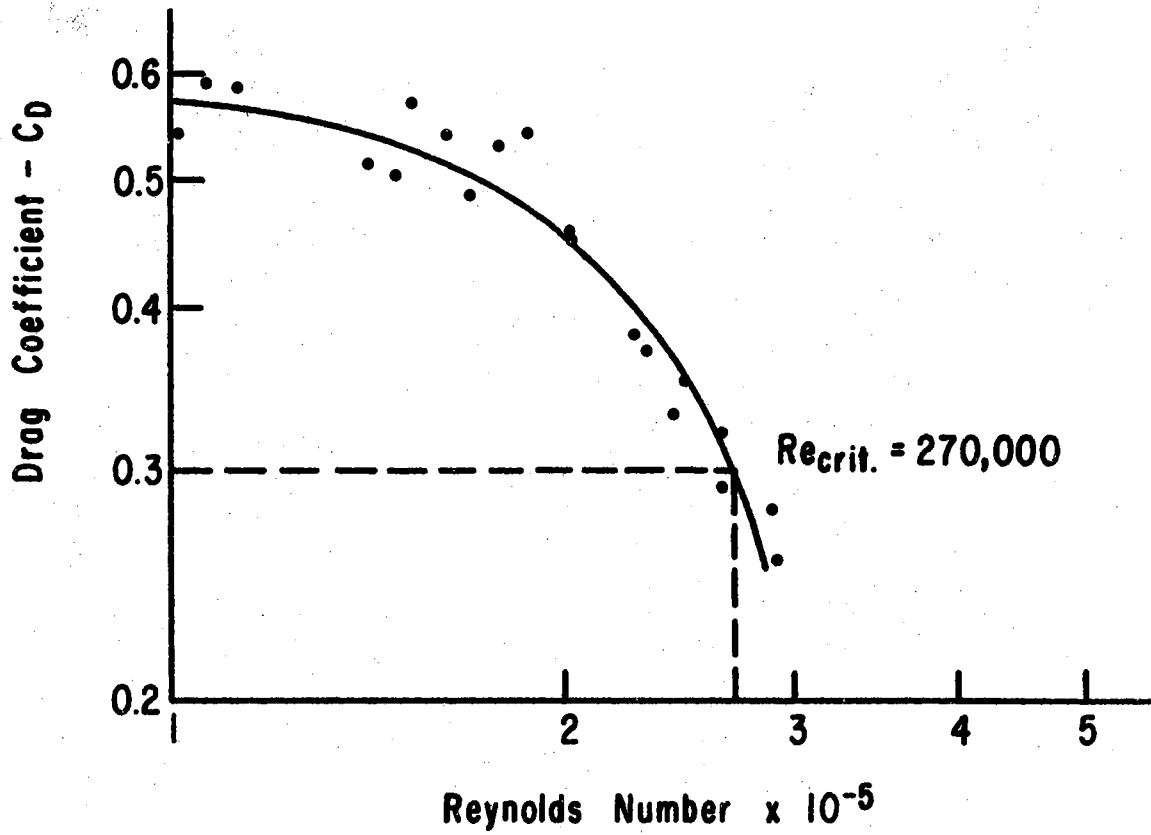


Figure 25. Drag coefficient on a sphere as a function of the Reynolds Number when tested in the OSU wind tunnel

## Summary of Turbulence Properties of the Tunnel

The following observations were made with regard to the turbulence properties of the wind tunnel in the Agricultural Engineering Laboratory at Oklahoma State University. The first point is from this work while the other observations are due to the work of Maher (23).

1. The turbulence properties of the wind tunnel are characterized by a critical Reynolds Number of 270,000.
2. The air in the wind tunnel was turbulent at all fan speeds.
3. For velocities less than 15 feet per second or approximately 10 mph, the fluctuations in velocity were extremely small at any distance greater than about 15 mesh diameters downstream from the screen.
4. When no screen was used in the entrance to the test section, the oscilloscope trace indicated small fluctuations were present, but extremely large peaks in the trace that occurred less frequently than about every five seconds were damped out when a screen was used.
5. The amplitude of velocity fluctuations were noted to increase when Reynolds Number was increased by increasing velocity. Some increase was also noted in frequency of occurrence of fluctuations having the same magnitude as velocity was increased.

## CHAPTER V

### DEVELOPMENT OF THE THEORY

Recall from the experimental design that 4 independent and dimensionless groups (or pi terms) are necessary to adequately describe the convective heat transfer coefficient from a general ellipsoidal model in gas flow with a specified orientation and surface roughness and in an air stream of specified turbulence. These pi terms are

$$\pi_1 = \frac{hc}{k} = Nu$$

$$\pi_3 = \frac{U_{\infty} c_p Ne}{\mu} = Re$$

$$\pi_4 = a/c$$

$$\pi_5 = b/c$$

The experimental plan shown in Table IV was conducted and component equations developed. Three "replications" of each test was conducted in order to minimize any error due to equipment malfunction, operator errors, etc. It will be observed that these repetitions are not true replications because the same model was used in each of the repeated tests. A semi-randomization procedure was used in determining the order in which tests were conducted. A period of three to four days was required for the

instrumenting and checking of each model prior to testing. Therefore to minimize the time and expense in the experimental phase of the work, all tests scheduled for a particular model were completed before the model was removed from the wind tunnel. However the order in which the models were tested was randomly selected by drawing numbers from a hat.

### Component Equations for the Ellipsoidal Model

The analysis requires the development of three component equations. They are:

$$Nu = \pi_1 = F_1(\pi_3, \bar{\pi}_4, \bar{\pi}_5) \quad (115)$$

$$Nu = \pi_1 = F_2(\bar{\pi}_3, \pi_4, \bar{\pi}_5) \quad (116)$$

and

$$Nu = \pi_1 = F_3(\bar{\pi}_3, \bar{\pi}_4, \pi_5) \quad (117)$$

Here the bar over the pi term indicates the group is held constant throughout the series of tests. The surface temperatures have been integrated over the surface to yield the average surface temperature. The reduced data for developing the Nusselt Number dependence on Reynolds Number is shown in Table VI.

The data in Table VI is plotted to yield a straight line in log-log space in Figure 26. The method of least

TABLE VI  
 NUSSELT NUMBER AS A FUNCTION OF REYNOLDS NUMBER  
 WITH  $\pi_4$  AND  $\pi_5$  HELD CONSTANT

Test No.	Reynolds Number	Heat Transfer Coefficient Btu/(hrft <sup>2</sup> °F)	Nusselt Number
1-1	30,522	4.83	108.7
1-2	30,522	4.99	112.4
1-3	30,228	5.81	121.6
2-1	40,819	5.96	134.3
2-2	40,819	5.67	127.7
2-3	41,038	5.91	133.2
3-1	52,697	6.71	151.2
3-2	52,697	6.90	155.5
3-3	52,527	7.08	159.4
4-1	70,447	8.69	195.8
4-2	70,319	8.13	183.2
4-3	70,192	9.13	205.6
5-1	88,078	9.57	215.4
5-2	88,100	8.90	200.5
5-3	87,976	6.40	215.9
6-1	105,734	10.32	232.6
6-2	105,734	10.20	229.7
6-3	105,649	10.06	226.7
7-1	123,187	9.78	244.5
7-2	123,041	11.30	254.5
7-3	123,114	11.08	249.5
8-1	140,894	11.99	270.0
8-2	140,894	11.63	262.0
8-3	140,639	11.83	266.4
9-1	144,410	10.06	256.2
9-2	145,769	12.51	281.8
9-3	146,321	11.99	270.3

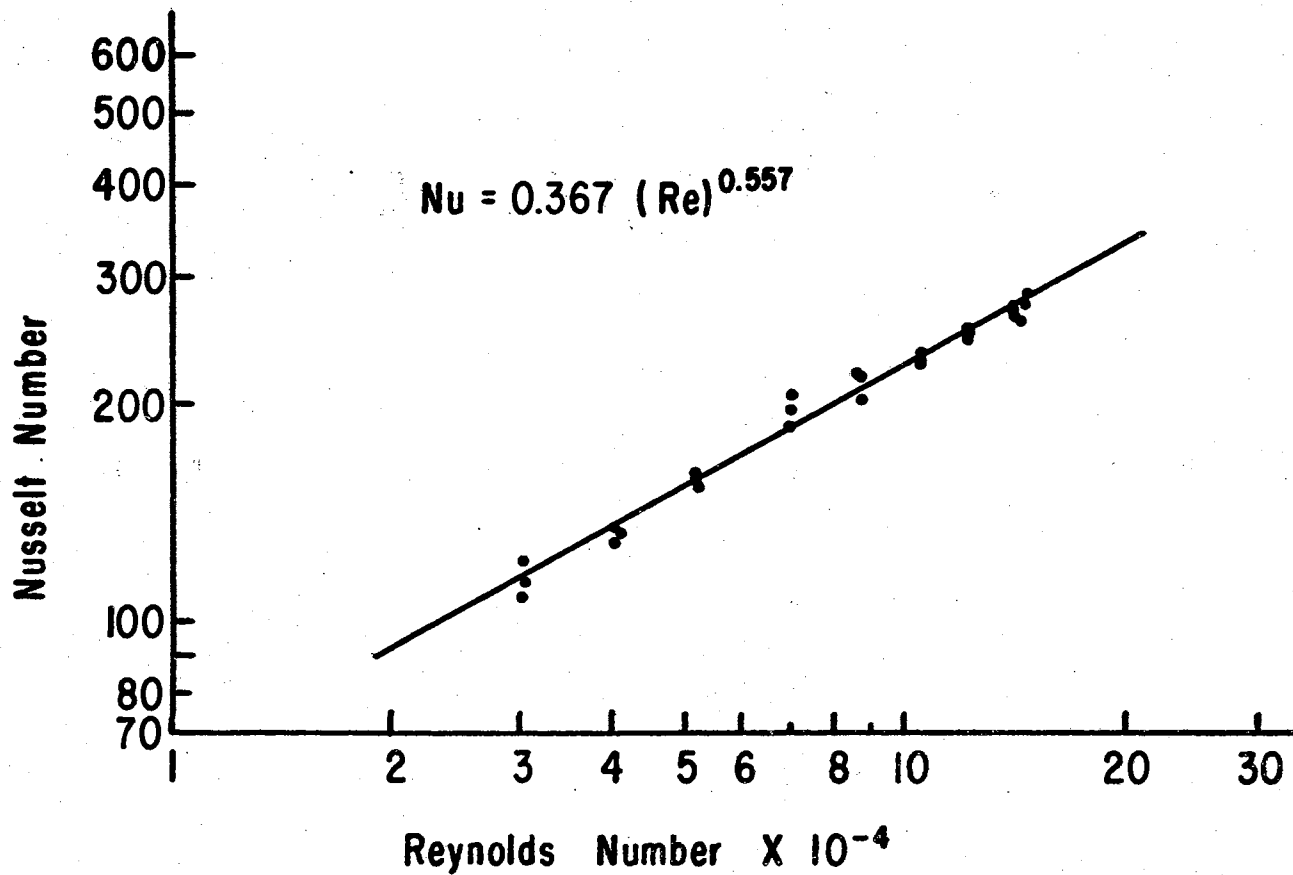


Figure 26. Nusselt Number vs. the Reynolds Number for the ellipsoidal model



squares was used to fit the straight line to the experimental data. The results are

$$Nu = 0.367(Re)^{0.557} \quad (118)$$

with a regression correlation coefficient,  $r = 0.991$  and a standard deviation,  $s = 0.018$  where the standard deviation is expressed in logarithmic units. Note that the results are valid over the Reynolds Number range from 30,000 to 150,000. The Prandtl Number is held constant at 0.72 by using air as the fluid medium. The other two pi terms,  $\pi_4$  and  $\pi_5$ , are held constant at the following values.

$$\bar{\pi}_4 = 2.50$$

$$\bar{\pi}_5 = 1.75$$

The dependence of the Nusselt Number on the length ratio,  $a/c$ , is tabulated in reduced form in Table VII. A logarithmic transformation is used to transform the data to a straight line in Figure 27. From a least squares analysis the function is

$$Nu = 230.21(a/c)^{-0.070} \quad (119)$$

The regression correlation coefficient is  $r = 0.559$  with a standard deviation in logarithmic units of 0.014. The Reynolds Number was held constant at approximately 123,000 and the length ratio,  $b/c$ , at 1.75. The small exponent on

TABLE VII  
 NUSSELT NUMBER AS A FUNCTION OF THE LENGTH RATIO,  $a/c$   
 WITH  $\pi_3$  AND  $\pi_5$  HELD CONSTANT

Run No.	Reynolds Number	Heat Transfer Coefficient Btu/(hrft <sup>2</sup> °F)	Nusselt Number	$\pi_4$ $a/c$
10-1	122,950	6.66	225.2	1.33
10-2	122,950	7.17	242.3	1.33
10-3	122,950	6.68	225.6	1.33
11-1	124,255	6.69	226.1	1.67
11-2	122,786	6.56	221.8	1.67
11-3	122,950	6.35	214.6	1.67
12-1	122,379	7.52	211.7	2.00
12-2	124,421	7.61	214.4	2.00
12-3	123,178	7.11	200.2	2.00
13-1	123,114	6.42	216.9	2.33
13-2	123,604	6.43	217.2	2.33
13-3	123,441	6.48	219.0	2.33
14-1	123,187	9.78	244.5	2.50
14-2	123,041	11.30	254.5	2.50
14-3	123,114	11.08	249.5	2.50
15-1	123,178	7.65	215.2	2.80
15-2	123,178	7.55	212.6	2.80
15-3	123,178	7.67	215.9	2.80
16-1	122,823	9.47	213.2	3.00
16-2	122,677	9.56	215.3	3.00
16-3	123,984	9.70	218.4	3.00

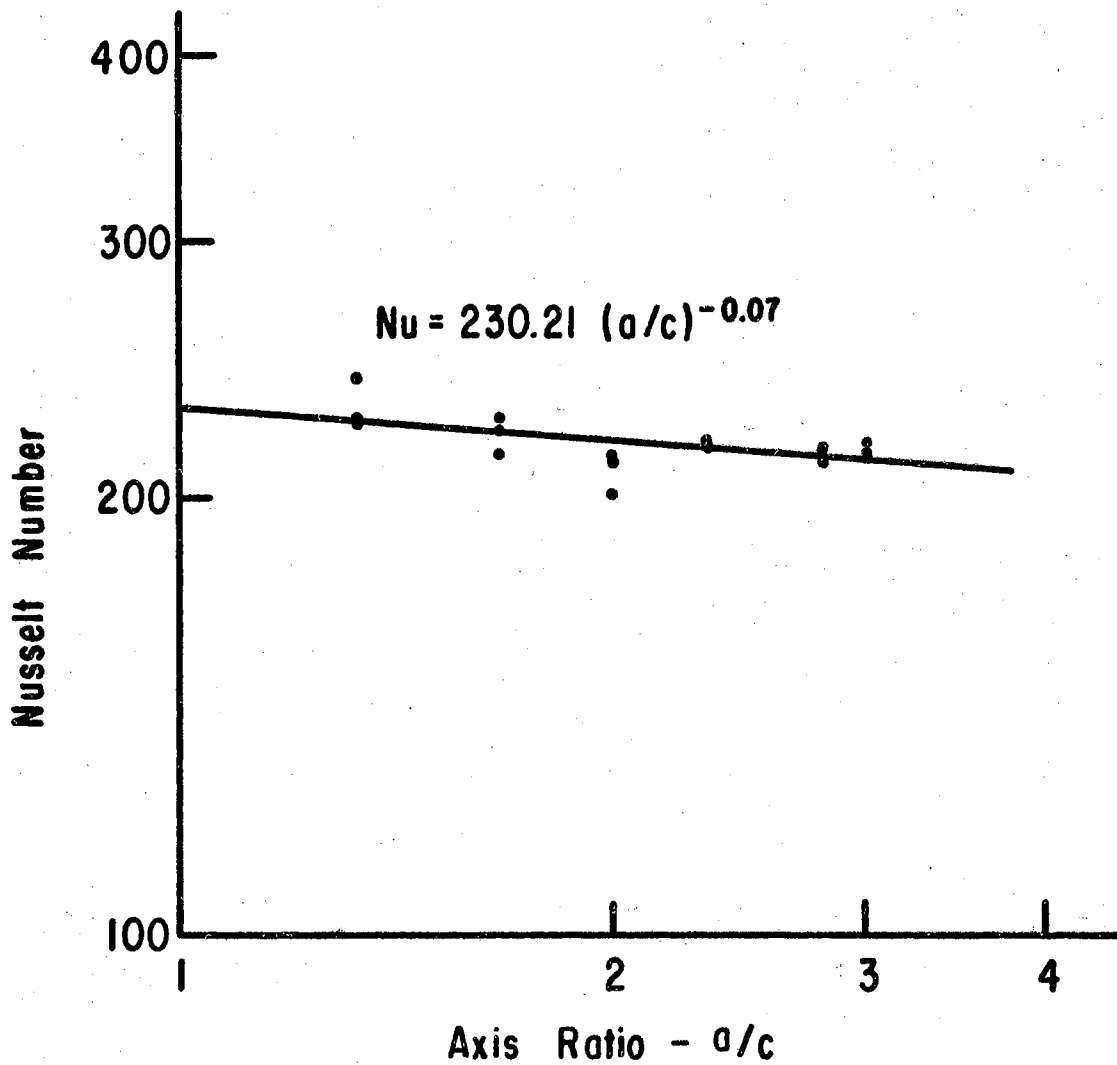


Figure 27. Nusselt Number vs. the length ratio,  $a/c$ , for the ellipsoidal model

the  $a/c$  ratio indicates very little change in the heat transfer coefficient with a change in the length of the ellipsoid, i.e., the horizontal dimension perpendicular to air flow. This, of course, is expected since the cross-sectional shape does not change as the length "a" changes within the range of values of  $a/c$  used in these tests. It seems plausible that the Nusselt Number dependence should take the form shown in Figure 28. This requires that as  $a/c \rightarrow 0$  that the heat transfer coefficient would approach the value for the finite flat plate that is elliptical in shape. As  $a/c \rightarrow \infty$  the shape would become an infinite elliptical cylinder. The range of values of  $a/c$  considered in this study is indicated by the portion of the curve between  $(a/c)_1$  and  $(a/c)_2$ . Sufficient data is not available to define completely the exponential curve in Figure 28. It would, therefore, be dangerous to extend the results to values of  $a/c$  less than 1.33. Values of  $a/c$  greater than the limits of these tests should not introduce large errors since the slope of the curve is close to zero.

The values for the Nusselt Number as a function of  $\pi_5$  is tabulated in Table VIII. Using the logarithmic transformation and a least squares analysis the correlation is described by

$$\text{Nu} = 256.38 (b/c)^{-0.440} \quad (120)$$

and is plotted in Figure 29. The correlation coefficient is  $r = 0.898$  with a standard deviation in logarithmic units

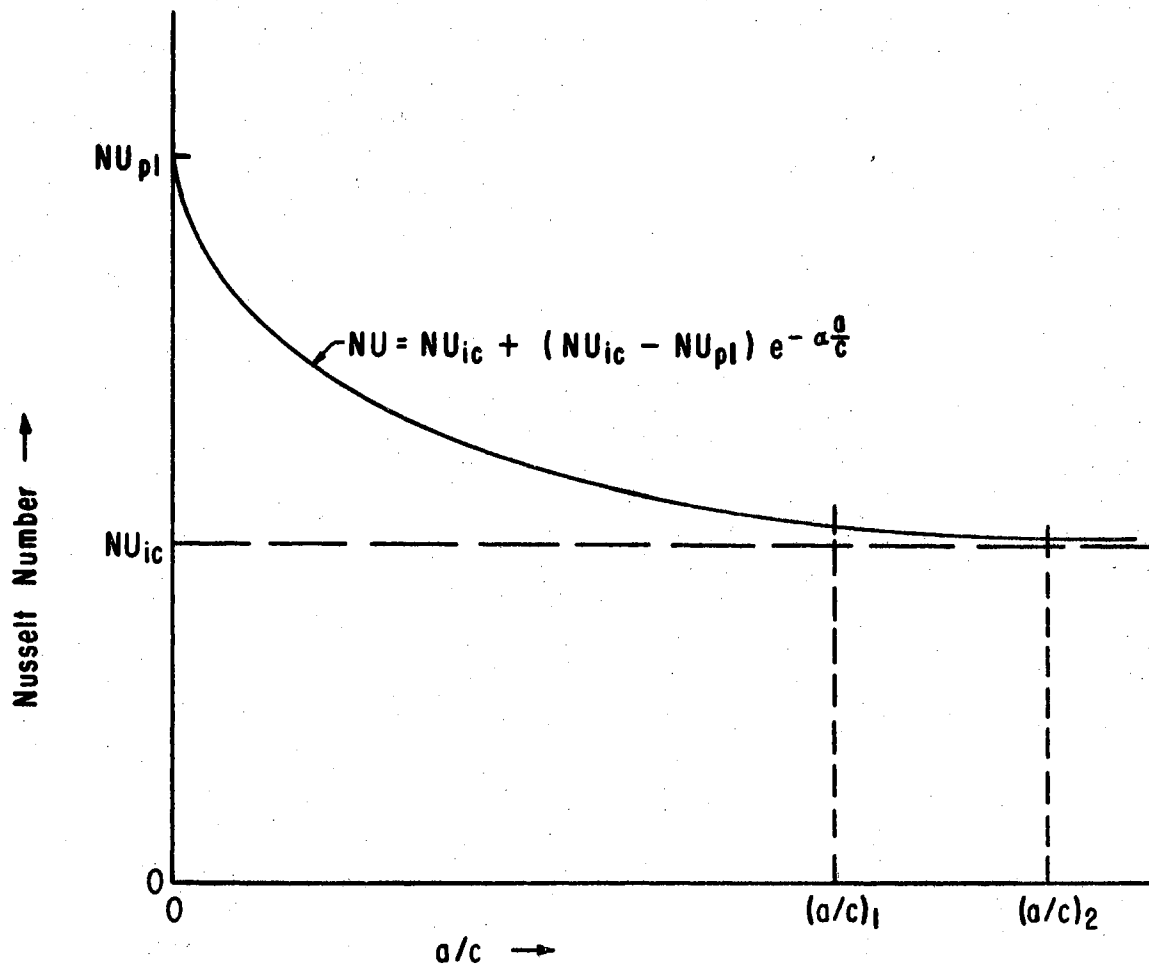


Figure 28. Hypothesized shape of the Nusselt Number vs. a/c function

TABLE VIII  
 NUSSELT NUMBER AS A FUNCTION OF THE LENGTH RATIO,  $b/c$ ,  
 WITH  $\pi_3$  AND  $\pi_4$  HELD CONSTANT

Run No.	Reynolds Number	Heat Transfer Coefficient Btu/(hrft <sup>2</sup> °F)	Nusselt Number	$\pi_5$ b/c
18-1	122,968	10.46	235.6	1.00
18-2	123,186	10.68	240.5	1.00
18-3	123,187	10.79	243.1	1.00
19-1	123,114	10.93	246.2	1.25
19-2	123,295	11.29	254.3	1.25
19-3	123,114	11.83	266.5	1.25
20-1	121,944	9.30	209.4	1.50
20-2	123,114	9.32	209.9	1.50
20-3	123,114	9.07	204.3	1.50
21-1	123,187	9.78	244.5	1.75
21-2	123,041	11.30	254.5	1.75
21-3	123,114	11.08	249.5	1.75
22-1	123,405	7.37	207.5	2.00
22-2	123,744	7.27	204.6	2.00
22-3	123,177	7.32	206.2	2.00
23-1	123,114	7.48	168.4	2.25
23-2	123,114	7.37	166.0	2.25
23-3	123,114	7.42	167.1	2.25
24-1	123,114	7.75	174.6	2.50
24-2	123,259	7.63	171.9	2.50
24-3	123,041		161.5	2.50

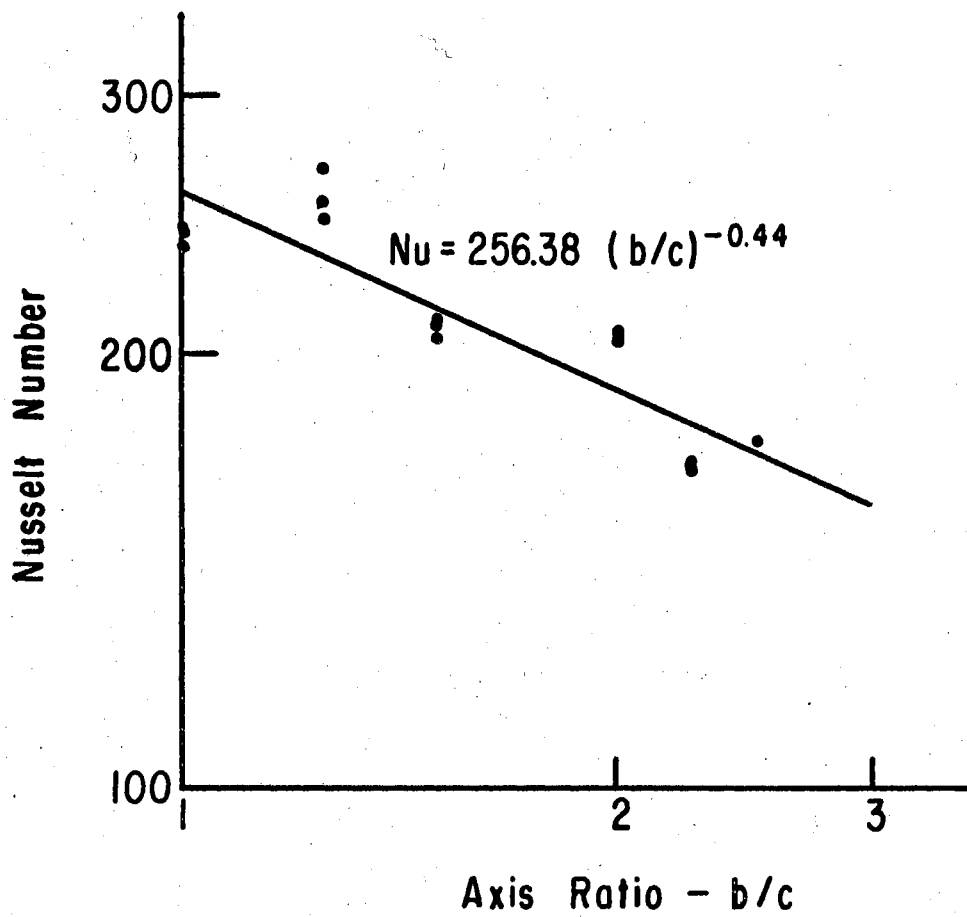


Figure 29. Nusselt Number as a function of the length ratio  $b/c$  for the ellipsoidal model.

of 0.032. Throughout the development of these results the values of  $\pi_3$  and  $\pi_4$  were held constant at

$$\pi_3 = 123,000$$

$$\pi_4 = 2.50$$

### Prediction Equation for the General Ellipsoid

Murphy (27) described methods for combining component equations to give the general prediction equation as provided on page 41. For component equations that form straight lines on log-log coordinates, combination is of the form

$$\pi_1 = \frac{F_1(\pi_3, \bar{\pi}_4, \bar{\pi}_5) F_2(\bar{\pi}_3, \pi_4, \bar{\pi}_5) F_3(\bar{\pi}_3, \bar{\pi}_4, \pi_5)}{[F_4(\bar{\pi}_3, \bar{\pi}_4, \bar{\pi}_5)]^2} \quad (121)$$

Again the bar over the pi terms indicate those quantities that are held constant during the indicated series of experimental tests.

The component equations from this study are

$$F_1(\pi_3, \bar{\pi}_4, \bar{\pi}_5) = 0.367(\text{Re})^{0.557} \quad (122)$$

$$F_2(\bar{\pi}_3, \pi_4, \bar{\pi}_5) = 230.2(a/c)^{-0.070} \quad (123)$$

$$F_3(\bar{\pi}_3, \bar{\pi}_4, \pi_5) = 256.38(b/c)^{-0.440} \quad (124)$$

The constant values for the pi terms are

$$\bar{\pi}_3 = \text{Re} = 123,000$$



$$\bar{\pi}_4 = a/c = 2.50$$

$$\bar{\pi}_5 = b/c = 1.75$$

$F_4(\pi_3, \pi_4, \pi_5)$  may be calculated from either equation 122, 123, or 124. The results are

$$[F_4(\bar{\pi}_3, \bar{\pi}_4, \bar{\pi}_5)] = 0.367(Re)^{0.557} = 0.367(123,000)^{0.557} = 251.03$$

$$[F_4(\bar{\pi}_3, \bar{\pi}_4, \bar{\pi}_5)] = 256.38(b/c)^{-0.44} = 256.38(1.75)^{-0.44} = 200.45$$

$$[F_4(\bar{\pi}_3, \bar{\pi}_4, \bar{\pi}_5)] = 230.21(a/c)^{-0.07} = 230.21(2.5)^{-0.07} = 215.95$$

therefore

$$F_4(\bar{\pi}_3, \bar{\pi}_4, \bar{\pi}_5) = \frac{[F_4(\bar{\pi}_3, \bar{\pi}_4, \bar{\pi}_5)]_1 + [F_4(\bar{\pi}_3, \bar{\pi}_4, \bar{\pi}_5)]_2 + [F_4(\bar{\pi}_3, \bar{\pi}_4, \bar{\pi}_5)]_3}{3}$$

$$= 222.48$$

substituting these values into equation 121 yields

$$Nu = \pi_1 = \frac{0.367(Re)^{0.557} (256.38)(b/c)^{-0.44} (230.21)(a/c)^{-0.07}}{(222.48)^2}$$

after simplifying

$$Nu = 0.438(Re)^{0.557} (a/c)^{-0.07} (b/c)^{-0.44} \quad (125)$$

Equation 125 was developed from experimental data with the following limits placed on each dimensionless group.

$$30,000 \leq Re \leq 150,000$$

$$1.33 \leq a/c \leq 3.00$$

$$1.00 \leq b/c \leq 2.50$$

Extrapolation beyond this range of values for the independent variables is not generally recommended. Equation 125 was developed using air as the fluid medium. The Prandtl Number for air at moderate temperatures and pressures is very closely estimated by considering it constant at 0.72. The Prandtl Number for most other gases is within 10% of the value for air so that applying this equation to systems where gases other than air is used would not induce large errors. However, when the Prandtl Number differs significantly from 0.72 as is the case for most liquids equation 125 is no longer valid.

Kays (19) noted the Nusselt Number varies approximately as the  $(Pr)^{1/3}$  for bodies with boundary layer separation, except for very low Prandtl Numbers, i.e. Prandtl Numbers on the order of those encountered in liquid metals. Based on this approximation equation 125 can be extended to cover fluids in the moderate Prandtl Number range. The result is

$$Nu = 0.489(Pr)^{1/3}(Re)^{0.557}(a/c)^{-0.07}(b/c)^{-0.44} \quad (126)$$

As reported earlier in this paper Ko and Sogin (20) determined the heat transfer coefficient from an ellipsoidal surface of axis ratio 4:1. By transliteration Ko showed the expression for the average heat transfer coefficient as

$$\left(\frac{h}{G_1 C_p}\right)(Pr)^{2/3} \left(\frac{G_1 S}{\mu}\right)^{1/2} = \beta \quad (93)$$

where

$h$  = Average heat transfer coefficient, Btu/(Hr ft<sup>2</sup>°F)

$G_1$  = Mass air velocity, lb<sub>m</sub>/(sec ft<sup>2</sup>)

$C_p$  = Fluid specific heat, Btu/(lb<sub>m</sub>°F)

$S$  = Total length of ellipsoidal surface measured from the stagnation point along the meridian profile, ft.

$\mu$  = Fluid viscosity, lb<sub>f</sub> sec/ft<sup>2</sup>.

Ko measured  $\beta$  to be 0.76 for an axis ratio of 4:1 and he reported that Lewis measured  $\beta$  to be 0.60 for the ellipsoid of revolution with an axis ratio of 3:1.

The results from Ko and Lewis are compared with the predicted results from equation 125 in Figure 30.

Variations in predicted values from both works are no more than five percent in the Reynolds Number range from 30,000 to 150,000. This variation probably needs no explanation since variation in experimental techniques could result in differences this large. However, it should be pointed out that no knowledge of the turbulence characteristics of the wind tunnels used by Ko and Lewis is available. As suggested in Chapter II a variation in wind tunnel turbulence could have large influences on the heat transfer coefficients from the ellipsoidal shapes and could account for the variation between these reports. **Nu calculated from equation 126 is plotted against Nu observed in Figure 31.**

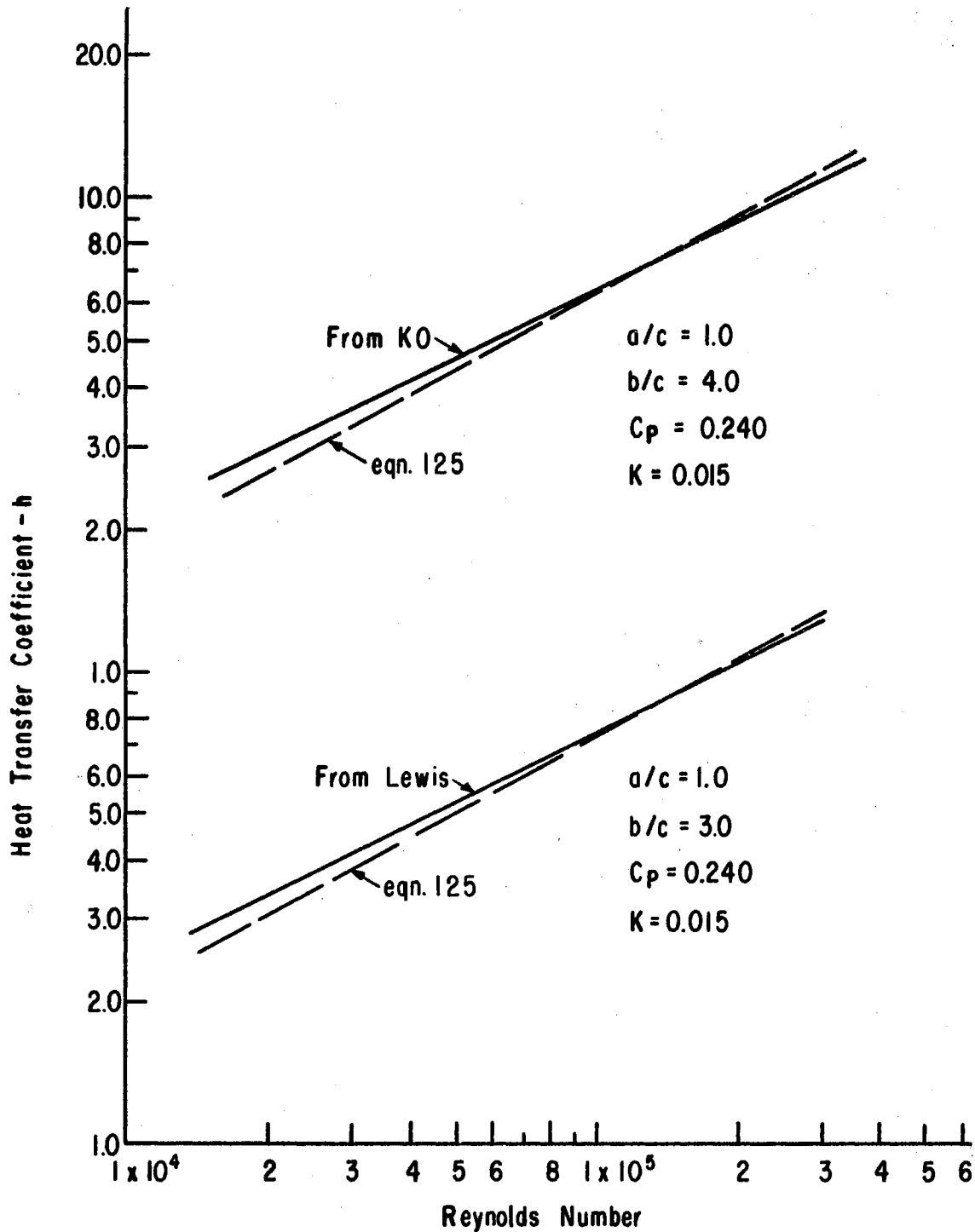


Figure 30. The Nusselt Number vs. Reynolds Number calculated from equation 125 and compared with the results of Ko and Lewis

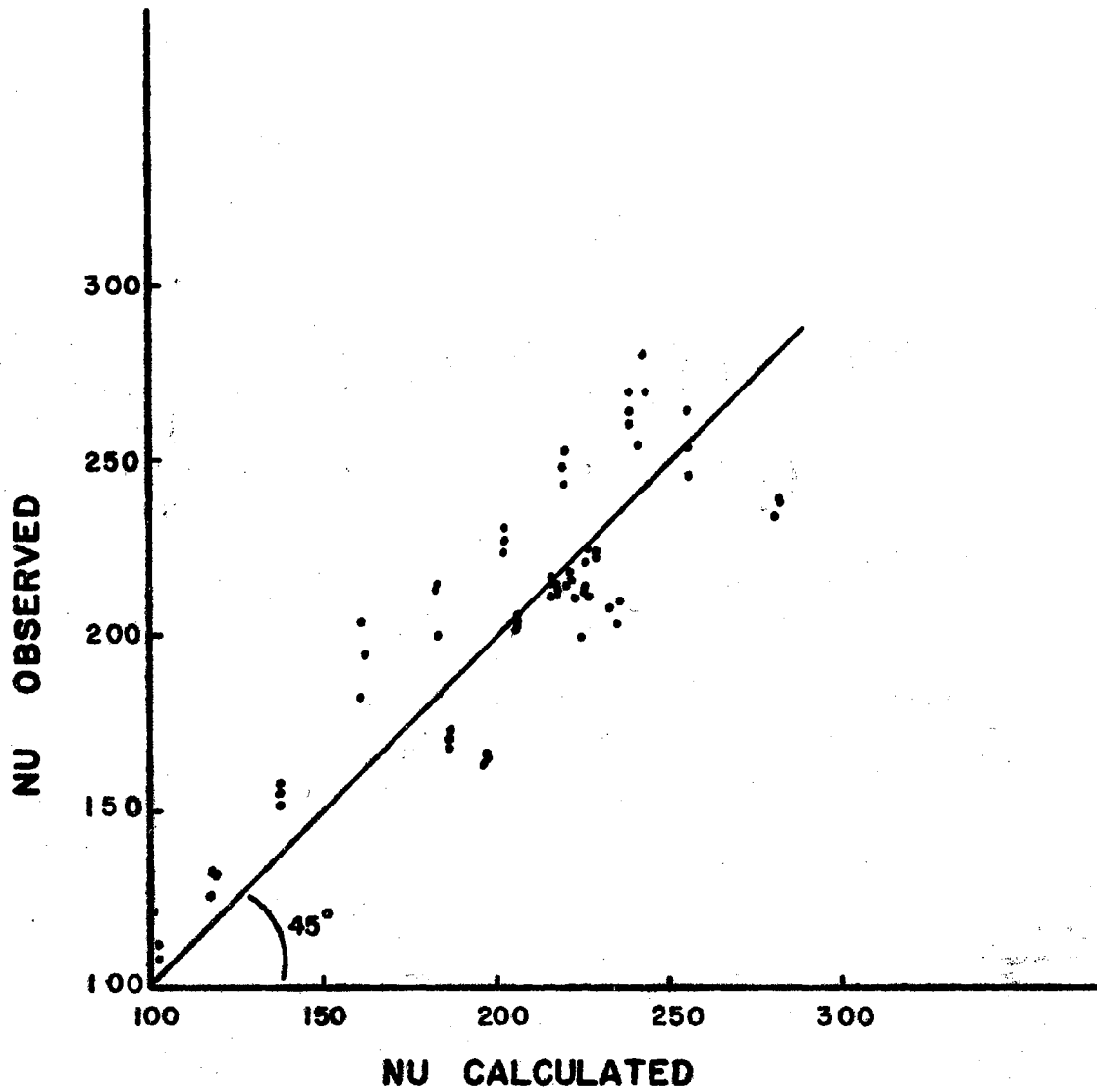


Figure 31. Nusselt Number Calculated vs. Nusselt Number Observed for the General Ellipsoid

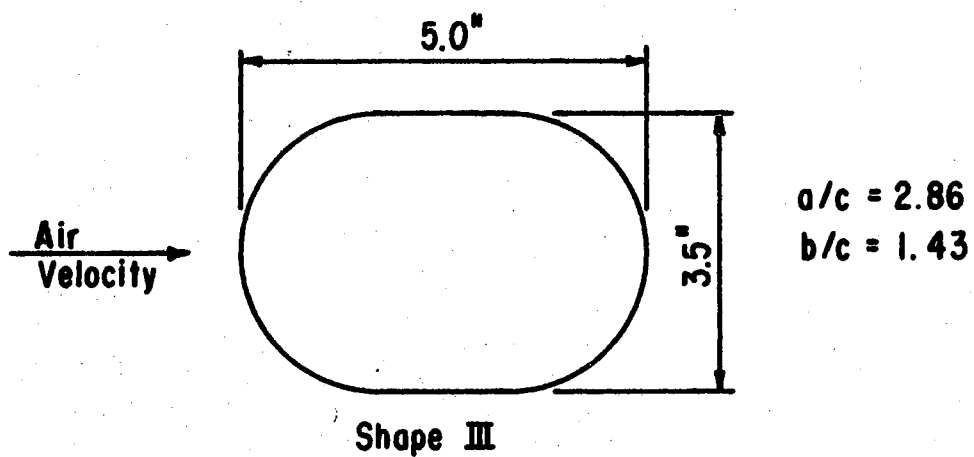
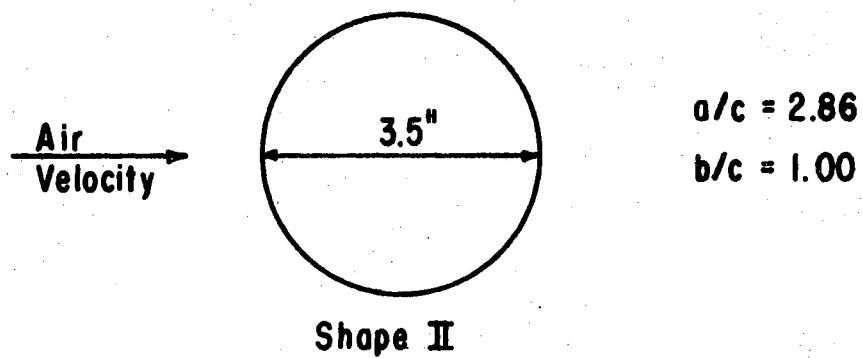
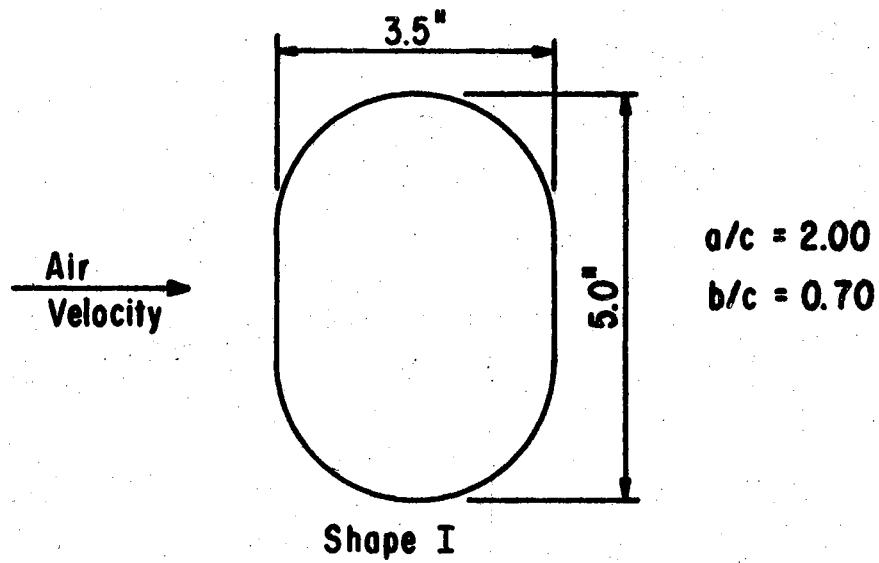


Figure 32. Orientation of Shapes I, II and III during the experimental tests

TABLE IX  
 NUSSELT NUMBER VS. REYNOLDS NUMBER FOR SHAPE I  
 a=10.0 in; b=3.50 in; c=5.0 in

Test Number	Heat Transfer Coefficient Btu/(hrft <sup>2</sup> °F)	Reynolds Number	Nusselt Number
1-1	5.19	32,616	146.2
1-2	4.94	35,493	139.1
2-1	5.36	43,308	151.0
2-2	5.39	43,630	151.6
3-1	6.84	65,659	192.6
3-2	6.67	65,659	187.6
4-1	7.90	87,740	222.3
4-2	7.43	88,218	209.2
5-1	9.25	109,843	260.5
5-2	9.37	110,097	263.8
6-1	11.13	131,956	313.5
6-2	10.78	132,062	303.5
7-1	11.52	153,802	324.4
7-2	11.81	153,984	332.4
8-1	14.69	171,201	410.9
8-2	12.79	172,098	360.0

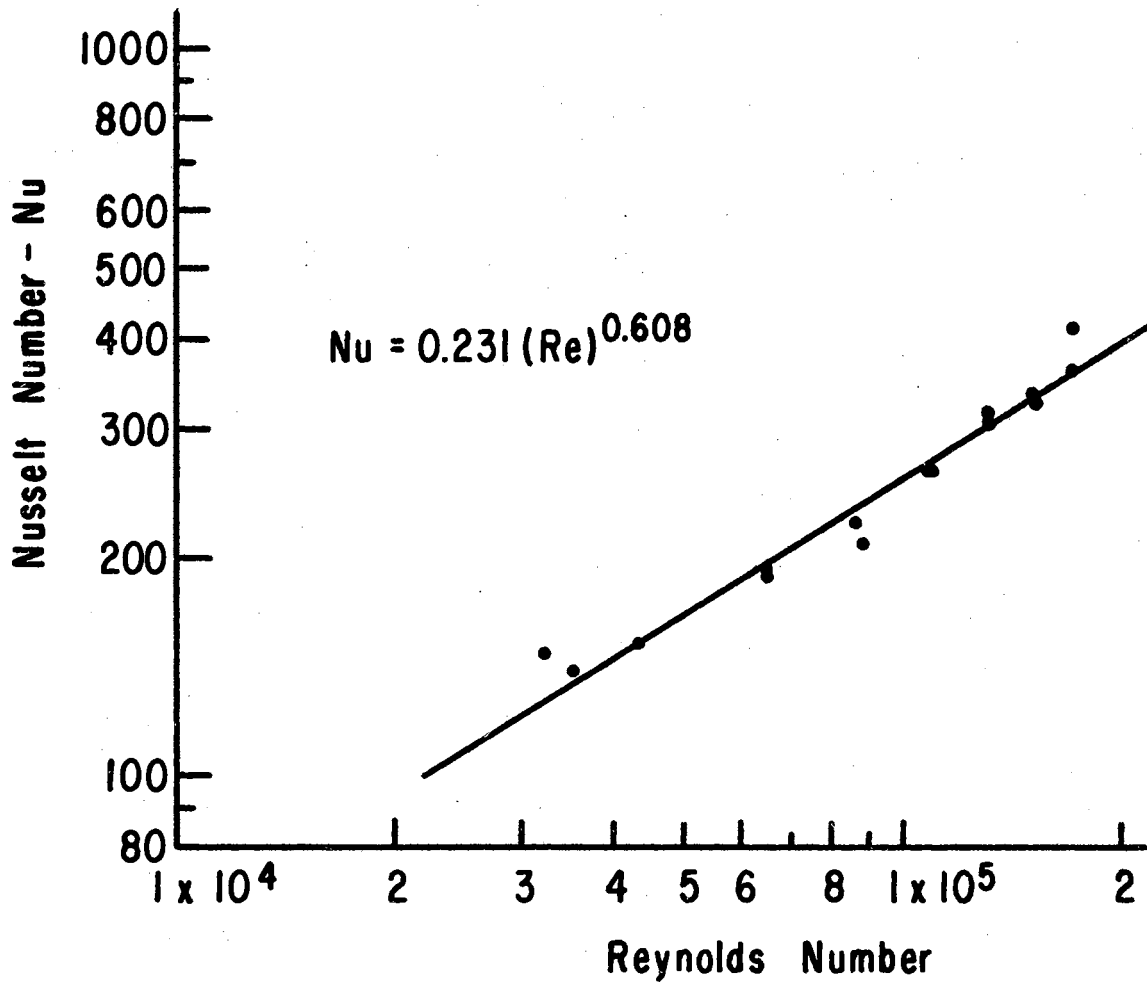


Figure 33. Nusselt Number vs. Reynolds Number for Shape I.



### Irregular Shapes

Three shapes were constructed of 3/16" thick aluminum and instrumented as described earlier for the ellipsoidal model. One of the shapes was a finite cylinder whose length was 10 inches and diameter was 3.5 inches. The other two shapes were designed to approximate the shape found in boneless processed hams. In all cases the length was 10 inches, however dimensions b and c varied. The cross-sections including dimensions b and c are shown in Figure 32. For convenience the irregular shapes will be referred to hereafter as

Shape I: a=10 in.; b=3.5 in.; c=5.0 in.

Shape II: a=10 in.; b=3.5 in.; c=3.5 in.

Shape III: a=10 in.; b=5.0 in.; c=3.5 in.

The dimension c is vertical and perpendicular to fluid flow. It is the length dimension used in the Reynolds Number.

After the shapes were instrumented, a series of tests were conducted varying the air velocity through the range available in the wind tunnel. The Nusselt Number as a function of Reynolds Number is tabulated in Table IX for Shape I. A linear regression was performed on the data after converting to logarithmic coordinates to yield

$$\text{Nu} = 0.231(\text{Re})^{0.608} \quad (127)$$

TABLE X  
 NUSSELT NUMBER VS. REYNOLDS NUMBER FOR SHAPE II  
 a=10.0 in; b=3.50 in; c=3.50 in

Test Number	Heat Transfer Coefficient Btu/(hrft <sup>2</sup> °F)	Reynolds Number	Nusselt Number
2-1	5.78	30,765	113.8
2-2	4.25	30,089	83.7
2-3	6.12	31,644	120.6
3-1	6.98	46,259	137.6
3-2	7.21	46,110	142.2
3-3	13.33	45,961	145.8
4-1	8.96	61,082	176.5
4-2	10.74	61,194	211.7
4-3	7.48	61,082	148.6
5-1	9.99	76,890	196.9
5-2	10.23	76,979	201.6
5-3	10.42	76,979	205.3
6-1	11.63	92,517	229.1
6-2	11.62	92,369	228.9
6-3	11.39	92,369	224.4
7-1	12.55	107,916	247.2
7-2	11.92	107,852	234.9
7-3	13.03	107,789	256.8
8-1	13.57	117,412	267.5
8-2	13.44	120,241	264.9

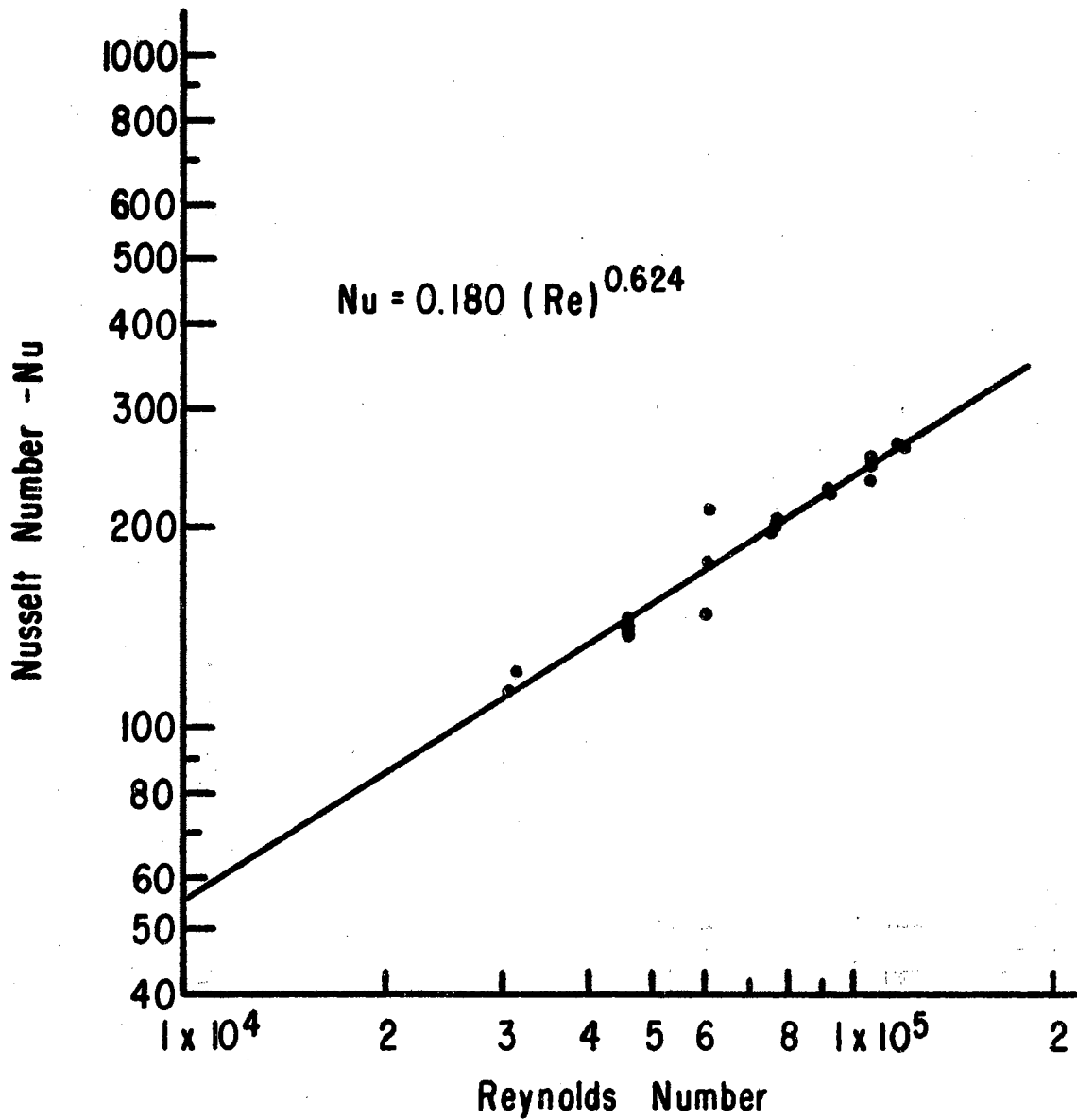


Figure 34. Nusselt Number vs. Reynolds Number for Shape II.

The data is plotted in Figure 33 and shows a regression correlation coefficient of 0.98 and a standard deviation of 0.0295 in the logarithmic coordinate system.

The results for Shape II, the finite cylinder are tabulated in Table X and plotted in Figure 34. The least squares analysis yields

$$\text{Nu} = 0.180(\text{Re})^{0.624} \quad (128)$$

with a regression correlation coefficient of 0.97 and a standard deviation 0.0289 in logarithmic coordinates. It is interesting to note that this result for the finite cylinder is almost identical to the values reported by Hilpert (18) for the Nusselt Number for infinite cylinders in the Reynolds Number range from 4,000 to 40,000. He reported that

$$\text{Nu} = 0.174(\text{Re})^{0.618} \quad (89)$$

This serves to help verify the earlier conclusion that the model length,  $a$ , has little effect on the average heat transfer coefficient as long as the cross-sectional shape is geometrically similar throughout.

Shape III is similar to Shape I except for the direction of air flow. In fact the orthogonal directions  $b$  and  $c$  are reversed in this shape compared to Shape I. The Nusselt Number for Shape III is tabulated in Table XI and plotted in log-log space in Figure 35. The least squares analysis yields

TABLE XI  
 NUSSELT NUMBER VS. REYNOLDS NUMBER FOR SHAPE III  
 a=10 in; b=5.0 in; c=3.5 in

Test Number	Heat Transfer Coefficient Btu/(hrft <sup>2</sup> °F)	Reynolds Number	Nusselt Number
1-1	5.26	24,567	103.7
1-2	5.76	26,189	113.5
2-1	6.69	30,765	131.8
2-2	6.65	30,765	131.0
3-1	7.67	45,961	151.2
3-2	7.97	46,110	157.2
4-1	10.22	61,863	201.4
4-2	10.75	61,641	211.8
5-1	11.89	77,246	234.4
5-2	11.78	76,890	232.2
6-1	13.49	92,369	265.8
6-2	13.08	92,517	257.8
7-1	14.74	107,661	290.4
7-2	14.82	107,852	292.0
8-1	16.43	119,612	323.9
8-2	15.42	118,227	303.9

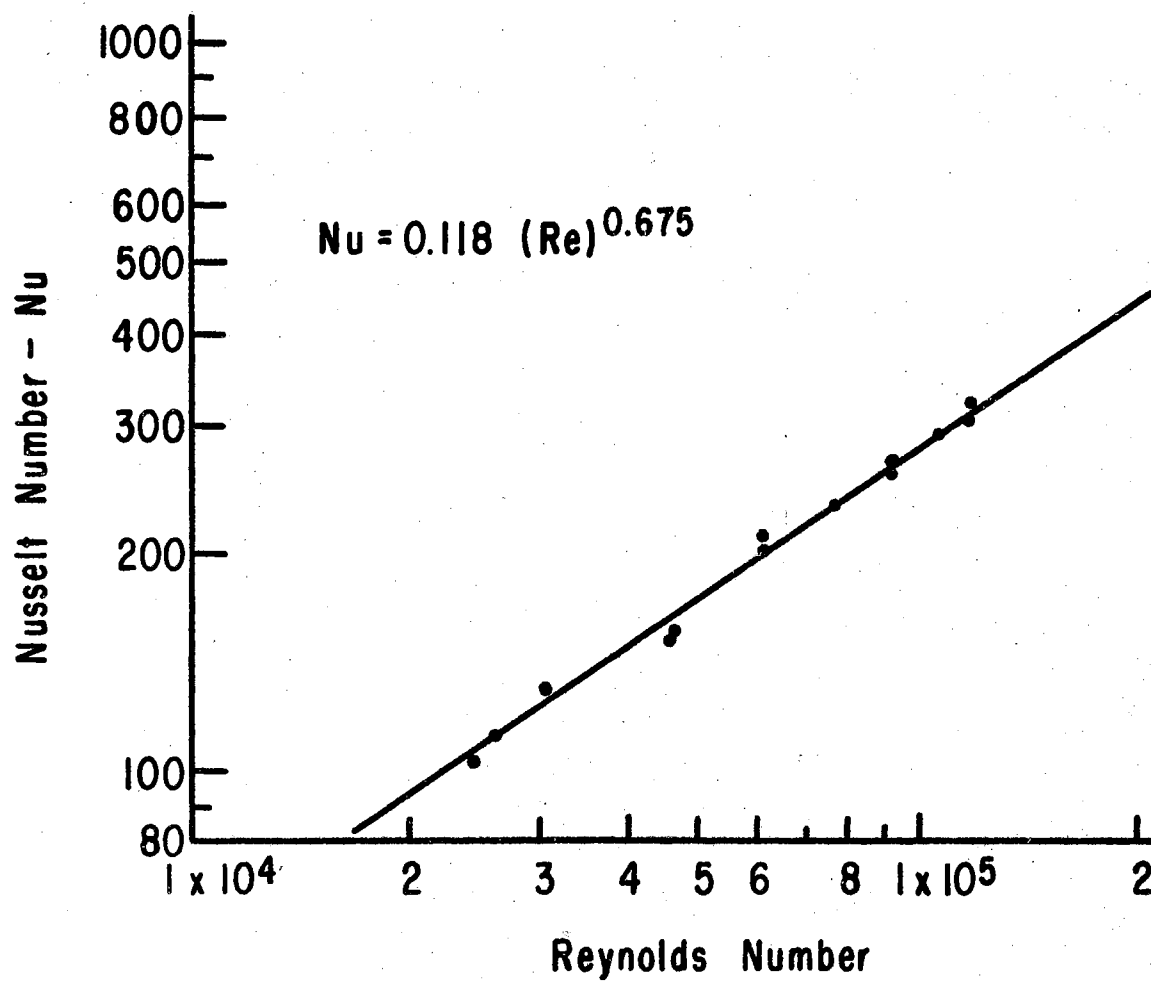


Figure 35. Nusselt Number vs. Reynolds Number for Shape III

$$\text{Nu} = 0.118(\text{Re})^{0.675} \quad (129)$$

with a linear regression correlation coefficient of 0.995 and a logarithmic standard deviation of 0.0165.

The exponent on the Reynolds Number and the constant coefficient varies as the geometry of the shape varies. Any criteria for replacing an irregular shape with an ellipsoidal model will have to operate on both ~~these quantities~~ to be successful.

It is interesting to look at the point at which the curves converge when the irregular shape is assumed to be replaced by an ellipsoidal model whose three orthogonal dimensions are the same as for the irregular shape. Call the point where the Nusselt Number for the irregular shape equals the Nusselt Number for the equivalent ellipsoid  $\text{Re}_{\text{conv}}$ . If we plot  $\text{Re}_{\text{conv}}$  as a function of  $b/c$  with both transformed logarithmically it yields a straight line as shown in Figure 36. The simple dots in Figure 36 are for the three irregular shapes used in this study. This result indicates no dependence on the length ratio,  $a/c$ . This is as should be expected because of the small dependence of the Nusselt Number on  $a/c$ .

To compare this result with other irregular shapes as reported by other investigators, correlations for four different irregular shapes were used. These correlations were for infinitely long shapes but since the Nusselt Number is not strongly dependent upon shape length, an  $a/c$  ratio

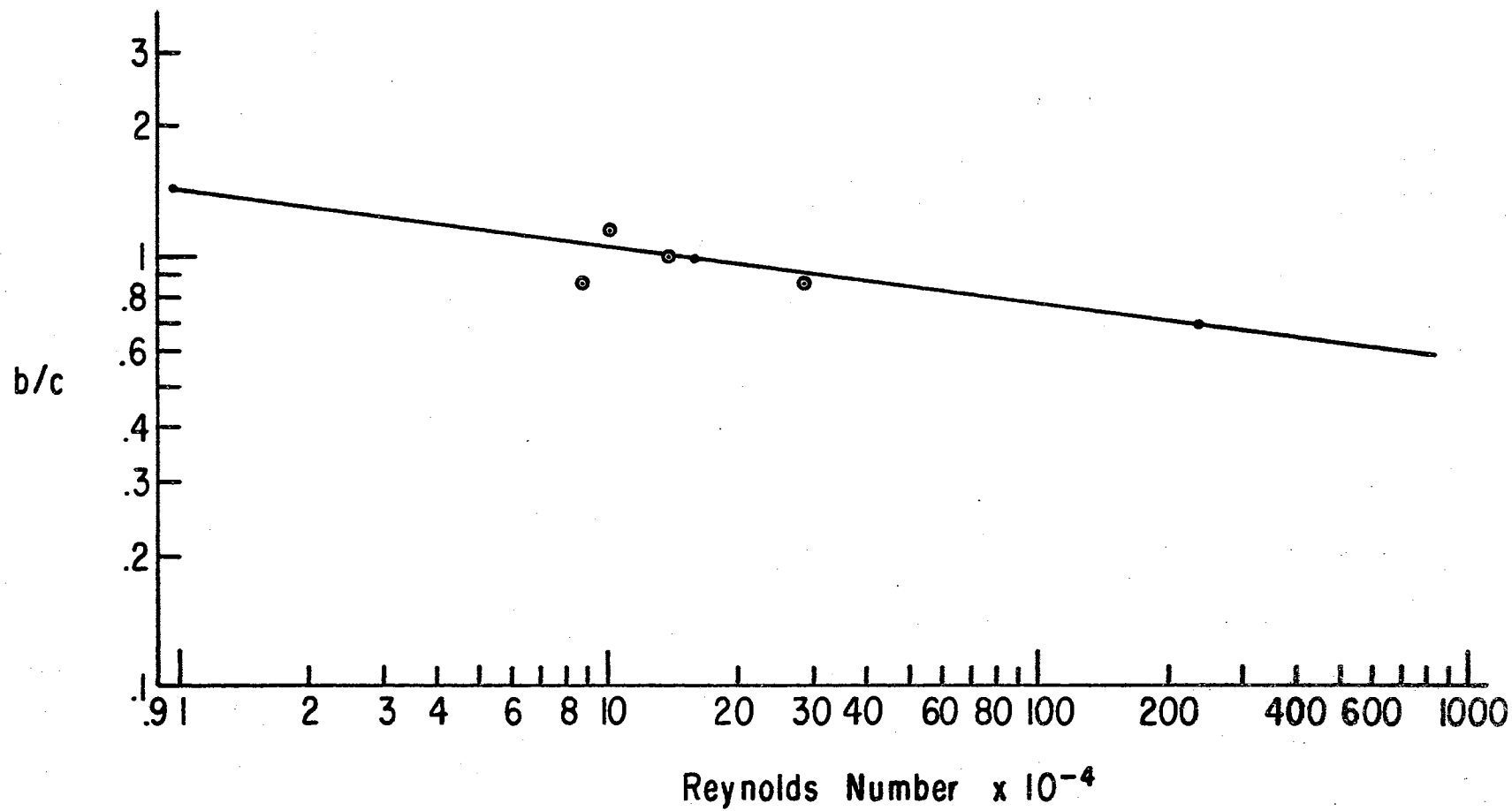


Figure 36. Reynolds Number at which Nusselt Number is equal for the irregular shape and ellipsoid with equivalent dimensions using equation 125



of 10 was arbitrarily selected and a value of  $Re_{conv}$  calculated for each shape. These values are the circled points in Figure 36. Note that the values for  $Re_{conv}$  lie very close to the line predicted from the models used in this study with some points falling above and some below the line. This variation may be due to the sharp corners that were present on these shapes and not on the models used in the tests. These differences could probably be accounted for by a "corner" effect as will be discussed in the following section.

#### Transforming the Irregular Shape

As discussed earlier the Nusselt Number for any specified shape has been shown to be a function of the Reynolds Number, Prandtl Number and geometry of the body. If we look at the component equation for Nusselt Number vs. Reynolds Number we find the type of expression shown in Figure 37 existing for the various geometries.

This form of the experimental data yields a component equation of the form

$$Nu_i = c_i (Re)^{n_i} \quad (130)$$

Analytical solution of the energy equation where possible and experimental observations indicate that the value of  $n$  varies between 0.5 for laminar boundary layer flow on a flat plate and 0.8 for a turbulent boundary layer on a

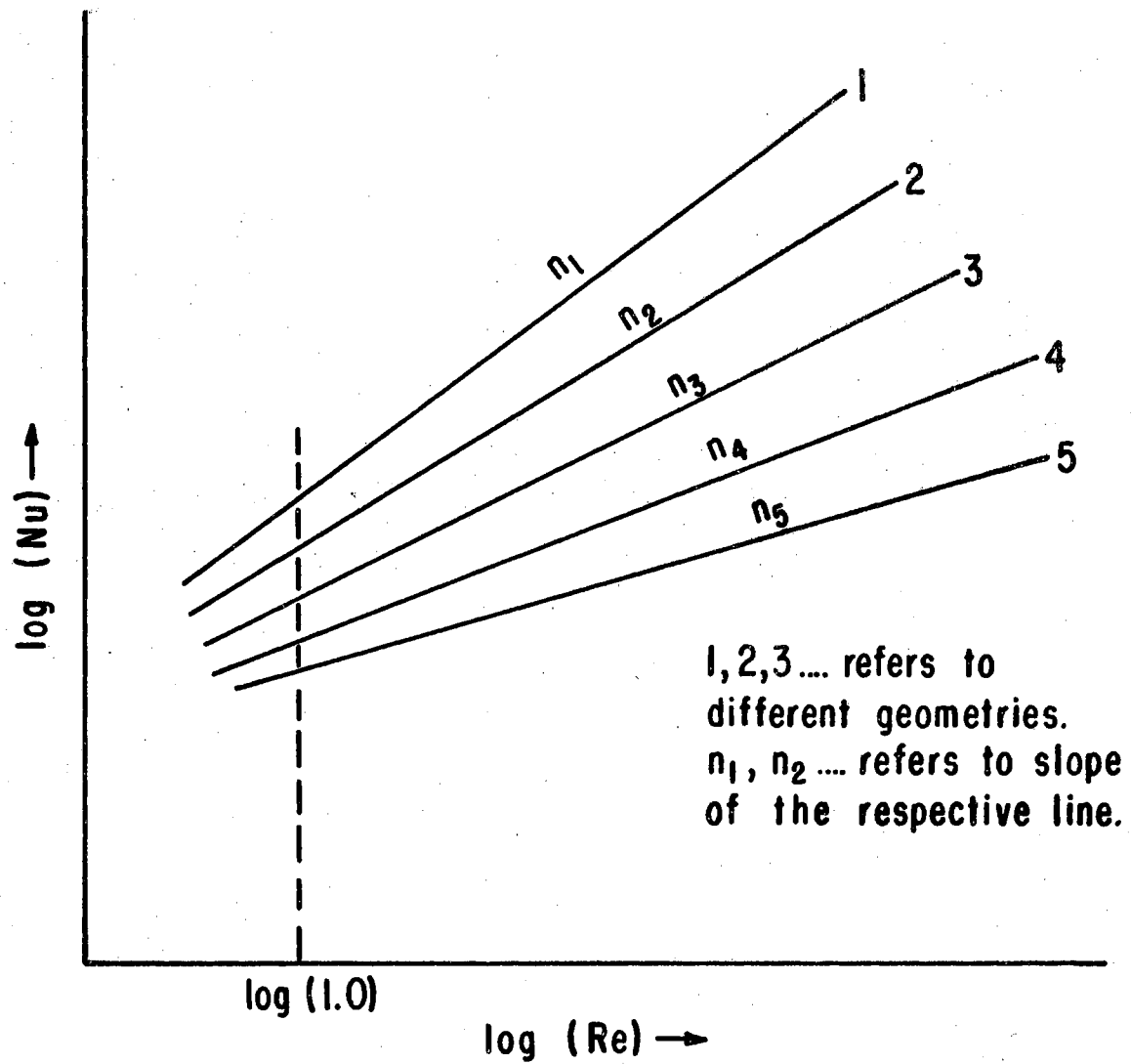


Figure 37. Effect of geometry of the object on the Nu vs. Re relationship

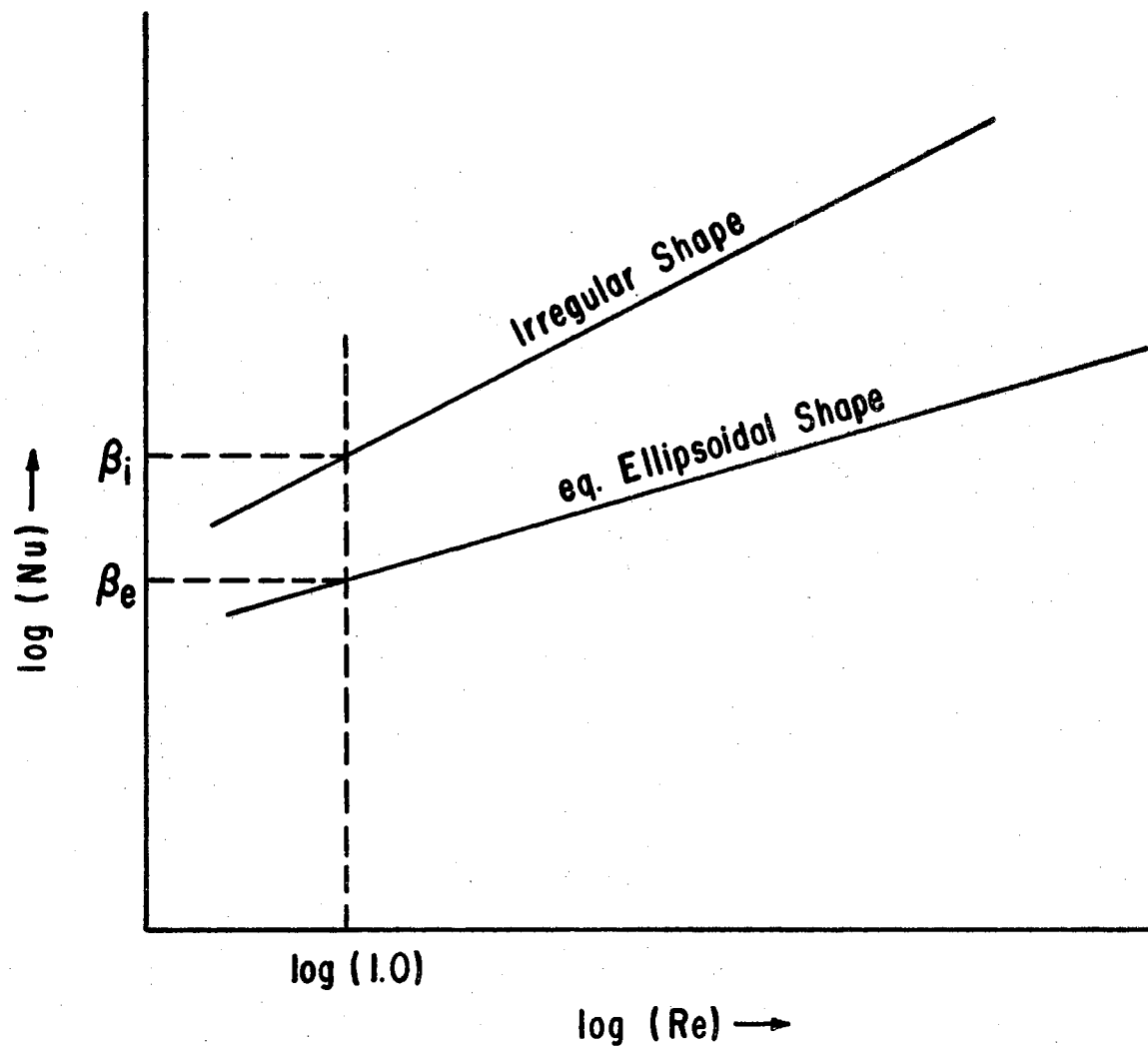


Figure 38. General shape of Nu vs. Re for an irregular shape and ellipsoidal shape

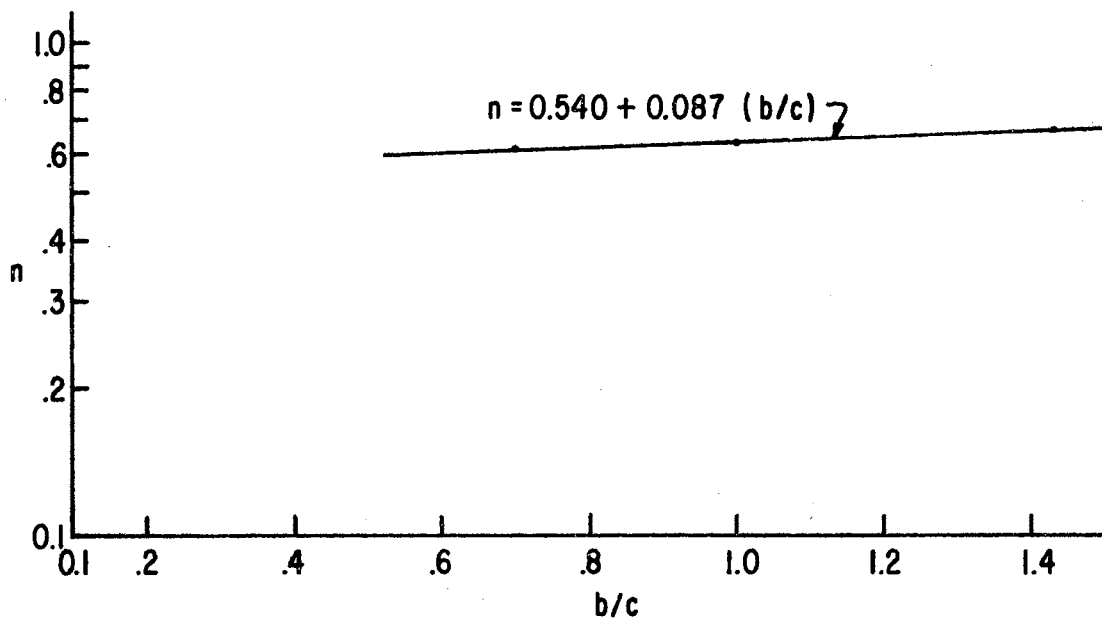
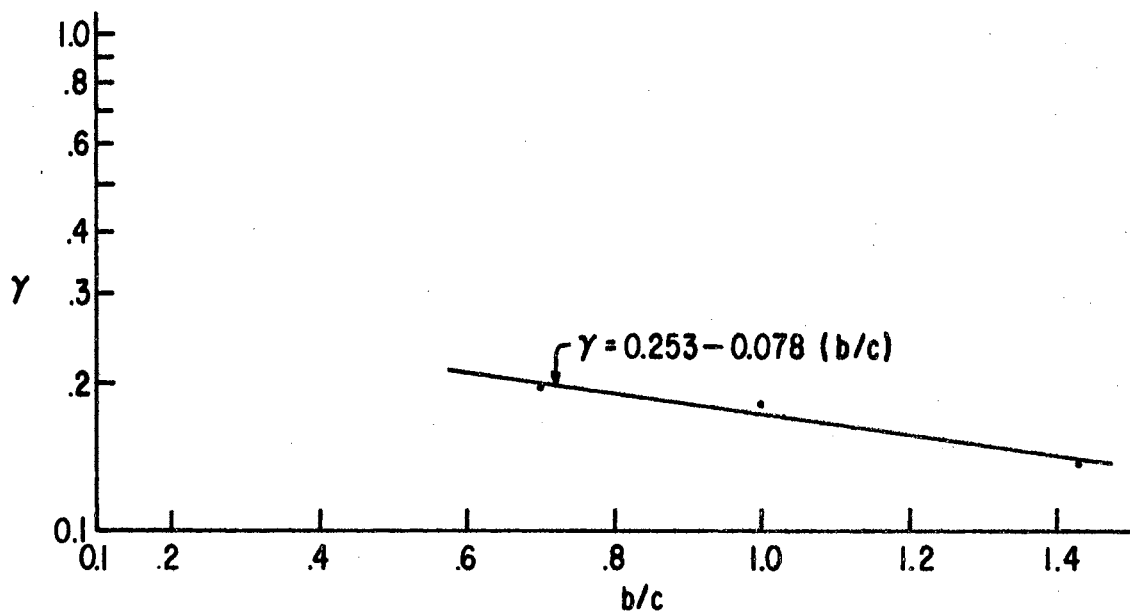


Figure 39. Values of  $\gamma$  and  $n$  as a function of the length ratio  $b/c$

flat plate. Values of  $n$  for other shapes and flow conditions fall within this range of values.

As observed previously the Nusselt Number plotted as a function of the Reynolds Number will be of the nature shown in Figure 38 for the irregular shape and for the equivalent ellipsoid when transformed by using equivalent orthogonal dimensions. We assert that since the Nusselt Number is not heavily dependent upon  $a/c$  and if we limit the analysis to irregular shaped bodies with smooth continuous surfaces, i.e. no sharp corners, that

$$n = f_9(b/c) \quad (131)$$

$$\text{and } \gamma = f_{10}(b/c) \quad (132)$$

The proof of this assertion will depend upon whether we are successful in obtaining a transformation that will indeed provide acceptable results for the irregular shaped objects.

In transforming the irregular shape to an ellipsoidal model the irregular shape is visualized as an ellipsoid inscribed inside the shape with orthogonal ellipsoid dimensions the same as the orthogonal dimensions of the irregular shape. This provides the simplest transformation possible with all length ratios and the length dimension in the Reynolds Number being based on the dimensions of the equivalent ellipsoid.

Both equations 131 and 132 fit as straight lines in semi-log space and the data is shown plotted in Figure 39. A least squares analysis of the data yields

$$n = 0.540 + 0.087(b/c) \quad (133)$$

$$\gamma = 0.253 - 0.078(b/c) \quad (134)$$

The experimentally derived equation for the general ellipsoid is from equation 125.

$$Nu_e = 0.438(Re)^{0.557}(a/c)^{-0.07}(b/c)^{-0.44} \quad (125)$$

For the irregular shape transformed on the basis of equivalent orthogonal dimensions for the irregular shape and equivalent ellipsoidal shape the equation becomes

$$Nu_s = \gamma(Re)^n(a/c)^{-0.07}(b/c)^{-0.44} \quad (135)$$

After substituting the derived expressions for  $n$  and  $\gamma$  the prediction equation for the transformed irregular shape becomes

$$Nu_s = (0.253 - 0.078(b/c))(Re)^{0.540 + 0.087(b/c)}(a/c)^{-0.07}(b/c)^{-0.44} \quad (136)$$

The Nusselt Number for the shape calculated from equation 136 is plotted against Nusselt Number observed in Figure 40.

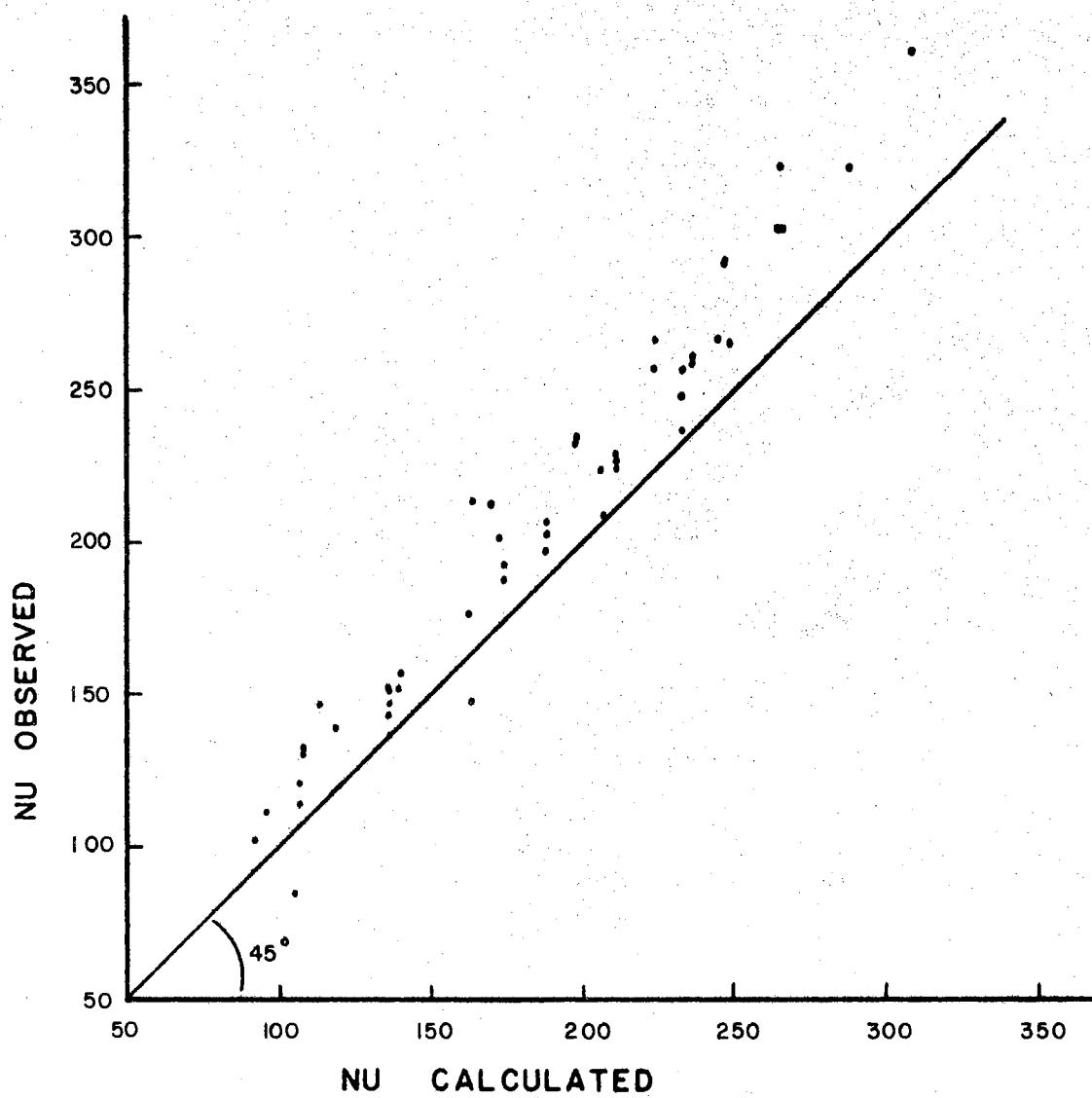


Figure 40. Nusselt Number Calculated from Equation 136 vs. Nusselt Number Observed for the Irregular Shape

## CHAPTER VI

### SUMMARY AND CONCLUSIONS

#### Summary

The primary objective of this study was to develop a method whereby the average convective heat transfer coefficients could be predicted with a reasonable degree of accuracy. The general ellipsoid serves as an adequate model for replacing the irregular shape for predicting the average heat transfer coefficient.

A series of thirteen ellipsoidal models were cast from aluminum for use in this study. Their dimensions were selected to span the range of sizes normally encountered in the processing of the pork carcass. The range of these dimensions are

$$8 \text{ in.} \leq a \leq 14 \text{ in.}$$

$$4 \text{ in.} \leq b \leq 11 \text{ in.}$$

$$4 \text{ in.} \leq c \leq 6 \text{ in.}$$

The prediction equation for the Nusselt Number from the general ellipsoid is of the form

$$\text{Nu} = f_{11}(\text{Re}, \text{Pr}, a/c, b/c, \lambda, \epsilon). \quad (137)$$



For this study the Prandtl Number,  $Pr$ , the orientation of the shape,  $\lambda$ , and the surface roughness,  $\epsilon$ , were all held constant so that they do not enter into the prediction equation. Equation 137 then reduces to

$$Nu = f_{12}(Re, a/c, b/c) \quad (138)$$

Employing the methods of similitude, component equations were developed that fitted to a straight line when transformed to logarithmic coordinates. Combining these component equations by multiplication yielded the following equation for predicting the average Nusselt Number for the general ellipsoid as

$$Nu = 0.438(Re)^{0.557}(a/c)^{-0.07}(b/c)^{-0.44} \quad (125)$$

This experimental correlation was developed over the following range of the independent pi terms.

$$30,000 \leq Re \leq 150,000$$

$$1.33 \leq a/c \leq 3.00$$

$$1.00 \leq b/c \leq 2.50$$

Using the non-ellipsoidal shapes described in the previous chapter a criteria was developed for replacing a smooth irregular shape with an ellipsoidal model for predicting the average convective heat transfer coefficient. All shapes used in this analysis were such that no sharp corners were present. The criteria established requires that the irregular shaped object be conceptually replaced

with an ellipsoid that has the same orthogonal dimensions as the irregular shape. The prediction equation then takes the form

$$\text{Nu} = \gamma(\text{Re})^n(\text{a/c})^{-0.07}(\text{b/c})^{-0.44} \quad (135)$$

where

$$n = f_9(\text{b/c}) \quad (131)$$

$$\gamma = f_{10}(\text{b/c}) \quad (132)$$

The functions for predicting  $n$  and  $\gamma$  were evaluated to yield

$$\text{Nu} = (0.253 - 0.078(\text{b/c}))(\text{Re})^{0.540 + 0.087(\text{b/c})}(\text{a/c})^{-0.07}(\text{b/c})^{-0.44} \quad (136)$$

### Conclusion

The following conclusions are based on the interpretation of the experimental results.

1. The influence of the length ratio,  $a/c$ , has little if any effect on the average Nusselt Number as long as the cross-sectional geometry of the shape remains constant throughout the length  $a$ . This could be expected to change as  $a/c$  approaches zero and becomes a flat plate whose shape is that of an ellipse. It is for this reason that the results of this study should not be extrapolated below the range of values used for  $a/c$ .

2. As would be expected the major geometry dependence is characterized by the length ratio  $b/c$ . As the length ratio,  $b/c$ , changes the percentage of the surface covered with laminar, transition, turbulent and separated flow regimes changes. This causes a change in the average Nusselt Number for the ellipsoidal shapes as predicted in equation 125.
3. The component equation for the Nusselt Number vs. Reynolds Number forms a straight line in log-log space for the ellipsoidal shape as well as all other shapes used in this study. This is in agreement with experimental results reported by other investigators.
4. For the non-ellipsoidal shapes with no sharp corners or edges the general ellipsoid can be used as an adequate model for predicting the average heat transfer coefficient. Where sharp corners exist the results probably are not valid because of the large change in the nature of the boundary layer in the vicinity of the sharp edge.
5. The coefficient,  $\gamma$ , in the expression for predicting the Nusselt Number can be adequately expressed as a function of the length ratio  $b/c$ . This expression is

$$\gamma = 0.253 - 0.078(b/c) \quad (134)$$

6. The exponent,  $n$ , on the Reynolds Number in the expression for predicting the Nusselt Number can be adequately expressed as a function of the length ratio  $b/c$ . This expression is

$$n = 0.540 + 0.087(b/c) \quad (133)$$

7. For the irregular shapes used in this study the criteria for using the general ellipsoid as an adequate model is that the orthogonal dimensions of the ellipsoid be the same as those for the irregular shape. With this criteria the Nusselt Number for the irregular shape is predicted by

$$Nu_s = \gamma(Re)^n(a/c)^{-0.07}(b/c)^{-0.44} \quad (135)$$

where  $\gamma$  and  $n$  are defined in 5 and 6 above.

## SELECTED BIBLIOGRAPHY

1. Allen, H. J. and B. C. Look. "A Method for Calculating Heat Transfer in the Laminar Flow Region of Bodies." National Advisory Committee for Aeronautics. Report 764, 1943.
2. Becker, K. M. "Measure of Convected Heat Transfer from a Horizontal Cylinder Rotating in a Tank of Water." International J. of Heat and Mass Transfer. Vol. 6, No. 12, December 1963, p. 1053.
3. Blasius, H. "Grenzschichten in Flüssigkeiten mit Kleiner Reibung." Z. Math. U. Phys., 56, 1, 1908. English translation in National Advisory Committee for Aeronautics. Technical Memo. 1256.
4. Buckingham, E. "On Physically Similar Systems: Illustrations of the Use of Dimensional Equations." Physical Review. Vol. 4, October, 1914, p. 345.
5. DeGroff, H. M. "On Viscous Heating." J. Aero. Science. Vol. 23, 1956, p. 395.
6. Drake, R. M. Jr., R. A. Seban, D. L. Doughty, and S. Levy. "Local Heat Transfer Coefficients on Surface of an Elliptical Cylinder, Axis Ratio 1:3, in a High-Speed Air Stream." Trans. American Society of Mechanical Engineers. Vol. 75, No. 7, October, 1953, p. 1291.
7. Dryden, H. L. and A. M. Kuethe. "Effect of Turbulence in Wind Tunnel Measurements." National Advisory Committee for Aeronautics. Technical Report 342, 1930.
8. Dryden, H. L., G. B. Schubauer, W. C. Mock, Jr., and H. K. Skramstad. "Measurements of Intensity and Scale of Wind Tunnel Turbulence and Their Relation to the Critical Reynolds Number of Spheres." National Advisory Committee for Aeronautics. TR581, 1935.
9. Eckert, E. R. G. and R. M. Drake, Jr. Heat and Mass Transfer. McGraw-Hill Book Company, New York, 1959.

10. Eckert, E. R. G. and J. N. B. Livingood. "Method for Calculation of Heat Transfer in Laminar Region of Air Flow Around Cylinders of Arbitrary Cross-Section." National Advisory Committee for Aeronautics. TN 2733, 1952.
11. Frick, C. W. Jr., and G. B. McCollough. "A Method for Determining the Rate of Heat Transfer from a Wing or Streamline Body." National Advisory Committee for Aeronautics. Report 830, 1945.
12. Froessling, N. "Verdunstung Wärmeübertragung und Geschwindigkeitsverteilung bei zweidimensionaler und rotationssymmetrischer Grenzschichtströmung." Lunds Universitets Arsskrift. N. F. Avd. 2, 36, No. 4, 1940.
13. Giedt, W. H. "Effect of Turbulence Level of Incident Air Stream on Local Heat Transfer and Skin Friction On a Cylinder." J. of the Aero-Space Sciences. Vol. 18, No. 11, November, 1951, p. 725.
14. Giedt, W. H. "Investigation of Variation of Point Unit Heat-Transfer Coefficient Around a Cylinder Normal to an Air Stream." Trans. of ASME, Vol. 71, May, 1949.
15. Griffith, E. and J. H. Awberry. "Heat Transfer Between Metal Pipe and a Stream of Air." Proceedings of the Institute of Mechanical Engineers. Vol. 125, 1933, p. 319.
16. Grigull, U. "Wärmeübertragung in Laminarer Strömung mit Reibungswärme." Chemie-Ingenieur Technik. 1955, p. 480.
17. Hausenblas, H. "Die Nicht Isotherme Strömung einer Zähnen Flüssigkeit durch enge Spalte und Kapillarröhren." Ing-Arch., Vol. 18, 1950, p. 151.
18. Hilpert, R. "Experimental Study of Heat Dissipation of Heated Wire and Pipe in an Air Current." Forschung auf dem Gebiete des Ingenieurwesen. Vol. 4, 1933, p. 215.
19. Kays, W. M. Convective Heat and Mass Transfer. McGraw Hill Book Co., New York, 1966.
20. Ko, Shao-Yen and H. H. Sogin. "Laminar Mass and Heat Transfer from Ellipsoidal Surfaces of Finesness Ratio 4 in Axisymmetrical Flow." Trans. of the ASME. February, 1958, p. 387.

21. Langhaar, H. L. Dimensional Analysis and Theory of Models. John Wiley and Sons, New York, 1951.
22. Lewis, J. P. and R. W. Ruggeri. "Investigation of Heat Transfer From a Stationary and Rotating Ellipsoidal Forebody of Fineness Ratio 3." National Advisory Committee for Aeronautics. TN 3837, November, 1956.
23. Maher, T. F. "An Investigation of the Transportation and Evaporation of Fog or Mist When Sprayed into an Air Stream." Ph.D. Thesis, Oklahoma State University, Stillwater, Oklahoma, 1961.
24. Martinelli, R. C. "Heat Transfer to Molten Metals." Trans. of the ASME, Vol. 69, 1947, p. 947.
25. McAdams, W. H. Heat Transmission. Third Edition, McGraw Hill Book Co., Inc., New York, 1953.
26. Millikan, C. B. and A. L. Klein. "The Effect of Turbulence." Aircraft Engineering. August, 1933, p. 169.
27. Murphy, Glenn. Similitude in Engineering. The Ronald Press Co., New York, 1950.
28. Panton, R. L. Class Notes for Boundary Layer Theory. Oklahoma State University, Fall Semester, 1966.
29. Pappas, C. C. "Measurement of Heat Transfer in the Turbulent Boundary Layer on a Flat Plate in Supersonic Flow and Comparison with Skin Friction Results." National Advisory Committee for Aeronautics. TN 3222, 1954.
30. Parker, J. D. and J. H. Boggs. Fluid Mechanics and Heat Transfer. Unpublished Manuscript, Oklahoma State University, Stillwater, Oklahoma, 1966.
31. Polhausen, E. "Der Wärmeaustausch Zwischen Festen Körpern und Flüssigkeiten mit kleiner Reibung und Kleiner Wärmeleitung." Zeitschrift für angewandte Mathematik und Physik. Vol. 1, 1921, p. 115.
32. Prandtl, L. "Der Luftwiderstand von Kugeln." Nachr. d. Ges. d. Wissensch., Göttingen, Math. Phys. Vol. 1, 1914, p. 177.
33. Prandtl, L. "Eine Beziehung Zwischen Wärmeaustausch und Strömungswiderstand der Flüssigkeiten." Phys. Zeitschr., Vol. 11, 1910, p. 1072.

34. Prandtl, L. "Fluid Motion with Very Small Friction." Mathematical Congress. Heidelberg, 1904.
35. Reynolds, O. "On the Extent and Action of the Heating Surface for Steam Boilers." Proceedings Manchester Lit. Phil. Soc., Vol. 14, 1874, p. 7.
36. Schlichting, H. Boundary Layer Theory. McGraw-Hill Book Co., Inc., New York, 1962.
37. Schmidt, E. and K. Wenner. "Heat Transfer Over the Circumference of a Heated Cylinder in Transverse Flow." National Advisory Committee for Aeronautics, TM 1050, 1943.
38. Seban, R. A., R. M. Drake, Jr. and S. Levy. "Local Heat Transfer Coefficients on the Surface of an Elliptical Cylinder in a High Speed Air Stream." Inst. of Engineering Research Report 41-6. University of California, Berkeley, Calif. January, 1952.
39. Seiff, A. "Examination of the Existing Data on the Heat Transfer of Turbulent Boundary Layers at Supersonic Speeds from the Point of View of Reynolds Analogy." National Advisory Committee for Aeronautics, TN 3284, 1954.
40. Smith, R. E. "Analyses on Transient Heat Transfer From Anomalous Shapes with Heterogeneous Properties." Ph.D. Thesis, Oklahoma State University, Stillwater, Oklahoma, 1961.
41. Squire, H. B. "Heat Transfer Calculation for Aerofoils." Aeronautical Research Council R and M, 1942, p. 1986.
42. Taylor, G. I. "Conditions at the Surface of a Hot Body Exposed to the Wind." Aeronautical Research Council R and M, 1919, p. 272.
43. Van Der Hegge Zijnen, B. G. "Modified Correlation Formulae for the Heat Transfer by Natural and by Forced Convection from Horizontal Cylinders." Applied Science Research. A6, 1957, p. 129.
44. Van Driest, E. R. "The Turbulent Boundary Layer with Variable Prandtl Number." Fifty Years of Boundary Layer Research, Memorial Volume, 1955, p. 257.



45. Van Meel, D. A. "A Method for the Determination of Local Convective Heat Transfer from a Cylinder Placed Normal to an Air Stream." International J. of Heat and Mass Transfer. Vol. 5, 1962, p. 715.
46. Von Karman, Th. "The Analogy Between Fluid Friction and Heat Transfer." Trans. of the ASME, Vol. 61, 1939, p. 705.
47. Zapp, G. M. M.S. Thesis, Oregon State University, Coravallis, 1950.
48. Alcoa Aluminum Handbook. Aluminum Company of America, Pittsburgh, Pa., 1957.

VITA

Bobby Leland Clary

Candidate for the Degree of  
Doctor of Philosophy

Thesis: CONVECTIVE HEAT TRANSFER COEFFICIENTS FROM  
ELLIPSOIDAL MODELS AND IRREGULAR SHAPES TO  
AIR

Major Field: Engineering

Biographical:

Personal Data: Born in Jesup, Wayne County, Georgia,  
August 14, 1938, the son of J. Edward and Ada  
Higginbotham Clary.

Education: Graduated from Odum High School in Odum,  
Georgia in 1956; received the degree of Bachelor  
of Science in Agricultural Engineering from the  
University of Georgia in June, 1960; studied at  
Alfred University in the spring of 1962; completed  
the National Science Foundation Summer Institute  
in Fluid Mechanics and Hydrology at Colorado  
State University in the summers of 1962 and 1963;  
completed the NSF Summer Institute in Structural  
Engineering at Oklahoma State University in the  
summer of 1964; completed the requirements for  
the Doctor of Philosophy degree from Oklahoma  
State University in May, 1969.

Professional Experience: Taught agricultural engineer-  
ing technology in the State University of New  
York, Agricultural and Technical Institute at  
Alfred, New York, 1960-1965; taught engineering  
technology in the Technical Institute Division  
of Polk Junior College, Winter Haven, Florida,  
1965-1966; graduate research assistant in the  
Agricultural Engineering Department, Oklahoma  
State University, 1966-present.

Professional Organizations: Member of American Society  
of Agricultural Engineers, Oklahoma Society of  
Professional Engineers, National Society of  
Professional Engineers, American Society for  
Engineering Education.